CARBON NANOCOMPOSITE MATERIALS FOR NON-ENZYMATIC ELECTROCHEMICAL GLUCOSE SENSING

Thesis

Submitted in partial fulfilment of the requirements for the degree of

DOCTOR OF PHILOSOPHY

By

RAGHAVENDRA PRASAD J

DEPARTMENT OF CHEMISTRY
NATIONAL INSTITUTE OF TECHNOLOGY KARNATAKA
SURATHKAL, MANGALORE - 575 025

March, 2017

My thesis is dedicated

- *....to my parents for their encouragement and support*
- *....to my brother and sister for their affection*
- *… to my soon to be better half Vinutha for her constant love*
- *... to my good friends for being with me in all ways*
- *… and to my teachers for their moral guidance*

during work

DECLARATION

I hereby *declare* that the Research Thesis entitled "**CARBON NANOCOMPOSITE MATERIALS FOR NON-ENZYMATIC ELECTROCHEMICAL GLUCOSE SENSING"** which is being submitted to the **National Institute of Technology Karnataka, Surathkal** in partial fulfillment of the requirements for the award of the degree of **Doctor of Philosophy** in **Chemistry** is a *bonafide report of the research work carried out by me*. The material contained in this Research Thesis has not been submitted to any University or Institution for the award of any degree.

Raghavendra Prasad J

Register Number: 123005CY12F08

Department of Chemistry

Place: NITK-Surathkal

Date: 8th March 2017

CERTIFICATE

This is to *certify* that the Research Thesis entitled "CARBON NANOCOMPOSITE MATERIALS FOR NON-ENZYMATIC ELECTROCHEMICAL GLUCOSE SENSING" submitted by **Raghavendra Prasad J** (**Register Number: 123005CY12F08**) as the record of the research work carried out by him, is accepted as the *Research Thesis submission* in partial fulfillment of the requirements for the award of degree of **Doctor of Philosophy.**

Research Guide

(Name and Signature with date and seal)

Chairman – DRPC

(Signature with date and seal)

ACKNOWLEDGEMENT

The culmination of a research work leading to degree of Doctor of Philosophy (Ph.D.) is result of constant encouragement and support from great number of people. This thesis could not be complete without acknowledging their contribution to make my research a successful one.

I pay my sincere and deepest gratitude towards my research supervisor, ***Prof. B. Ramachandra Bhat, Dept. of Chemistry.*** *His encouragement and teachings provided me freedom to explore, critically evaluate and express ideas. His patience and support helped me overcome many crisis situations and finish this dissertation.*

I would like to thank ***Prof. A. Chitaranjan Hegde, Prof.B. Ramachadra Bhat*** *and* ***Prof. D. Krishna Bhat****, Head of the Department of Chemistry from 2013-14, 2014-16 and 2016-Current respectively, for extending administrative facility for tranquil progress of my Ph.D. work.*

I am also grateful to my RPAC members ***Prof. A. Chitharanjan Hegde, Dept. of Chemistry*** *and* ***Dr. B. D. Prasanna, Dept. of Chemical Engineering.*** *Their insightful comments and constructive criticisms at different stages of my research were thought-provoking and helped me focus on my research objectives.*

I thank ***Dr. Gangamma S., Dept. of Chemical Engineering****, for her support to obtain ethical committee clearance to work on biological samples.*

I am thankful to the ***CeNSE, IISc-Bangalore*** *and* ***SMaRT@UNSW, Australia*** *for extending the characterization facilities needed to complete this research work.*

I would also like to acknowledge ***Ravindra Rajarao, Kiran, Suresh Dara, Pooja Bhat, Lolaskshi Mahesh Kumar, Ansari Rashida Bano Maqbool Hasan, Praveen Mishra, Madhu N. Nimbalkar and Anuma Saroja*** *for their constant support and encouragement during the thick and thins of my Ph.D. journey.*

I cannot forget to mention my deepest regards towards ***The Faculty and Non-Teaching Staff*** *of the* ***Department of Chemistry*** *for extending their support at various stage of my research journey and* ***NITK-Surathkal*** *for providing research infrastructure and fellowship.*

Most importantly, none of this would have been possible without the support and patience of my family. They have been a constant source of love, concern and strength all these years. I would like to express my extreme sense of gratefulness to my ***family****.*

I conclude with gratitude towards all individuals who have made this dissertation possible and my research experience rewarding and to be cherished forever.

Raghavendra Prasad J

ABSTRACT

Unique and Extraordinary electrical and mechanical properties of carbon nanotubes (CNTs) and their composites have stimulated extensive research activities across the world since their discovery by Sumio Iijima in 1991. The range of application of CNTs is indeed wide as it ranges from nano-electronics, with quantum wire interconnects and field emission devices to composites, chemical sensors and biosensors. However, because of low production capacity and high production costs at present, their applications cannot be extended until large-scale production is achieved.

In present research work titled "**Carbon nanocomposite materials for non-enzymatic electrochemical glucose sensing**", the principal objective is to synthesize bulk scale CNTs and explore the possible application to design efficient, improved and economical non-enzymatic glucose sensor. The work describes eco-friendly synthesis of CNTs and its metal oxide composites (NiO-MWCNT, CuO-MWCNT and Co_3O_4) using metal formates as an eco-friendly precursor by low temperature thermal reduction method using chemical vapour deposition. The surface and structural morphology were studied by FESEM, TEM, whereas, elemental composition was determined by XRD and Raman spectroscopy. Using these materials the modified glassy carbon electrodes were fabricated to investigate the electro-catalytic properties towards the direct glucose oxidation. The electrochemical properties were characterised by cyclic voltammetry and chronoamperometry techniques in NaOH electrolyte. The sensor parameters like sensitivity, selectivity, stability, reproducibility, response time, limit of detection (LOD) and linear concentration range was investigated for the fabricated electrodes and results obtained were compared with the ones reported in literature. It is notable that the composite materials show significantly enhanced catalytic performance towards direct glucose oxidation due to the synergistic effect of carbon nanomaterials and metal oxide. This composite martials also shows properties like high surface area, fast electron movement, biocompatible and antifouling properties, etc. making these material as promising candidate for the fabrication of non-enzymatic glucose sensors.

Keywords: Carbon nanotubes, Graphene, Composite, Non-enzymatic, Electro catalyst.

CONTENTS

NOMENCLATURE

ABBREVIATIONS

AA	Ascorbic acid
ATP	Adenosine triphosphate
CA	Chronoamperometry
CNT	Carbon nanotube
CPE	Carbon paste electrode
CV	Cyclic voltammetry
CVD	Chemical vapour deposition
DA	Dopamine
FAD	Flavin adenine dinucleotide
GCE	Glassy carbon electrode
GO	Graphene oxide
GOx	Glucose oxidase
HBS	human blood serum
I	Current
IUPAC	International Union of Pure and Applied Chemistry
LOD	Limit of detection
MWCNT	Multiwall carbon nanotube
NP	Nanoparticle
NW	Nanowire
rGO	Reduced graphene oxide
RSD	Relative standard deviation
SCE	standard calomel electrode
SWCNT	Single wall carbon nanotube
Trp	Tryptophan
UA	Uric acid
VLS	vapour-liquid-solid
FESEM	Field Emission Scanning Electron Microscope
TEM	Transmission Electron Microscope
PXRD	Powder X-Ray Diffraction

EDXA	Energy-dispersive X-ray spectroscopy
CNT	Carbon nanotube
WHO	World Health Organization
TGA	Thermogravimetric analysis
JCPDS	Joint Committee on Powder Diffraction Standards
DFT	Density Functional theory
VASP	Vienna Ab-initio Simulation package
PAW	Projected augmented-wave
CNF	Carbon Nano Fibre

CHAPTER 1

INTRODUCTION

Chapter1 *presents a brief overview of carbon nanomaterials, carbon-metal/metal oxide composites and their importance in bio-sensing application. It also covers a brief introduction to working principles, advantages and limitations of enzymatic and non-enzymatic glucose biosensors. The importance of metal formates in composite synthesis and different electrochemical techniques employed in the work are also discussed.*

In living organisms, biomolecules play crucial role in the metabolic activities. It is well known that any change in their concentration level adversely affects the well-being of organisms (McDowell 1989, Simpson and Ortwerth 2000, Cooper et al. 2003). Maintenance of optimal level of biomolecules demand their selective and accurate determination, thereby posing a great challenge to analytical chemists, biomedical engineers and biotechnologists. As a part of medical diagnosis, classical method followed in clinical laboratories to analyse the body fluid of patients, often lead to experimental or human errors (Connolly 1995). However, with progress in biosensor technology, use of biosensor devices reduce errors, cost and time of analysis (Strasinger and Lorenzo 2001). Current medical diagnosis depends on the sensitivity, selectivity, accuracy of the device and also the experimental skill of the lab personnel. These aspects also limit the use of many instruments for accurate monitoring of the biomolecules (Marazuela and Moreno-Bondi 2002, Malhotra and Chaubey 2003). Hence, to overcome these limitations, simple electrochemical device called biosensors were developed, where in analytes are converted into the measurable electrical response.

1.1 BIOSENSOR

A biosensor is an analytical device which can detect the analyte that combines a biological component with a physico-chemical detector (Wang 2008, Wang and Liu 2011). The International Union of Pure and Applied Chemistry (IUPAC) define biosensor as self-containing integrated device, capable of analysing quantitative or semi-quantitative analytical information using a biological recognition element which is in contact with a transduction element (Figure1.1).

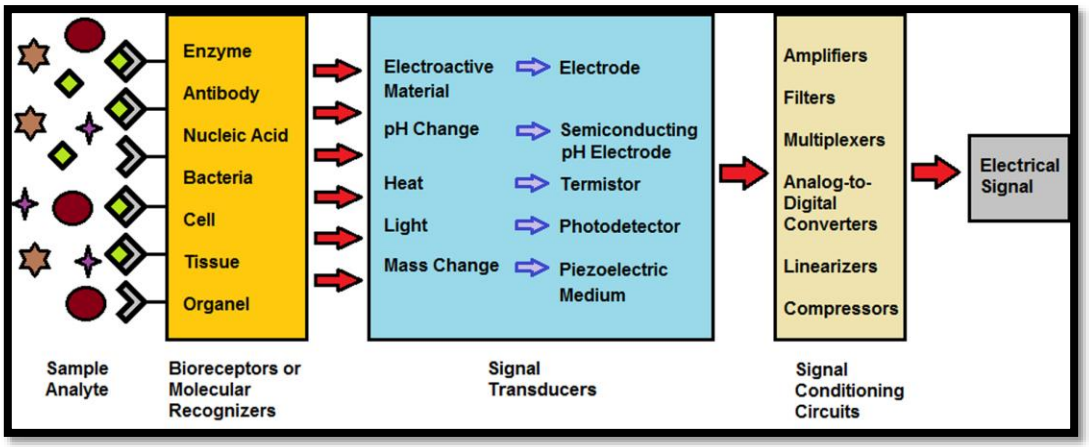

Figure 1.1 Biosensor operating principle.

The biosensor consists of three components:

a) A receptor/ biological element which is sensitive to the biological analyte.
b) The transducer, that converts a signal in one form of energy to another form of energy.
c) The detector element, which works in a physicochemical way; optical, piezoelectric electrochemical, thermometric and magnetic.

The main component of a biosensor is the receptor (i.e. enzymes, antibodies, lipid layers, immobilized cells, metal, metal oxide, etc.) which is very sensitive to the analyte in the sample that makes the detection very selective. This detection by the receptor is converted to a readable signal from the transducer. The conversion can be to an electrical signal, light signal or as a mass change, etc. The detector later detects the signal and converts to observable output for user.

1.1.1 Desirable Characteristics of a Biosensor

Biosensor performance and efficiency is evaluated in terms of well-defined technical and functional characteristics according to guidelines laid down by IUPAC (Cass 1990, Buerk 1995). These desirable characteristics for any biosensor are:

(a) Sensitivity

Sensitivity of the sensing electrode can be defined by the slope of the calibration curve or the rate of change of response function with analyte concentration. It is further defined as the potential of the sensor to analyse accurately with less than 1% error in concentration. For accuracy purposes, sensitivity is always calculated over the linear portion of calibration curve.

(b) Selectivity

Selectivity of a biosensor can be defined as the specificity of the sensing electrode towards single analyte or to avoid false results caused by potentially interfering species. Two major aspects which decides the selectivity of the sensor includes bio-molecule type and transducer element. Enzymes and antibodies are very distinct for specific analyte and have been extensively used for biosensor development, while whole biomolecules like, microorganisms, are highly non-specific and are comparatively less explored. Biosensor response could either be enhanced or decreased in the presence of potentially interfering species. Enhanced interference is recorded when the interfering species share structural and chemical similarity with the sensor substrate and are recognized by a biocatalyst. On the contrary, if the interfering species show decreased effects towards the immobilized biocatalyst a drastic reduction in response of the sensing electrode is observed.

(c) Detection Limit

Detection limit of the biosensor is the lowest concentration of the analyte that can be measured accurately by sensing electrode with an acceptable signal to noise (S/N) ratio. Sensor response with low signal to noise ratio is required to achieve lower limit of detection and high sensitivity.

(d) Response Time

Response time is one of the important parameters in biosensor for technology transfer from lab to industries. It can be designated into two types, 1) Steady state response time which can be defined as the time required for response signal to reach

95% of the steady state value. 2) Transient response time, which is the time required for derivation of the response signal to reach its maximum value after the addition of the substrates. Desirably, the response time of biosensor should be as low as possible.

(e) Recovery Time

Recovery time is defined as the minimum time required between two successive measurements. The baseline potential can be achieved with sufficient washing of the electrode after every measurement by removing the accumulated un-reacted substrate and formed product from the electrode surface.

Factors influencing recovery time of the biosensor:

a) High concentration of substrate.
b) Thickness and permeability of the membrane on which biocatalyst is immobilized.
c) Nature of the catalyst.

(f) Reproducibility

The reliability of the biosensor is highly dependent on reproducibility of the results. It is defined as the ability of a device to produce the concordant results for same inputs applied each time. Signal baseline drift and/or sensitivity drift is the primary limit on reproducibility.

(g) Storage and Operational Stability

Commercial worth of a biosensor is dictated by its stability in addition to other factors like high sensitivity, response time or selectivity. The stability of biosensor is evaluated in terms of operational stability and storage stability.

1.1.2 Successful Biosensor Features

a) The catalyst or receptor must be highly selective for the choice of analyte, should be stable under normal storage conditions and show greater stability and reproducibility over a number of assays.

b) Sensor results should be independent of physical parameters like, pH, stirring, humidity and temperature.
c) The sensor response should be accurate, precise, reproducible and linear over the useful analytical range, without dilution or concentration. It should also be free from electronic noise.
d) If the biosensor is to be used for invasive monitoring in clinical situations, the probe must be tiny and biocompatible, having no toxic or antigenic effects.
e) The biosensor device should be small, cost effective, portable and can be easily used by semi-skilled operators.
f) There should be a greater market for the biosensor.

1.2 GLUCOSE

Glucose is a well-known monosaccharide, measured as blood sugar and serves as an energy source for a living cell and a metabolic intermediate. It is one of the important products of photosynthesis and in case of both prokaryotes and eukaryotes, glucose is responsible for cellular respiration. In biochemical process, the dextrose−glucose (D-glucose) is biologically active and easily get converted into energy, whereas, L−glucose is biologically inactive and cannot be metabolized by cells. Specificity of enzyme make it favourable catalyst for reduction of glucose. In human beings, carbohydrates are the major source of energy, where it can contribute 3.75 kcal (16 kJ) per gram of food material through aerobic respiration (Pomeranz, 2013). The breakdown of these carbohydrates lead to glucose which is oxidised to give carbon dioxide and water and energy. Glucose being a major energy source for the brain, influences psychological processes, however, when the concentration decreases, psychological processes are impaired (Fairclough and Houston 2004, Gailliot and Baumeister 2007). The glucose level in the human blood is regulated by the insulin and other metabolic activity. The normal blood glucose level in human beings is 80-120 mg/dL (4.4-6.6 mM) and any imbalance in the production of insulin by pancreas leads to the metabolic disorder called diabetes mellitus that results in hyperglycaemia. A high fasting blood sugar level is an indication of pre-diabetes and diabetic conditions

Diabetes is one of metabolic disease affecting major group of people around the world (~150 million people) and leading cause of death and many disabilities, such as nervous disorder, blindness, blood related issues and kidney failure (WHO, Diabetes mellitus). Currently there is no cure for diabetes, hence, control of elevated blood glucose levels, without causing abnormally low levels, is the major goal in treating diabetes (Shao et al. 2009). The diagnosis and management of diabetic patients require precise monitoring and control of the glucose level in the body. Therefore, frequent testing of the physiological glucose level is critical to confirm treatment efficiency, prevent long-term complications and avoid a diabetic emergency, such as hypoglycaemia (low blood sugar, < 3 mM). Currently, diabetics must frequently check their blood glucose levels by "finger-pricking" and adjust their insulin dosage to keep the glucose level as close to "normal" as possible. Compared to conventional methods of glucose testing, electrochemical biosensors provide a rapid and easy method of testing blood glucose levels. Glucose sensors are therefore a highly active area of biosensor research and accordingly they account for approximately 85% of the biosensor industry worth approximately $12 billion. This figure will reach $19 billion by 2018 according to the Global Industry Analysts.

1.3 ENZYME BIOSENSOR

In Enzyme biosensor, enzyme shows specific binding and catalytic activity towards analyte making them most commonly available biosensors. The plausible mechanisms for analyte detection are:

- Enzyme catalysed conversion of analyte to a product, which is subsequently detected by sensor,
- Detection of enzyme inhibition or activation in presence of analyte (Pohanka, 2013),
- Interaction of analyte with enzyme leading to change in properties of enzyme which is detected by sensor (Marazuela and Moreno-Bondi, 2002).

Similarly, major reason for the use of enzyme in biosensors are

- Ability to catalyse a large number of reactions,

- Potential to detect a group of analytes (substrates, products, inhibitors and modulators of the catalytic activity) and
- Suitability with several different transduction methods for detecting the analyte.

Notably, since enzymes are not consumed in reactions, the biosensor can be easily repeatedly used. The catalytic activity of enzymes also allows lower detection limits compared to common binding techniques. However, the stability of sensor, shelf-life, cost, reproducibility is limited by the stability of the enzyme.

1.3.1 Glucose Oxidase-based Glucose Biosensor

The glucose oxidase (GOx) is well known enzyme employed in glucose biosensor due to its high catalytic activity to reduce the glucose, high selectivity, high catalytic activity over broad range of temperature (~ upto 40 °C), pH and ionic strength. GOx requires less harsh conditions for the fabrication, manufacturing and storage process hence it has been extensively used in glucose sensor industry (Wang et al. 2006, Deng et al. 2009, Wang et al. 2009, Ding et al. 2010).

GOx is an elongated spherical protein (Wilson and Turner 1992) and it functions as a biocatalyst when it is associated with the redox cofactor-flavin adenine dinucleotide (FAD). During oxidation of glucose, FAD serves as the initial electron acceptor and is reduced to $FADH_2$, which is regenerated by reacting with oxygen, leading to the formation of hydrogen peroxides (Wang 2008, Yoo and Lee 2010). Hence two important methodologies were used for GOx-based electrochemical glucose sensing: 1) by measuring oxygen consumption (Gamburzev et al. 1995, 1996, 1997) and 2) by measuring the amount of hydrogen peroxide produced through the enzyme reaction (the first generation glucose biosensor) (Cespedes et al. 1993, Karyakin et al. 1994, Celej and Rivas 1998, Dai and Shiu 2004, Du et al. 2008). However, many factors affect the performance of GOx-based biosensor such as protein shell which usually covers the GOx, restrict the direct electron transfer from enzyme to electrode (Park et al. 2008).

Variety of materials have been employed to enhance the electron transfer process between GOx and electrode (Zhao et al. 2008), in which metals, polymers,

carbon nano materials and composite materials have attracted increasing attention (Shin et al. 2009, Liu et al. 2009, Wang et al. 2009b). Nanomaterials have unique benefit in enzyme immobilization and retain their bio-catalytic activity due to their high surface to volume ratio, the favourable micro-environment and the enhanced direct electron transfer between the enzyme's active sites and the electrode (Lu et al. 2008). Thus the glucose biosensor's performance can be potentially improved by using novel functional nanostructured materials.

1.3.2 The Limitations of Enzymatic Glucose Sensor

Even though the enzyme based glucose sensor dominates in biosensor industry, enzymatic sensors have many critical flaws which still needs to be addressed. The biosensor working principle depends on oxygen and therefore are unsuitable for practical use and reliable analytical use. The major problem is ability of the sensor to selectively detect the choice of analyte, where many potentially electroactive interference molecules commonly co-exists in blood samples. Furthermore, due to its instability to many physical parameters, use of GOx is restricted to conditions such as temperature below 44 ^{o}C, pH ranges of 5-8 and ambient humidity level. Hence, stability of the GOx glucose sensor is still a major concern, which also hinders the development and application of enzymatic glucose sensors (Zhang and Wang 2002, Shen et al. 2007, Deng et al. 2009). Despite these limitations, enzymatic glucose sensors remain commercially unchallenged.

1.4 NON-ENZYMATIC BIOSENSOR

Due to the insufficient stability, simplicity and reproducibility of the enzymatic glucose biosensor, which are hard to overcome, enzymeless glucose sensor have been studied and improved. Continuous efforts were made to realize this idea on the electrochemistry of glucose itself (Vassilyev et al. 1985, Park et al. 2006). In last decades, considerable attention has been given to develop the nonenzymatic sensor with good glucose sensitivity, stability and selectivity. With this concern precious metals and metal alloys (e.g. Au (Li et al. 2007), Pt (Park et al. 2003), Ni (You et al. 2003), Cu (Nagy et al. 2001), Pt-Pb (Sun et al. 2001), Ni-Cu (Yeo and Johnson 2001) and Au-Ag

(Tominaga et al. 2006) have been extensively investigated towards nonenzymatic glucose sensors. Although both bulk and nanoscale materials are used for electro-catalyzing glucose oxidation, the nanostructured materials have triggered considerable research activities due to their large surface-to-volume ratio which can greatly improve the sensitivity, selectivity and potentially minimize the adsorption of poisoning intermediates.

Enzyme-free glucose sensor have overcome some essential drawbacks of the biosensor based on enzyme. Non-enzymatic glucose biosensor can work in severe condition, for example, pure platinum electrode with nanoporous surface shows high sensitivity and selectivity to glucose even after exposure to 1 M NaOH or H_2SO_4 (Park et al. 2003). Further, for an enzyme modified electrode, the most important factor in fabrication is enzyme immobilization which includes one or more enzyme layers to be placed on the bare electrode through carefully optimized process. Many different methods have been reported for enzyme immobilization, such as direct adsorption, sol–gel entrapment, cross-linking, all of which are cost and time consuming. In this respect, the nonenzymatic sensor is an attractive alternative to the GOx based glucose sensor.

Non-enzymatic glucose sensor is still limited for practical application due to the major drawbacks like low sensitivity, poor selectivity, requirement of alkaline electrolyte and also suffers from chloride ion poisoning (Park et al. 2003, Ye et al. 2004, Zhuang et al. 2007). Therefore, there is great demand for the development of new generation non-enzymatic sensor which is cheap, shows high sensitivity, high selectivity and greater stability (Wang et al. 2007). Recently, many research groups explored the possible application of metal/metal oxides in the development of a variety of enzyme-free glucose sensors such as nanoscale Co_3O_4 (Ding et al. 2010a), NiO (Ding et al. 2010b), CuO (Reitz et al. 2008) and bulk metal oxides (Cu_2O, RuO_2, CoO and NiO) (Chen et al. 1993). Besides this, many carbon nanomaterials were also used with metal particles to enhance the sensor features of metal or metal oxide based non-enzymatic glucose sensors, e.g. gold nanoparticles/MWCNTs nanocomposites (Zhu et al. 2009), Cu_2O/MWCNTs nanocomposites (Zhang et al. 2009) and electrodeposited MnO_2 on MWCNTs (Chen et al. 2008). Recent activity in practical non-enzymatic glucose sensor has been focusing on major advances in electro-catalysis. The first goal

was to enhance the sensitivity towards glucose. Another goal was to reduce the interference of co-existing electroactive species. Most of the reported non-enzymatic glucose sensors lack a glucose recognition unit. Thus, it is difficult to distinguish glucose from other electroactive interferences (e.g. uric acid (UA), ascorbic acid (AA), dopamine (DA) etc.) and other sugars (e.g. maltose).

To overcome these limitations of non-enzymatic glucose sensor, nanotechnology is certainly providing new dimension in the fabrication of non-enzymatic glucose sensor. Numerous nano-materials, because of their surface properties and their catalytic features suggest new chances and inspirations. Hence, in this concern, significant focus is required for fabrication of nanoparticle based non-enzymatic glucose sensor. The commercialization of non-enzymatic glucose sensor for human blood may be one of the key issues. The future research on non-enzymatic glucose sensor will be extended beyond the use in disposable strips for determining human blood glucose levels.

1.5 NANOMATERIALS FOR THE DETECTION OF BIO-MOLECULES

Nano science and Nanotechnology address the study, control, manipulation and assembly of nanometre scale components into materials, systems and devices for human interest and needs (Pujado 2012). The rapid progress of nanotechnology and advanced nanomaterial production offers significant opportunities for designing powerful sensing devices with enhanced performances. Such nanomaterials can exhibit properties and functions different from the ones corresponding to bulk or macroscopic version of them. Additionally, such nanostructures can become suitable materials that favour the integration with biomaterials or biological systems. Under this context, carbon based nanomaterials like CNT and graphene have been exploited as a novel material with huge potential in bio-analytical and bio-sensing applications.

As it was mentioned before, the sensitivity of the biosensors depends a lot on the characteristics of transducer (shape, type of the material, size). High surface-to-volume ratio of the transducing element can increase the efficiency of the signal transfer. Thus, nanomaterials are ideal candidates to be used as components of transducers. The first and foremost feature that nanostructures offer is their size (a few

Angstrom to 100 nm), which is in the range of the size of various biomolecules such as nucleic acids, small proteins and viruses. The small size brings a tremendous increase in the surface-to-volume ratio that is essential for maximizing the sensitivity. A major advantage of using nanostructures in a label-free sensing is that the amount of receptors immobilized on the detector surface can be as low as a single molecule (Yun et al. 2009, Kurkina and Balasubramanian 2011, Reimhult and Hook 2015). As a result, the amount of analyte required to generate a measurable signal could be just a few providing for very low limits of detection (LOD). Secondly, nanostructures exhibit specialized physical and chemical properties that are generally not available in the bulk. For example, the binding of analytes to receptors immobilized on carbon nanotubes brings significant changes in the resistance of the CNT that is used as a sensor signal (Maroto et al. 2007). Such a phenomenon does not occur in bulk metals. Furthermore, surface plasmons in thin metal films (2D) and nanoparticles (one dimensional, OD) (Homola 2006) are characteristic properties at the nanoscale that are otherwise not available in bulk microscale materials. These unusual properties arise due to confinement in one to three dimensions.

1.5.1 Carbon Nanotube

CNTs, discovered by Iijima, S. (Iijima 1991), can be described as a graphene sheet rolled up into a nanoscale-tube (Nakada et al. 1996). A single sheet generates single walled carbon nanotubes (SWCNTs) while multiple sheets produce multi-walled carbon nanotubes (MWCNTs).

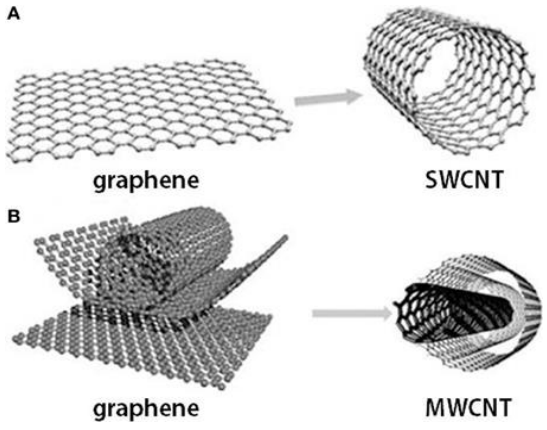

Figure 1.2 Schematic representation of CNT formation

Typically, the length of CNTs can range from several hundred nanometres to several millimetres while diameters are 0.4 - 2 nm and 2 - 100 nm for SWCNTs and MWCNTs, respectively (Gooding 2005). The CNTs behave either like a metal (SWCNTs, MWCNTs) or a semiconductor (SWCNTs). The electrical conductivity of SWCNTs depends on their chirality and diameter, while for MWCNTs such dependence is not observed. The unique properties of CNTs such as greater strength, stiffness, chemical and thermal stability, electrical conductivity, high surface area of 1600 m^2 g^{-1} (SWCNTs) and the presence of a hollow core suitable for storing guest molecules, have revolutionized various fields such as electronics and medicine (Kim et al. 2007). CNTs are also applicable in various energy storage devices (supercapacitors, fuel cells and accumulators), transistors, photovoltaic devices, sensors and biosensors (Wang 2005, Yang et al. 2010).

There are numerous ways for preparation of CNT for modified electrodes, among which notable few are, chemical vapour deposition (CVD) (Coquay 2005), laser evaporation (Guo et al. 1995) and arc discharge method (Park et al. 2002). The CNTs owing to advantages such as, small size with large surface area, high sensitivity to target analyte, fast response time in analyte detection and diminishing surface fouling effects have found wide application in the electrochemical sensing. However, CNTs gain considerable attention in modified electrodes area, because of enhancement of their electrochemical sensing performance through their functionalization by covalent bonding or non-covalent attachment of various objects to the CNTs sidewalls (eg. conducting polymer, metal nanoparticles, graphene). Even the impurities that may remain after synthesis, such as metallic compounds or nanoparticles have a great impact on their electro catalytic activity (Hong et al. 2010)

1.5.2 Graphene based Biosensors

Graphene ideally forms two dimensional structures and comprises a single layer of sp^2-hybridized carbon atoms joined by covalent bonds to form a flat hexagonal lattice. An isolated single layer of graphene is difficult to fabricate (Castro Neto et al. 2009). Although the electrochemical properties of graphene are not clearly understood, most work has confirmed that fast electron transfer between enzymes and electrodes

can be obtained due to the unique electronic structure of graphene (Shang et al. 2008, McCreery 2008). This mainly comes from the delocalized π bonds above and below the basal plane. These delocalized electrons create high electrical conductivity and mobility within the plane of the graphene (Yang et al. 2010). The use of graphene in biosensors can avoid the problem of electrochemical oxidation associated with the transition metals, like Fe, Ni, Co, etc. The fast electron transport, high thermal conductivity, excellent mechanical flexibility and good biocompatibility make the graphene an ideal candidate for bio-sensing application.

1.5.3 Metal Oxides based Glucose Sensors

Metal-oxide based sensors are very sensitive, relatively inexpensive and have the advantage of rapid response associated with specific nanostructures such as nanowire, nanorod, nanotube, nanoparticle, nanofiber. It should be mentioned that during the last two decade, tremendous efforts have been made for the detection of glucose based on nanostructured metal oxides and their composites. In Table 1.1 we tabulated metal oxides applicable to glucose sensors reported so far and have given brief descriptions in terms of the detection methods, availability of enzymatic or non-enzymatic operations, sensitivity, detection limit, response time and applied potential.

Table 1.1 Important non-enzymatic electrodes from reported literature.

Electrode type	Sensitivity ($\mu A\ mM^{-1}cm^{-2}$)	Linear range (mM)	LOD (μM)	Working Potential (V)
MWCNTs (Ye et al. 2004)	0.00436	11.0	1.0	0.10
SWNT electrode (Wang et al. 2007)	248.6	2.1	10.0	0.60
Cu–CNTs–GCE (Kang et al. 2007)	17.7	3.5	0.2	0.60

MnO_2/MWNT (Chen et al. 2008)	0.03	28.0	-	0.30
Pd-SWNTs (Meng et al. 2009)	0.16	17.0	0.2	0.35
CuO–MWCNTs (Yang et al. 2010a)	2190.0	3.0	0.8	0.55
CNT/Ni NAs (Zhu et al. 2011)	1381.0	10	1.0	0.55
RGO-$Ni(OH)_2$/GCE (Gan and Hu 2011)	11.43	3.1	0.6	0.54
$Ni(OH)_2$/graphene (Qiao and Zheng,2012)	494.0	10.0	0.6	0.45
Co_3O_4 microspheres (Guo et al. 2013)	1440.0	12.0	0.08	0.55

The literature studies demonstrate that non-enzymatic electro-oxidation of glucose varies considerably depending on the electrode material used (Park et al. 2006, Mu et al. 2011). Hence, development of novel electrode materials with high electrocatalytic activity and high stability for glucose attains major attention in developing the practical non-enzymatic sensor. Many different transition metals and their oxides (Pt, Co, Ni, Au, WO_3, Co_3O_4, NiO, RuO_2, etc.) have been explored as the electrode substrates toward the oxidation of glucose (Wang et al. 2012, Si et al. 2013). Among these, NiO, CuO and Co_3O_4 materials are preferred choice because of their excellent electrocatalytic properties, low toxicity and low cost construction of non-enzymatic glucose sensors (Fleischmann et al. 1971, Cao et al. 2011, Luo et al. 2013). Hence, extensive research was carried out on non-enzyme biosensors using oxides of Ni, Cu and Co based nano-materials. There are many number of these metal based non-

enzymatic glucose sensors constructed by modifying the substrate with metal nanoparticles, metal-carbon hybrids, metal-CNT composite, metal-graphene composites, etc. (Lu et al. 2009, Xiao et al. 2012, Wang et al. 2012b, Wang et al. 2014). The recent developments in electrochemical sensor technology shows significant increase in electrocatalytic activity for nano-materials as compared to the bulk materials (Gangopadhyay and De 2000, Zhang et al. 2010).

1.6 METAL FORMATES

Metal formate, a simple metal-organic precursor consists of only metal (M), oxygen (O), carbon (C) and hydrogen (H) and this on thermal decomposition gives highly pure metal or metal-oxide along with the few by-products like carbon dioxide (CO_2), carbon monoxide (CO), hydrogen (H_2) and water (H_2O) which are harmless to the environment (Mouche et al.1995, Kenfack and Langbein 2005). Metal formate is used as a precursor as it is easy to produce and economical as compared to the other generally used metal precursors. It also requires relatively lesser temperature to yield pure metal or metal oxide. Metal formates are considered a green precursor as they are easy to synthesis, eco-friendly, cheaper and efficient in producing high yield pure metal or metal oxide nanoparticles.

1.7 METHODS OF PREPARING CARBON NANO MATERIAL/ METAL OXIDE COMPOSITE

Hybrid nanomaterials, such as CNT/graphene-metal oxide/metal nanoparticle composites, will be important building blocks in a variety of future nano systems. The extraordinary properties associated with CNTs and graphene make them potential material in many applications. In order to enhance efficiencies in various applications, CNTs/graphene have been modified according to demands of each field. In particular, the hybrid materials composed of nano metal/metal oxide and CNTs/graphene have been paid more attention. Until now, a series of metal oxides, such as SnO_2, Fe_2O_3, NiO, CuO, PdO and metals such as Ni, Pd, Co, Fe have been successfully explored to decorate carbon nanomaterials via microwave irradiation, hydrothermal, solvothermal, chemical vapor deposition and electrophoretic deposition (Xia et al. 2007, Liu et al. 2008). The resultant carbon nanotube-based composites show promising applications

for solar cells, catalysts, chemo sensors, hydrogen storage, lithium batteries and gas storage/separation. However, the cost effective and scalable synthesis is still quite challenging.

1.8 ELECTROCHEMICAL BIOSENSORS

Several methods have been established to study electrochemical reactions, which are reviewed elsewhere (Frew and Hill 1987, Wang 2008, Faridbod et al. 2012). Thus, only the techniques relevant to this work are described here, namely:

1. Cyclic Voltammetry (CV)
2. Chronoamperometry (CA)

1.8.1 Cyclic Voltammetry (CV)

Cyclic voltammetry is a type of potentiodynamic electrochemical measurement that is widely used for obtaining qualitative information about electrochemical reactions. This technique provides a fast and simple method for initial characterization of a redox-active system and interfacial structure. In addition to providing an estimate of the redox potential, it can also provide information about the rate of electron transfer between the electrode and the analyte and the stability of the analyte in the electrolyzed oxidation states.

The basic cyclic voltammetry scheme gives the electrode potential follows a linearly ramping potential vs. time as shown in Figure 1.3.

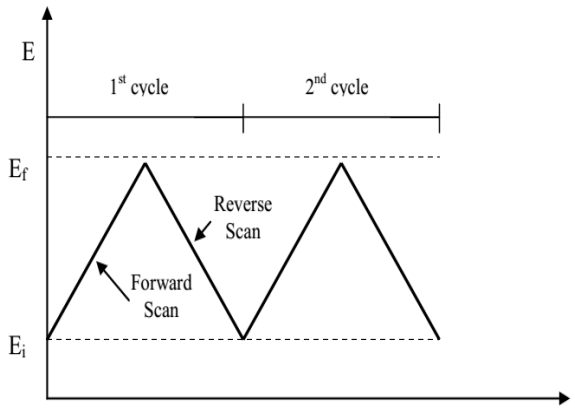

Figure 1.3 Triangular potential waveform for cyclic voltammetry.

As the waveform shows, the forward scan produces a current peak for an analyte that can be reduced through the range of the potential scan. The current will increase as the potential reaches the reduction potential of the analyte, but then falls off as the concentration of the analyte is depleted close to the electrode surface. As the applied potential is reversed, it will reach a potential that will re-oxidize the product formed in the first reduction reaction and produce a current of reverse polarity from the forward scan. This oxidation peak will usually have a similar shape to the reduction peak. As a result, information about the redox potential and electrochemical reaction rates of the compounds is obtained.

In a cyclic voltammetry experiment, the three-electrode method is most widely used because the electrical potential of reference does not change easily during the measurement. The potential is measured between the reference electrode and the working electrode whereas the current is measured between the working electrode and the counter electrode. When the potential is applied to the system, the faradaic current response due to the redox reaction of an electroactive species is measured as well as the double layer charge called capacitive current. This data is then plotted as current (I) vs. potential (E) (Figure 1.4). For instance, if the electronic transfer at the surface is fast and the current is limited by the diffusion of species to the electrode surface, then the current peak will be proportional to the square root of the scan rate. The dependence of the peak current to the scan rate is given by the Randles-Sevcik equation (Kissinger and Heineman 1983, Stromme et al. 1995).

$$i_p = 2.69x10^5 n^{3/2} A D^{1/2} C v^{1/2} \qquad 1.1$$

Where i_p is the peak current, n is the number of electrons involved in redox reaction, D is the diffusion coefficient (cm^2/s), C is the bulk concentration (mol/cm^3), v is the scan rate (V/s) and A is the electrode area (cm^2).

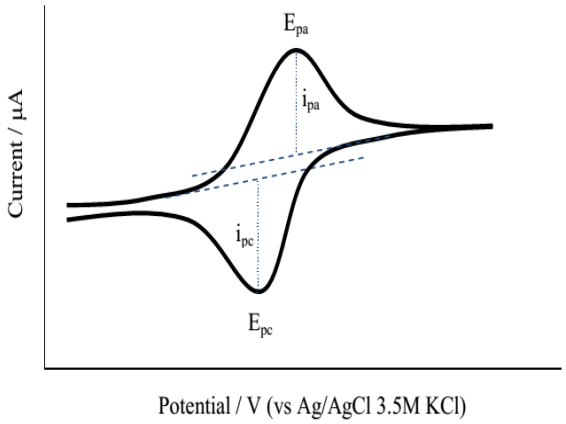

Figure 1.4 Cyclic voltammogram of a reversible redox couple during a single potential cycle.

For a reversible electron-transfer (Nernstian) process, the following information can be obtained from a cyclic voltammogram using microelectrodes:

- The cathodic peak current (i_{pc}) is equal to the anodic peak current (i_pa) which is $i_{pc} = i_{pa}$.
- The peak potentials (E_{pc} and E_{pa}) are independent of the scan rate (v).
- The formal potential (E^o) is centred between E_{pc} and E_{pa}, which is $E^o = (E_{pc} + E_{pa})/2$.
- The peak current (i_p) is proportional to the square root of the scan rate ($v^{1/2}$).
- The separation between the peak potentials (ΔE) is 59/n mV for an n-electron couple. This information can be used to determine the number of electrons transferred and as a benchmark for a Nernstian behaviour.

For an irreversible reaction, the individual peaks are reduced and become widely separated. The peak current in irreversible reaction is given by:

$$i_p = (2.99\text{x}10^5)\, n(\alpha n)^{1/2} A C D^{1/2} v^{1/2} \qquad 1.2$$

Intermediate case for reversible and irreversible reactions can also exist in between of these reactions. It is called the quasi-reversible reaction. For a quarsireversible reaction, the current is controlled by both the charge transfer and mass

transport (Wang 2005). A reverse peak of similar magnitude of the forward peak is observed on the reverse sweep, but the separation of the two peaks is dependent on the scan rate and the peak current is not proportional to the square root of the scan rate (unlike the case of reversible reaction).

Besides the qualitative information about electrochemical reaction at the electrode obtained from the cyclic voltammogram, multiple cyclic voltammetry experiments can also be used for a variety of applications including,

- The number of electrons transferred in an oxidation or reduction processes.
- The determination of reversible and irreversible behaviour of redox couple.
- Formal potentials.
- Rate constants.
- Reaction mechanisms.
- Diffusion coefficients.

1.8.2 Chronoamperometry (CA)

CA technique is used to study the sensor response to a change of substrate concentration which is referred as titration. It involves the current measurements of a sensor under constant potential immersed in an electrolyte solution, while changing the analyte concentration (stepwise). The results are plotted on a current versus time curve. The time between the changes of analyte concentration is determined by the properties of the sensor, namely by the time required for the current to reach equilibrium state.

CA is a technique where the electrode potential is stepped to a region where the analyte is electroactive and the decaying current reflects the growth of the diffusion layer with time. Figure 1.5 shows the waveform for a step experiment which is the basis concept in CA experiment. The potential of the working electrode is stepped from a value E_1 at which the oxidized or reduced species is electro-inactive (no faradaic reaction occurs), to the value of E_2 where the oxidation or reduction process could occur. At this time the surface concentration of the electroactive species is effectively zero.

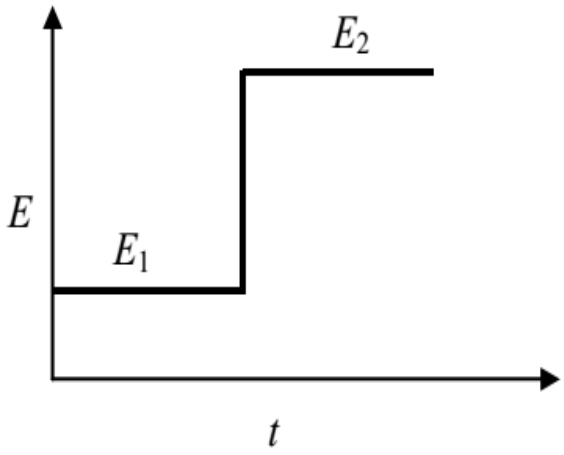

Figure 1.5 The variation of applied potential in a potential step experiment.

At the same time, a large current is detected which falls steadily with time (Figure 1.6). This arises since the mass transport under this condition is controlled by the rate of diffusion of the electroactive species to the electrode surface. The initial process has created an extremely large concentration gradient as well as large flowing current, since there has been little time for any depletion of the electroactive species. Current produced is proportional to the concentration gradient at the electrode surface. But then, as depletion occurs gradually, the diffusion layer thickness increases and the slope of the concentration profile decline with time. Accordingly, the flowing current decays as time progress.

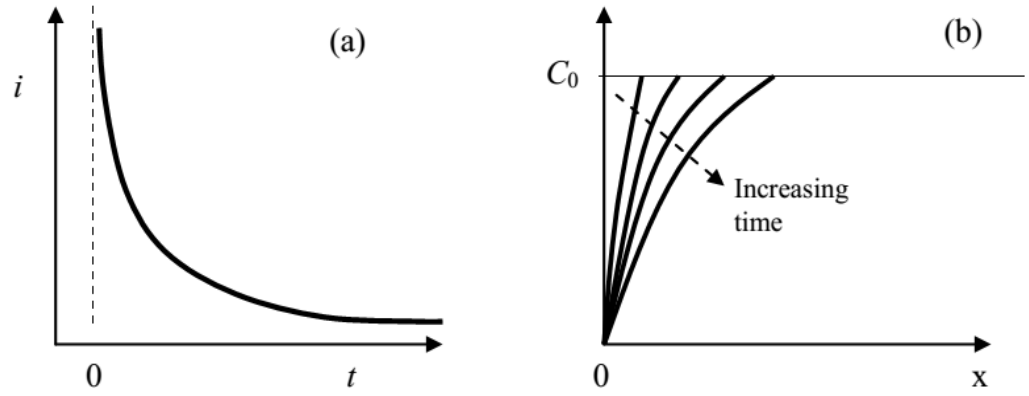

Figure 1.6 The current response vs. time (a) and concentration profile (b) at the electrode in a potential step experiment.

CA is often used to measure the diffusion coefficient of electroactive species or the surface area of the working electrode according to the Cottrell equation:

$$\boldsymbol{i} = nFACD^{\frac{1}{2}}\pi^{\frac{-1}{2}}t^{\frac{-1}{2}} \qquad 1.3$$

Where *n* is the number of electrons involved in redox reaction, *F* is the Faraday constant (96,500 C mol^{-1}), *A* is the electrode area (cm^2), *C* is the bulk concentration (mol/cm^3), *D* is the diffusion coefficient ($cm^2\ s^{-1}$) and *t* is the time (s).

Emerging nanotechnology has inspired and brought new opportunities for the fabrication and development of advanced non-enzymatic glucose sensors. The nanostructure electro catalysts expect to resolve the limitations associated with enzymatic electrode such as, low sensitivity, poor selectivity, lesser stability and surface fouling.

CHAPTER 2

LITRATUTRE REVIEW AND OBJECTIVES

Chapter 2 *describes the evolution of non-enzymatic glucose biosensor and advantages over enzymatic glucose sensor. Different nano composite materials explored for glucose sensing are discussed and results of few are tabulated. The scope and objectives of the present work has been listed.*

The detection of glucose is extremely important in many fields such as medicine, biotechnology and food industry. Accurate, fast and reliable measurement of glucose is greatly needed, especially in clinical diagnostics. Therefore, sustained effort of more than two decades has been devoted for development of electro-catalytic glucose sensors (Guilbault and Lubrano 1969). The most common glucose sensors are enzymatic type which is based on immobilization of glucose oxidase (GOx) onto various substrates, have demonstrated some useful applications (Wilson and Turner 1992). However, the major problem for this type of oxidase-based sensor is poor stability arising from the loss of enzyme activity during the immobilization process and even in the storage period, which impairs sensitivity and reproducibility of these sensors. Another drawback is the high operating potential that leads to limited selectivity of glucose in blood samples in the presence of uric acid (UA), acetaminophen (AC) and ascorbic acid (AA) (Liu et al. 1999). Thus, many elaborate fabrication and immobilization techniques are required to overcome these issues. As a result, there is an ever-growing demand to create non-enzymatic amperometric electrochemical glucose sensors with high sensitivity, high reliability, short response times, good recyclability and low cost (Park et al. 2006).

2.1 NANOMATERIALS USED FOR ELECTROCATALYTIC GLUCOSE SENSING

2.1.1 Carbon

In last two-decade carbon based materials are greatly used as a substrate for the development and fabrication of biosensors due to their electronic conductivity, biocompatibility and electrochemical inertia. Glassy carbon electrode (GCE) and carbon paste electrode (CPE) are the commonly used electrodes in laboratories for electrochemical study and biosensor research. Because of its electrochemical

inactivity, bare GCE and bare CPE could exhibit very negligible current response to the addition of glucose, according to the investigation by Vassilyev et al. in 1985. CPE has been widely employed for research purposes because of its easy preparation, low cost and easily renewable surface. However, screen printed enzymatic electrodes have been industrialized for revolutionising personal glucose monitors since 1990 (Wring et al. 1990a, Newman et al. 1992).

Many new carbon based nano-materials have emerged in the last decade with the rapid development of nanotechnology. Among them, CNTs, carbon nanofibers and graphene have been intensively studied as enzymatic and nonenzymatic electrochemical biosensors (Wang 2005b). Because of their excellent conductivity, ease of functionalization, high surface area and biocompatibility, the nanostructured carbon materials are believed to improve the performance of electrochemical glucose biosensors. In the following sections, we explore the recent advances of non-enzymatic electrochemical glucose biosensors based on CNTs, graphene and a number of other carbon nanomaterials are briefly explained.

2.1.2 Carbon Nanotubes

CNT based sensors show, greater sensitivity and faster response time, than the traditional electrodes. The improved performance can be attributed to the one-dimensional hollow tubular morphology which is responsible for the efficient capture and transfer of electron from analytes. Furthermore, the significant decrease in the over potentials of hydrogen peroxide is observed at CNT-modified electrodes. Hence, CNTs considered as very promising material in the glucose sensing.

2.1.3 Transition Metals and Metal Oxides

Transition metals are well known to be good electrocatalysts due to their ability to adopt multiple oxidation states, absorb other species on their surfaces and catalyse to form intermediates and activate them in the reaction process. The advantages of nanostructure transition metals are their unique physical, chemical, optical and electrical properties such as high surface-to-volume ratio, higher surface area, excellent electrical conductivity, tuneable optical property and greater electro

catalytic activity (Huang and Kim 2011). Hence, transition metal nanomaterials could serve as effective catalysts due to their high ratio of surface atoms with free valances to the cluster of total atoms and the resulting enhanced mass transport property. A wide range of transition metal nanomaterials have been studied in recent years for the electrocatalytic bio-sensing. According to the literatures platinum (Pt) (Yuan et al. 2005), copper (Cu) (Kang et al. 2007), gold (Au) (Bai et al. 2008), palladium (Pd) (Bai et al. 2010), nickel (Ni) (Mu et al. 2011), cobalt (Co) (Lee et al. 2012) and respective oxides are the most intensively studied. However, due to the excellent electro-catalytic activity, stability, bio-compatibility and abundance, the oxides of Ni, Co and Cu were examined in present studies. Because of these excellent electro catalytic effect of metal nanoparticles towards glucose sensor and electronic properties of CNTs, there has been greater efforts to fabricate nano-sensors using CNTs with metals/metal oxides through various fabrication techniques.

Over the past four decades the efforts to develop and improve glucose sensors, particularly based on amperometry have been made since Clark and Lyons first reported the enzyme electrode in 1962 (Clark and Lyons 1962). Updike and Hicks (1967) for first time immobilized enzyme glucose oxidase (GOx) in a gel on an oxygen electrode and analysed glucose concentration in biological fluids. Guilbault and Montalvo (1969) developed the urea sensor by entrapping urease enzyme on an ammonia electrode as another kind of glucose sensors.

Iijima (1991) first announced in nature journal, the preparation of nanometre-size, needle-like tubes of carbon, now familiar as “carbon nanotubes” (CNTs). These CNTs used in optoelectronic, microelectronic circuitry, microscopy and as a tool to test quantum mechanics and model biological systems, nanotubes seem to have unlimited potential.

Park et al. (2003) reported mesoporous platinum based non-enzymatic glucose sensor, in which they demonstrated that roughness of nanoscopic dimensions can be used to selectively enhance the faradaic current of a sluggish reaction. Using this principle, they constructed mesoporous structures on the surfaces of pure platinum electrodes responding even more sensitively to glucose than to common interfering

species, such as l-ascorbic acid and 4-acetamidophenol. Good sensitivities, as high as 9.6 μA cm^{-2} mM^{-1}, were reproducibly observed in the presence of high concentration of chloride ion. The experimentally determined selectivity, sensitivities and stabilities have demonstrated the potential of mesoporous platinum as a novel candidate for non-enzymatic glucose sensors.

Ye et al. (2004) have reported the first non-enzymatic glucose detection using well aligned multi-walled carbon nanotube electrodes. The electrocatalytic effect observed is mainly attributed to carbon nanotubes with possible minor contributions from the Co catalysts used to synthesize the MWCNTs present on the tantalum (Ta) substrate. At an applied potential of +0.20 V, MWCNTs electrodes shows a high and reproducible sensitivity of 4.36 μA cm^{-2} mM^{-1} in the presence of high concentration of chloride ion. The well-aligned MWCNTs electrode thus allows highly sensitive, low-potential, stable and fast amperometric sensing of glucose, promising for the development of non-enzymatic glucose sensors.

Salimi and Roushani (2005) reported a new enzyme-less glucose by using a nickel powder dispersed sol-gel derived ceramic graphite composite.

Xu et al. (2006) reported dimethylglycoxime (DMG) functionalized copper nanoparticles (DMG-CuNPs) prepared by a microwave heating method and investigated for non-enzymatic glucose detection. The sensor showed good selectivity and sensitivity. A wide linearity range and a low detection limit have been assessed for it. A linear response to glucose in the concentration range between 1.0×10^{-6} and 5.0×10^{-3} M and a detection limit of 5.0×10^{-7} M were observed. Most important of all, the common drawback of copper electrode fouling was overcome in this sensor.

Kang et al. (2007) reported glucose sensor, wherein copper (Cu) nanoclusters were electrochemically deposited on the film of a Nafion-solubilized MWCNTs modified glassy carbon electrode (MWCNTs–GCE), which fabricated a Cu–MWCNTs composite sensor (Cu–CNTs–GCE) to detect glucose with non-enzyme. The study shows that the non-enzymatic sensor has synergistic electrocatalytic activity to the oxidation of glucose in alkaline media. A well applicable sensor was

constructed to use for the analysis of the glucose in real blood serum samples due to the large number of electrons taking part in the oxidation process, the high apparent kinetic rate constant and the stable operation of the electrode. The linear range for the detection of the glucose is 7.0×10^{-7} to 3.5×10^{-3} M with a high sensitivity of 17.76 μA mM^{-1}, a low detection limit of 2.1×10^{-7} M and a fast response time within 5s. Experiment results also showed that the sensor has good reproducibility and long-term stability and is interference free.

Lu et al. (2009) synthesized highly ordered Ni nanowire arrays (NiNWAs) for the first time using a template-directed electro polymerization strategy with a nanopore polycarbonate (PC) membrane template. This nano-NiWAs electrode was investigated for non-enzymatic electrochemical glucose sensing in alkaline medium. The sensor results show that, can be applied to the quantification of glucose with a linear range covering from 5.0×10^{-7} to 7.0×10^{-3} M, a high sensitivity of 1043 μA mM^{-1} cm^{-2} and a low detection limit of 1×10^{-7} M. The experiment results also showed that the sensor exhibits good reproducibility and long-term stability, as well as high selectivity with no interference from other oxidisable species.

Yang et al. (2010), potentiostatically electrodeposited metallic Cu nanocubes from a precursor solution onto vertically well-aligned multi-walled carbon nanotube arrays (MWCNTs) and fabricated the non-enzymatic glucose sensor. The electrochemical characteristics of the sensor were studied by electrochemical impedance spectroscopy (EIS) and cyclic voltammetry (CV). The sensor shows significantly higher electrocatalytic activity to the oxidation of glucose in 0.1 M NaOH alkaline solution after modification of Cu nanocubes than before. The sensor response is rapid (<1 s) and highly sensitive (1096 μA mM^{-1} cm^{-2}) with a wide linear range (up to 7.5 mM) and low detection limit (1.0 μM at signal/noise ratio (S/N) = 3). It also exhibits high stability and specificity to glucose and performs very well in detecting glucose concentration in human blood serum.

Kung et al. 2011 have reported cobalt oxide acicular nanorods with high sensitivity for the non-enzymatic detection of glucose. The pertinent sensor could be successfully used for the quantification of glucose by amperometric method. The

sensing parameters include wide linear range up to 3.5 mM, a high sensitivity of 571.8 μA/ (cm^2 mM) and a remarkable low detection limit of 0.058 μM. The coblt-oxide nanorods modified electrode exhibited a high selectivity for glucose in human serum, against ascorbic acid, uric acid and acetaminophen.

Dong et al. 2012a have synthesized 3D graphene–cobalt oxide nano composite using simple hydrothermal techniques and demonstrated it as a sensor to detect glucose with a ultrahigh sensitivity of 3.39 mA mM^{-1} cm^{-2} and a remarkable lower detection limit of <25 nM (S/N = 8.5).

Lang et al. 2013 have reported flexible and self-supported microelectrodes with a seamless solid/nanoporous gold/cobalt oxide hybrid structure for electrochemical non-enzymatic glucose biosensors. As a result of synergistic electrocatalytic activity of the gold and cobalt oxide nanoparticles hybrid microelectrodes towards glucose oxidation, exhibit multi-linear detection ranges with ultrahigh sensitivities at a low potential of 0.26 V (versus Ag/AgCl). The sensitivity up to 12.5 mA mM^{-1} cm^{-2} with a short response time of less than 1 s gives rise to ultralow detection limit of 5 nM. The outstanding performance originates from a novel nano- architecture in which the cobalt oxide nanoparticles are incorporated into pore channels of the seamless solid/nanoporous Au microwires, providing excellent electronic/ionic conductivity and mass transport for the enhanced electro-catalysis.

Niu et al. (2013) have fabricated enzyme-free sensor through in situ growing porous nickel networks on a homemade screen-printed carbon electrode substrate via electrochemically reducing the Ni^{2+} precursor, along with continuously liberating hydrogen bubbles. Cyclic voltammetry, alternating-current impedance and amperometric methods were used to investigate the catalytic properties of the assembled sensor for glucose electro-oxidation in alkaline media. Under optimized conditions, the enzyme-less sensor exhibited excellent performance for glucose analysis selectively, offering a much wider linear range (from 0.5 μM to 4 mM), an extremely low detection limit (0.07 μM, signal-to-noise ratio (S/N) of 3) and an ultrahigh sensitivity of 2.9 mA cm^{-2} mM^{-1}. Importantly, favourable reproducibility

and long-term performance stability were obtained. He also demonstrated blood glucose detection using this sensor.

Bao et al. (2015) have reported synthesis of copper oxide nanowires (CuO NWs) and single-walled carbon nanotubes (SWCNTs) hybrid electro-catalyst and fabricated to detect glucose in alkaline environment. The biosensor realized an excellent sensitivity of 2191.3 μA cm^{-2} mM^{-1} for glucose in low concentration from 1 μM to 34 μM and a fine overall sensitivity of 761.5 μA cm^{-2} mM^{-1} within a wide linear range from 1 μM to 2.67 mM. The lowest limit of detection (LOD) was measured down to 45.6 nM (S/N = 3) with a fast response time of 1–2 s. It was also found that CuO NWs in the hybrid composite greatly improved the selectivity of the sensor, while SWCNTs largely benefited the response toward glucose.

Soomro et al. 2015 have reported the synthesis of cobalt oxide (Co_3O_4) nanostructures and their application in enzyme free electrochemical sensing of glucose. The as-synthesized nanostructures of Co_3O_4 were found to exhibit nanodisc like morphology with the size dimension in range of 300–500 nm. The obtained morphological features were evaluated for their electrochemical potential towards oxidation of glucose which enabled development of sensitivity (27.33 μA mM^{-1} cm^{-2}) and stable enzyme free glucose sensor. In addition, the developed sensor showed excellent linearity (r^2=0.9995), wide detection range (0.5–5.0 mM), lower detection limit (0.8 μM) and extreme selectivity towards glucose in the presence of common interferons like dopamine (DP), ascorbic acid (AA) and uric acid (UA). The successful application of developed sensor for real blood glucose analysis further reflects its capability for routine glucose measurement.

From literature, it is observed that in the last decade, carbon nanotubes (CNTs) have been intensively studied to improve the performance of first and second generation glucose biosensors. Reports to facilitate the direct electron transfer of GOx and to develop third-generation glucose sensors also exists. In addition, both MWCNTs and SWCNTs have demonstrated their capability for non-enzymatic glucose detection, but most often CNTs are used as support for other electrocatalysts. In addition, the MWCNTs based non-enzymatic glucose sensor exhibited

reproducible current response for glucose in the presence of high concentration of chloride ions, indicating excellent anti-poisoning property of the electrode. However, the interferons species such as ascorbic acid (AA) and uric acid (UA) had a significant impact on glucose detection, possibly due to the overlapped oxidation potentials of these species with glucose.

In Table 2.1 we have tabulated few well cited non-enzymatic sensors towards glucose sensing reported so far and brief descriptions about the same in terms of sensor parameters like, sensitivity, selectivity, detection limit, response time and applied potential are listed.

Table 2.1. Comparison of non-enzymatic glucose sensors from the reported literature.

Electrode composition	**Sensitivity ($mA\ mM^{-1}\ cm^{-2}$)**	**Linear Range (mM)**	**LOD (µM)**	**Working Potential (V)**
Ni powder modified electrode (You et al., 2003)	40.0	5.0	-	0.55
Pt–Pb/CNTs (Cui et al. 2007)	18.0	0.5	1.8	0.30
Nickel electrode (Zhao et al., 2007)	-	2.5	40.0	0.50
CuO nanospheres (Reitz et al. 2008)	404.5	2.6	1.0	0.60
MnO_2/MWNTs (Chen et al. 2008)	33.2	28.0	-	0.30
Ni-NPs-CNF paste electrode (Liu et al. 2009)	420.4	2.5	1.0	0.55

CuO nanofibers (Wang et al. 2009b)	431.3	2.5	0.8	0.60
SA-CNT- Cu-NPs thin films (Li et al. 2009)	602.0	1.8	0.1	0.60
Ni nanowire arrays (Lu et al. 2009)	1043.0	7.0	0.1	0.55
Co_3O_4 nanofibers (Ding et al. 2010a)	36.2	2.0	0.97	0.16
Cu_xO flowers (Li et al. 2010)	1620.0	6.0	49.0	0.50
NA/NiONF-rGO/GCE (Zhang et al. 2010)	1100.0	0.6	0.8	0.55
CuO–MWCNTs array electrode (Yang et al. 2010a)	2190.0	3.0	0.8	0.55
CuO NR-graphite electrode (Wang et al. 2010)	371.4	8.0	4.0	0.60
NiO/MWCNTs electrode (Zhang et al. 2010b)	1768.8	7.0	2.0	0.50
CS–GA–GOx–Nafion–PtPd–MWCNT (Chen et al. 2012)	112.0	14.0	31.0	0.60
Ni–MWCNT (Sun et al. 2012)	67.2	17.5	0.8	0.6

Ni–Cu/TiO_2/Ti (Li et al. 2013)	1591.0	3.2	5.0	0.5
NiO/Pt/ERGO/GCE (Li et al. 2014)	668.2	05.6	0.2	0.6

It is evident from the literature that the field of non-enzymatic glucose sensing electrodes is developing rapidly in the past decade. The surge in interest and improved success no doubt coincides with the development of nanomaterials, allowing for higher surface areas, improved glucose oxidation kinetics and better selectivity. However, it is also evident that much of the research surrounding non-enzymatic glucose sensors is becoming repetitive and greatly lacks innovative approaches beyond designing new nanomaterials. This advancement may depend on research into new carbon based materials and the technology involving is certain to rapidly develop in the near future, possibly leading to a useful non-enzymatic glucose sensor.

2.2 DECORATION OF CNTs BY NANO METAL OR METAL OXIDE

Metal/metal oxide nanoparticles coated over CNTs and graphene provide a way to obtain novel materials with useful electro chemical properties for sensor and catalyst application. Metal oxides are well-known materials which are suitable to directly catalyse the glucose with high sensitivity. Hence, synthesising decorated nano-metal/metal oxide carbon nanotubes is of great importance. A few important work reported about different method of composite synthesis are listed in Table 2.2

Table 2.2 Decoration of CNTs by nano metal or metal oxide

Authors	Metal type	Synthesis method	Result
Ang et al. 2000	Ni and Cu	Electroless plating method	Decoration of activated carbon nanotubes with copper and nickel by electroless plating method was achieved in this study.

Stoffelbach et al. 2005	Magnetite nanoparticles	Reduction method	An easy and economically viable route for the decoration of carbon nanotubes by magnetite nanoparticles and their orientation in a magnetic field was achieved.
Sun et al. 2006	Pt, Ru, Pt-Ru, Rh, Ru-Sn	Supercritical methanol was used as solvent and as reducing agent.	CNTs were decorated by metal nanoparticles with uniform sizes and a narrow particle size distribution and mechanism were also discussed.
Ping et al. 2006	Cu	Chemical reduction method	Preparation of Cu/CNT composite particles and catalytic performance on thermal decomposition of ammonium per chlorate was studied in this paper.
Huiqun et al. 2006	Iron oxide	Precipitation method	Decoration of carbon nanotubes by iron oxide was fabricated by precipitation method.
Xia et al. 2007	TiO_2	Hydrothermal method and sol gel method	Multi-walled carbon nanotube -TiO_2 composite catalysts were prepared by sol-gel and hydrothermal methods.
Byrappa et al. 2008	Pt, Ni, Co	Supercritical fluids (SCFs)	The SCF methods provide a green route for the synthesis of nano metal CNT composites. SCFs show unusual advantages for the synthesis of composites.
Kim et al. 2008	ZnO	Atomic layer deposition (ALD) method	CNTs functionalized by ZnO or Al_2O_3 shells realizing coaxial nanotubes were

			prepared by ALD and composite was investigated for the Photo Luminencscence property.
Khanderi et al. 2009	ZnO	*In situ* decomposition method	ZnO nanoparticles of size 2-10 nm were generated in-situ from the single source precursor [2- (methoxyimino) propanoato] zinc(II) onto multiwalled carbon nanotubes. The nanostructured ZnO/MWCNT composite showed a better sensing performance when compared to bare MWCNTs in the detection of low CO levels.
Li et al. 2008	ZnO	Thermal decomposition of Zinc oleate in an organic medium	Carbon nanotubes decorated with ZnO nanoparticles were produced by thermally decomposing a Zn-oleate complex in an octadecene medium. The nanoparticles had the wurtzite hexagonal crystal structure and showed good adhesion to the nanotubes.
Li et al. 2010	Pt	Ethylene glycol, H_2PtCl_{16}, sodium citrate was used to prepare Pt/CNTs by Polyol Method.	Results of synthesis of carbon nanotubes decorated with platinum nanoparticles by organic colloidal process were demonstrated in this work.
Ren et al. 2010	CuO, PbO	Microemulsion process was used to synthesize CNT nano metal oxide composite	Microemulsion method was adopted to synthesize nano-metal oxide deposited on carbon nanotubes. Ternary diagram was used to study influencing factors of W/O microemulsion system.

Zhoa et al. 2011	Fe_2O_3, SnO_2, CeO_2 and Er_2O_3	Hydrothermal method	A general strategy for synthesis of a large variety of metal oxide nano particles on carbon nanomaterials, including SWNTs, MWNTs and a few-layer graphene by hydrothermal route was reported.
Belesi et al. 2011	CoO, Co	Thermal decomposition of $Co(acac)_2$ in oleyl amine	Nanocomposite CoO or Co/CNT materials were synthesized by one pot chemical route. The structural and phase transformation of CoO/MWNTs composite was investigated using XRD, TEM, magnetic and NMR measurements.

From the literature, it is observed that, many different methods were explored for carbon-metal/metal oxides composites. These synthetic methods are of high cost and also bulk scale synthesis and uniform decoration of nano particles remains a greater challenge. Therefore, a facile and cost effective method for large scale synthesis of uniformly decorated composites synthesis is of prime importance.

2.3 SCOPE OF WORK

Due to the most outstanding mechanical, thermal and electrical properties, carbon nanomaterials and its few metal/metal oxide composites are considered to be the most promising materials for future high performance electronic devices such as biosensors. However, because of low production capacity and high production costs at present, their applications cannot be extended until large-scale production is realized. High yield synthesis is essential for applications. So detailed investigation should be done to synthesize carbon nano materials in bulk quantity.

High-surface-area and conducting carbons have been the choice of supports for many metal/metal oxide decorations for electrochemical application. A special

type of carbon that is attracting much interest is CNT, in particular multi-walled carbon nanotubes and graphene. CNTs and graphene attract a growing interest as catalytic support in biosensor applications due to their specific characteristics such as: (i) resistance to acid/basic media, (ii) high surface area, (iii) possibility to control the porosity and surface chemistry (iv) biocompatibility, (v) fast electron transfer and (vi) easy to functionalise by the choice of materials, etc.

Numerous efforts have been made to devise an ultrasensitive biosensor for monitoring blood glucose without interference from other electroactive species. With the advent of nanotechnology, the regulation of sensing devices at molecular level is possible to some extent. Since metal-oxide nanomaterials have basically large surface-to-volume ratio provide a better surface area for GOx immobilization and direct glucose oxidation. Scientists have paid much attention to these electrode materials in anticipation of more stable, more sensitive but less interference. Additionally, the metal-oxide based nonenzymatic glucose sensor enables cost-effective direct determination of blood glucose level without any electron transfer mediator and there is no loss of sensitivity due to denaturation of protein enzymes in the immobilization or detection procedures.

Several new carbon based modified electrodes have emerged over the past decade for use in electrocatalysis, including glucose oxidation. Carbon electrodes have been explored as potential electrodes for direct glucose oxidation for a long time however, with the fabrication of carbon based, screen printed enzymatic electrodes revolutionising finger-stick electrodes in the early 1990s, allowing for mass production and lower cost sensor fabrication (Wring et al. 1990b). Generally, carbon substrates are used due to their electronically conductive, yet electrocatalytically inert properties. Thus, the scientists wanted to explore the composite of metal/metal oxide and carbon composite materials for direct glucose oxidation. Interestingly, excellent performance was recorded for the direct glucose oxidation. The great performance of carbon and its metal nanocomposite electrodes towards the oxidation of glucose is mainly attributed to the increase of the electroactive working electrode surface by the use of carbon nanomaterials and the electrocatalytic activity by the homogeneous dispersion of the metal nanoparticles. Nevertheless, glucose sensing based on novel

metal-oxide nanomaterials still has many advantages for the glucose detection in terms of miniaturization and development of semi-invasive or finally non-invasive sensing devices especially for the in vivo detection even though it requires more academic and technical studies for commercialization. The proposed research activity is on the bulk scale synthesis of highly purified MWCNTs and its nanocomposites by metal/metal oxide.

2.4 OBJECTIVES

The main objectives of the present research work are as follows.

- To synthesize the CNTs by CCVD method and purification.
- To synthesize eco-friendly metal precursors (nickel formate, cobalt formate, copper formate).
- To synthesize metal/metal oxide nanoparticle (nickel, cobalt, copper) decorated carbon nanostructures by simple solvent-free, low temperature, thermal decomposition method using eco-friendly metal formate precursors.
- To characterise the composite materials by using FESEM, TEM, XRD, EDX and Raman analysis.
- To fabricate the metal oxide-CNTs composite electrodes for non-enzymatic glucose sensing.
- To optimise the electrochemical parameters and investigate for glucose detection and finally extend the application to detect glucose in real human blood samples.

CHAPTER 3

CHEMICALS, INSTRUMENTS AND

EXPERIMENTAL PROCEDURE

Chapter 3 *describes the common experimental procedures, chemicals, electrode fabrication and instruments used in this work.*

3.1 MATERIALS AND METHODS

3.1.1 Chemicals

Ferrocene, ferrocene carboxaldehyde, copper (II) acetate monohydrate, nickel acetate, cobalt (II) acetate tetrahydrate, nickel sulphate, formic acid, cobalt sulphate, graphite flakes (average particle size 20 μm), D- (+)-glucose, tryptophan (Trp), dopamine (DA), L-ascorbic acid (AA), uric acid (UA), fructose, sucrose and maltose were purchased from Sigma–Aldrich India. Hydrogen peroxide (H_2O_2, 30% w/v), alcohol, sodium formate, N,N-dimethylformamide (DMF), was purchased from Fisher Scientific. All the chemicals used were of analytical grade and used as received. Argon (99.95% purity) and acetylene gas (99.99% purity) were procured from Buruka agencies, Bangalore. The MWCNTs obtained using ferrocene as catalyst precursor was synthesized by decomposition of acetylene in chemical vapour deposition (CVD). Metal formate precursors were synthesized by using the reported procedure. All the electrochemical studies and synthesis were done using ultrapure water from millipore system.

3.1.2 Real-time Samples

The human blood serum (HBS) samples were voluntarily given by the patients for conducting the experiments and study protocol was approved by the Institutional review board at National Institute of Technology Karnataka. Patients had given written informed consent before their participation. The glucose concentration was confirmed by WHO approved commercial glucose meter (Freestyle Freedom Lite Glucose monitoring system, Abbott Diabetic Care) and compared with the results of fabricated carbon composite electrodes in our work.

3.2 CARBON NANOTUBE SYNTHESIS

3.2.1 CVD set up

Figure 3.1 shows a schematic representation of double stage CVD set-up which was designed and developed for the catalytic synthesis of CNTs using ferrocene as catalyst precursor. The apparatus consists of a double-stage furnace system fitted with a quartz tube of inner diameter 25 mm and 1500 mm long. The pre-heated furnace and high temperature furnace were connected as shown in the Figure 3.1. Argon and acetylene gas cylinders were connected to the gas flow lines through respective gas regulators. The gas flow rates were measured using mass-flow controller. The catalysts were placed in a quartz boat of 60 mm in length. Water bubbler was used to monitor the exhaust gas at the outlet and to prevent the reverse flow of air into the furnace.

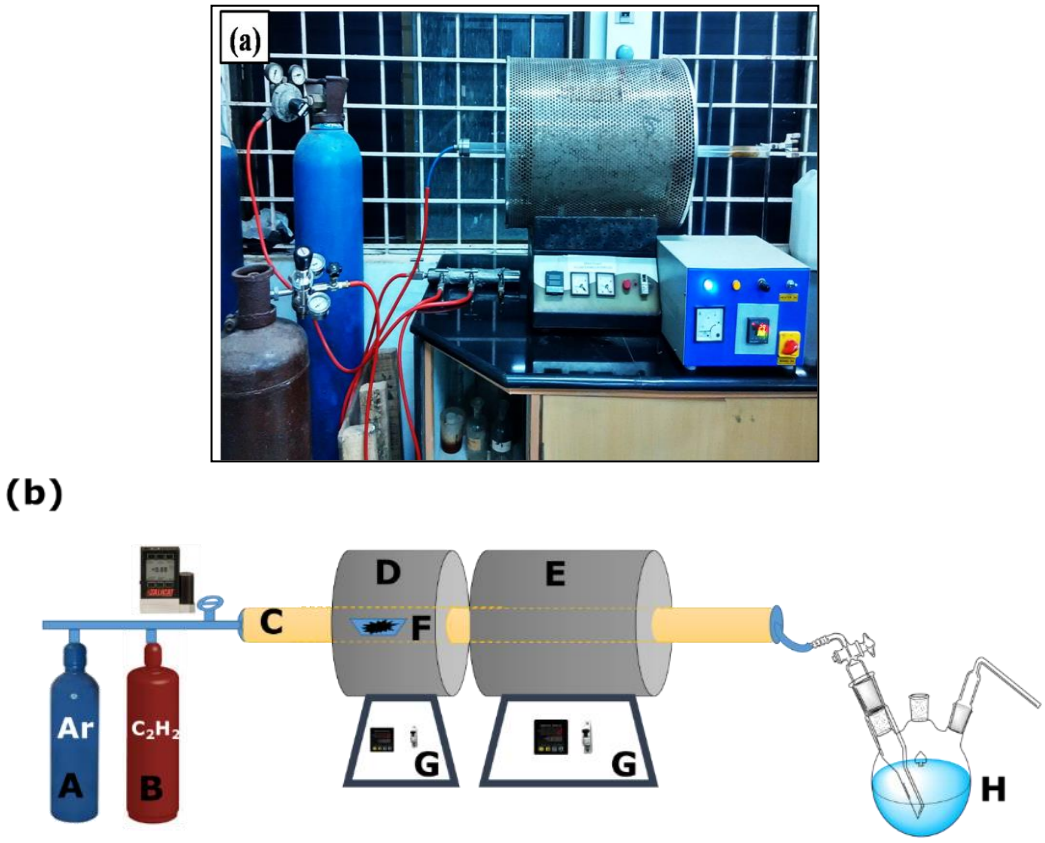

Figure 3.1 (a) CVD set up used in lab and (b) Schematic representation of CVD set-up. (A-Argon gas cylinder, B-Acetylene gas cylinder, C-Quartz tube, D-Pre heater, E-Reaction zone, F-Quartz boat, G- Controller and H-Water bubbler).

The carbon nanotubes were synthesized, purified and functionalized using the reported procedure from our research group (Rajarao and Bhat 2013). Briefly, CNTs were grown using the double stage CVD technique. Argon gas was used as carrier gas and acetylene gas was used as carbon precursor. Ferrocene was used as catalyst precursor. 100 mg of ferrocene was taken in the quartz boat and placed inside the quartz reactor. The furnace was pre-heated to 230 °C, after the temperature in the second furnace reached to desired temperature (1000 °C). Acetylene gas flow was allowed for 10 min. Finally, the furnace was cooled to room temperature in the argon flow. Carbonaceous material was deposited as a black film onto the walls of quartz tube, which was collected.

3.2.2 Purification of Carbon Nanotubes

The as obtained products contain catalyst particles which were removed by an acid treatment with 5 N HCl at 80 °C for 30 minutes. To eliminate the acid, the samples were washed with distilled water. The samples were dried in an oven at 100 °C. This was followed by air oxidation to remove the amorphous carbon.

3.3 PREPARATION OF METAL FORMATE CATALYST PRECURSORS

Nickel formate was synthesized by mixing the solutions of nickel acetate (1Eq) and formic acid (2 Eq) at 100 °C in stoichiometric amount. The green coloured solution was cooled in an ice bath and small amount of ethanol was added with stirring. The light green microcrystalline precipitate was filtered, washed with ethanol and dried in air.

Copper formate was synthesized by refluxing the solution of copper sulphate (1 Eq) and sodium formate (3 Eq) in stoichiometric amount. The light green crystals precipitate out after cooling. The crystals were washed with ethanol and dried in air.

Cobalt formate was synthesized by refluxing the solutions mixture of cobalt sulphate (1 Eq) and sodium formate (3 Eq) in stoichiometric amount. On cooling, red coloured cobalt formate crystallized which was filtered, washed with ethanol and allow to dry.

3.4 SYNTHESIS OF METAL OXIDE DECORATED MWCNT COMPOSITES

The MWCNTs (0.25 g) were dry mixed with metal formate (different wt.%) using mortar and pestle until the homogeneous mixture was obtained. The mixture was then sonicated and transferred to quartz boat followed by thermal treatment in an air atmosphere at 380 °C for 2 h using CVD setup. The final product, metal oxide decorated CNTs were collected as a black powder and were used without further purification. For the comparison studies the pure metal oxides were also synthesized similarly without using CNT. Figure 3.2 represents the set up used for decorating of CNTs by metal oxide nanoparticles.

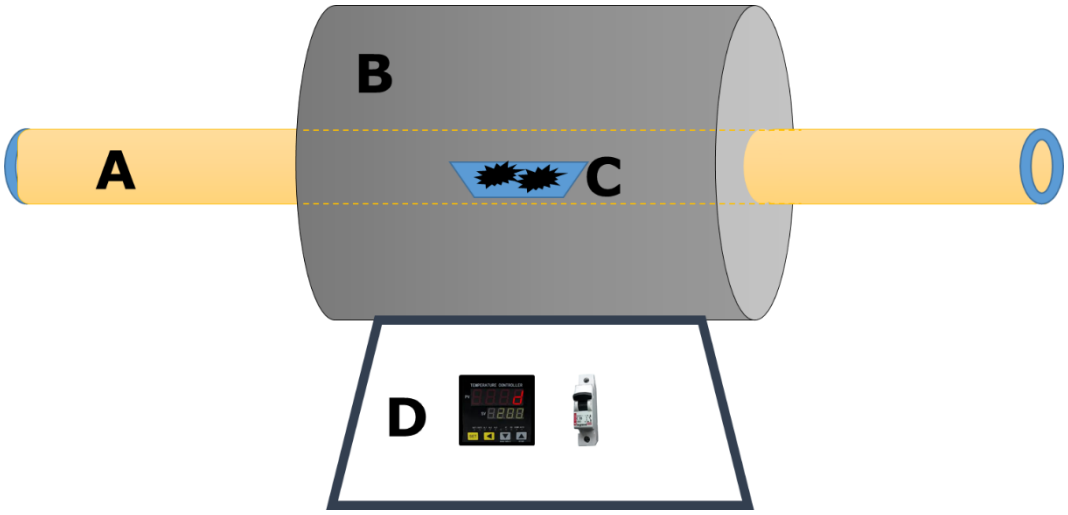

Figure 3.2 Set up for synthesizing decorated CNTs by nano metal oxide particles. A- quartz tube, B-furnace, C-quartz boat and D- controller

3.5 CHARACTERIZATION TECHNIQUES

Performance characteristics of fabricated biosensors are controlled by achieving an understanding and control over the properties and behaviour of the materials used. To accomplish the same, physical and chemical characterization of materials were used in addition to response characteristics of biosensor after each modification step becomes pertinent. Current biosensor technology exploits carbon nanostructure composites and their varied electronic, mechanical, catalytic and other properties for enhancing performance and efficiency. Morphological and elemental characterization of these nanostructures is of paramount importance since their

properties vary drastically with their size and shape. The brief overview of different techniques employed to characterise the materials are as follows.

(a) X-ray Diffraction (XRD)

The phase content and structure of materials was determined by X-ray diffractometry (XRD). In this work, phase content of the material synthesized were obtained using JEOL JDX 8P diffractometer. The diffraction patterns were recorded at room temperature with a CuK_{α} radiation (λ = 1.5418 Å) at a scan rate of 0.5 degree/min. This technique was used to determine the crystallinity and purity of samples.

(b) Thermo-Gravimetric Analysis (TGA)

Thermogravimetric analysis (TGA) is an analytical technique used to determine the material's thermal stability and its fraction of volatile components by monitoring the weight change that occurs as a specimen is heated. The measurement is normally carried out in air or in an inert atmosphere and the weight is recorded as a function of increasing temperature. In this work, TGA measurements were performed on SDT Q600 (TA, USA) using dry air as the carrier gas (flow rate: 50 mL/min). The heating rate was 10 °C/min. Samples of approximately 20 mg were heated in an air atmosphere from 30 °C to 700 °C. TGA was used to determine the purity and structure stability of metal formates.

(c) Field Emission Scanning Electron Microscopy (FESEM)

The scanning electron microscope (SEM) is a type of electron microscope that images the morphology of sample surface by scanning it with a high-energy beam of electrons in a scan pattern. The electrons interact with the atoms that make up the image producing signals that contain information about the sample's surface topography, composition and other properties.

The morphology of the synthesized samples was analyzed using SIGMA field emission scanning electron microscope (FESEM, CARL ZEISS). The samples were coated with gold using a sputter coating unit, to avoid charging during the recording.

(d) Transmission Electron Microscopy (TEM)

Transmission electron microscopy (TEM) studies were carried out using PHILIPS CM 200 transmission electron microscope. The sample was initially sonicated in acetone for 1 hour. It was then allowed to settle and a drop of the supernatant liquid was transferred on to a carbon coated copper grid and mounted onto the microscope and the micrographs were recorded.

(e) Laser Raman Spectroscopy (LRS)

A Raman scattering spectrophotometer was used to understand the relative intensity of G-band (Graphitized band) and D-band (Defective band) of CNTs (Renishaw, RM 1000, He-Ne laser excitation line at 514.0 nm) at ambient condition.

3.6 ELECTROCHEMICAL CHARACTERIZATION

Sensor behaviour of the fabricated electrodes was studied using a Potentiostat at PGSTAT30 (Autolab, Eco Chemie) electrochemical workstation driven by NOVA 1.10 software. Electrochemical studies were performed using a standard three-electrode cell containing alkaline NaOH solution. The working electrode was modified carbon paste electrode and modified glassy carbon paste electrode with the diameter of 4 mm and 3 mm, respectively. The counter electrode was a platinum wire and standard calomel electrode (SCE) was the reference electrode. All the measurements were carried out at room temperature.

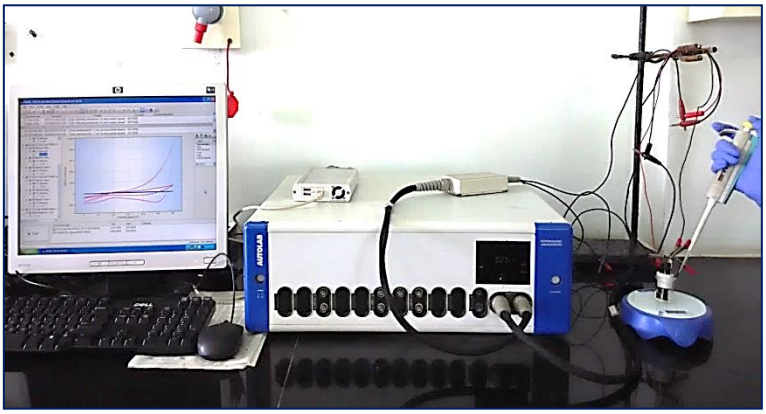

Figure 3.3 Electrochemical workstation (AUTOLAB)

3.7 ELECTRODE FABRICATION

3.7.1 Fabrication of Modified Carbon Paste Electrode

The carbon paste electrode (CPE) was constructed by mixing synthesized composite material (0.05 g), graphite powder (0.7 g) and of silicone oil (0.3 g) in a mortar and pestle to produce a homogeneous paste. This paste was then packed into the cavity of Teflon tube and electrical contact was established using a copper wire and surface was smoothened on a weighing paper (Figure 3.4 a).

3.7.2 Fabrication of Modified Glassy Carbon Electrode

Prior to the fabrication of modified electrode, it is important to clean the surface of glassy carbon electrode. First, the GCE was polished with 0.3 μm and 0.05 μm alumina slurries, respectively to obtain a mirror-like surface and was then ultrasonically cleaned in ethanol and water successively. After these pre-treatments, the electrode was allowed to dry at room temperature.

For the preparation of modified GCE, 5 mg of composite sample and 0.5 mL of 0.5 wt.% Nafion solution was mixed ultrasonically. Then resulting suspensions (5.0 μL) was drop casted onto the GCE surface and allowed to dry prior to use. After experiments, the modified electrodes were preserved at atmospheric conditions until further use.

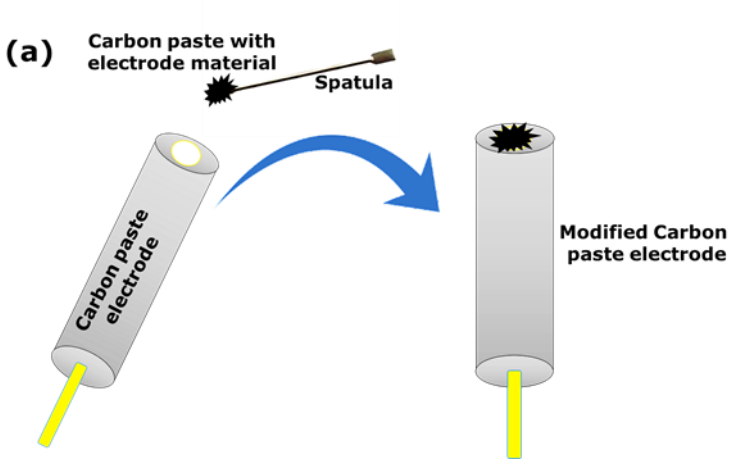

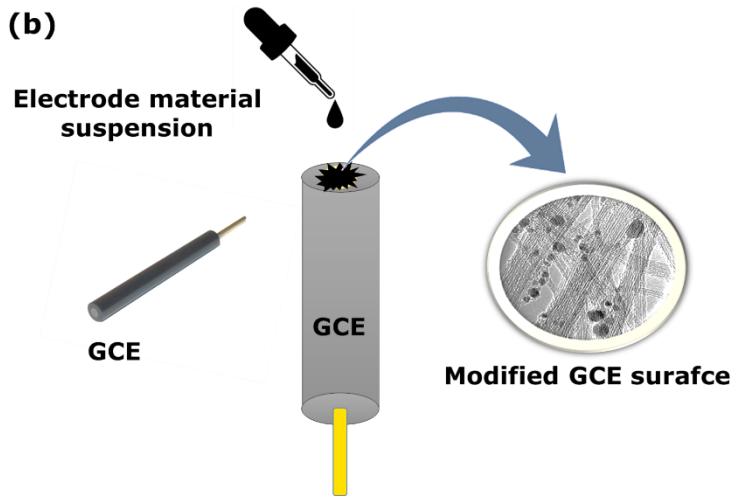

Figure 3.4 Schematic representation of electrode fabrication (a) carbon paste electrode and (b) glassy carbon electrode.

CHAPTER 4

RESULTS AND DISCUSSION

Chapter 4 *describes the characterization for morphology and elemental composition of the synthesized composite materials. This chapter also describes about electro-catalytic activity, oxidation mechanism and sensor parameters like sensitivity, selectivity, stability, reproducibility, response time towards glucose sensing of the synthesized materials.*

4.1 INTRODUCTION

Characterization, when used in material science, refers to the broad and general process by which a material's structure and properties are probed and measured. It is a fundamental process in the field of materials science, without which no scientific understanding of engineering materials could be ascertained. Several analytical techniques are used for the characterization of the chemical composition, morphology, shape and structural homogeneity of materials. In this chapter, we describe the characterisation of the synthesized materials by using different analytical techniques. The surface morphology was obtained by field emission scanning electron microscopy (FESEM) and transmission electron microscopy (TEM). Similarly, the phase identification, elemental composition and defects on the carbon nanotubes which were obtained by powdered X-ray diffraction (PXRD) and Raman analysis, have been described.

Enzymatic glucose sensor based on glucose oxidase (GOx) with good selectivity and high sensitivity, have played a key role in simple easy-to-use blood sugar testing (Chen et al. 2013). Yet enzymatic sensors possess inevitable drawbacks for enzymes by intrinsic lack of chemical and thermal stability. As an alternative strategy, non-enzymatic glucose sensors can overcome the disadvantages of enzymatic glucose sensors to some extent through direct electro-catalytic oxidation of glucose. Thus, non-enzymatic glucose sensors have achieved great attention in recent years (Tian et al. 2014). In the fabricating of enzyme-free glucose sensing devices, it is crucial to explore materials with high electro-catalytic activity. The nanomaterials show exceptional electro-catalytic performance due to their high surface area, surface atomic structures and shapes, which can be further enhanced by controlling their shape and size during

synthesis. In this chapter, synthesis and characterisation of MWCNTs composite with NiO, CuO and Co_3O_4 materials are described and are named as NiO-MWCNT, CuO-MWCNT and Co_3O_4-MWCNTs respectively. These synthesized materials were employed for the construction of the modified fabricated electrode for enzyme-free glucose sensing application. The sensor performance factors like sensitivity, selectivity, stability and linear range, limit of detection (LOD), interference effect and reproducibility of the sensor was systematically investigated and compared with other non-enzymatic glucose sensors reported. Finally, the sensor was also tested for its practical usage by detecting glucose in human blood serum (HBS).

4.2 CHARACTERIZATION OF CARBON NANOTUBES

4.2.1 Morphological Characterization

The synthesized CNTs were characterized for its morphology, crystallinity and purity by using FESEM, TEM, PXRD and Raman studies, respectively. Figure 4.1 represents the FESEM micrographs of the purified CNTs at different magnification (Figure 4.1 A and B). Images show that, most of the CNTs are straight, tubular in nature however, some are helical and twisted CNTs are also present in the bulk. From the particle size distribution histogram obtained from particle size analyser, it is observed that the CNTs grown have an average diameter of 5 nm and few microns in length (Figure 4.1C).

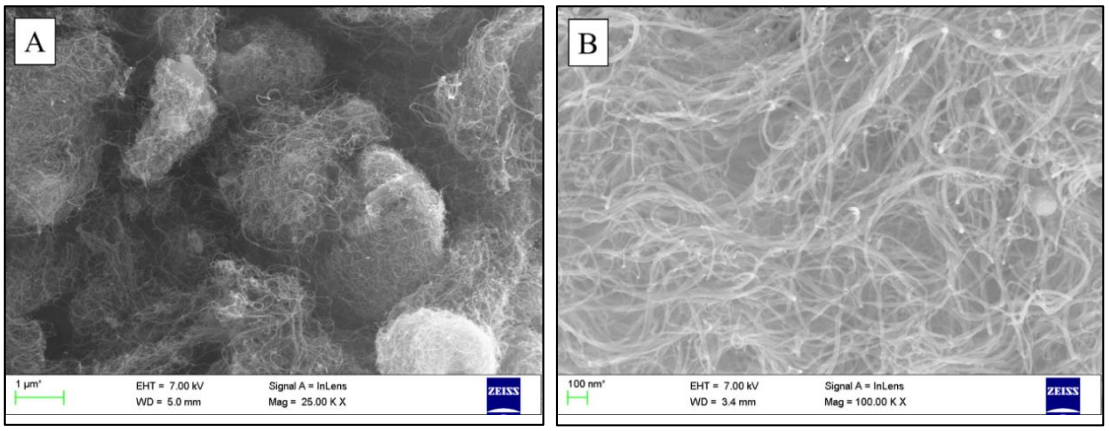

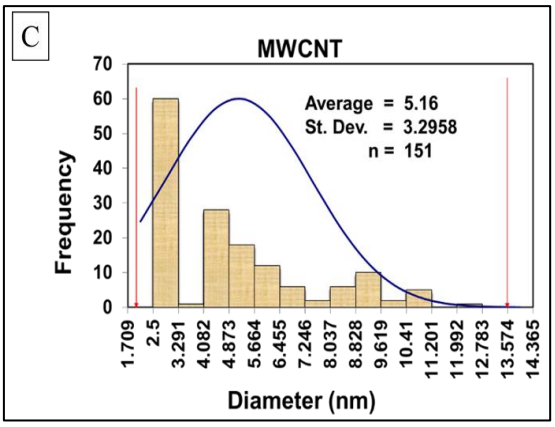

Figure 4.1 FESEM images of purified CNTs at different resolution (A) 1 µm, (B) 100 nm and (C) Size distribution Histograms for CNTs.

Figure 4.2 shows the TEM images of purified CNTs at different resolution. The micrographs clearly show that the carbon nanostructures formed are multi walled carbon nanotubes (MWCNTs). TEM images of purified MWCNTs are very clean and almost all impurities have been removed without destroying the basic structure suggesting the purity of the MWCNTs synthesized.

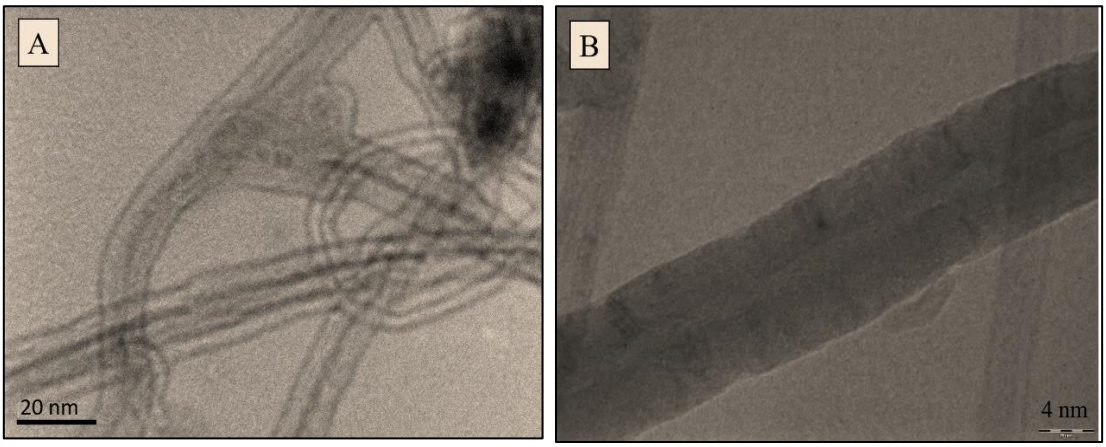

Figure 4.2 TEM images of purified MWCNTs at different magnification (A) 50 nm and (B) 4 nm.

Raman spectroscopy is a useful technique to analyse the degree of graphitization of synthesized MWCNTs. It provides information about the crystal structure and the presence of the disorder and defects (Eklund et al. 1995, Reich and Thomsen 2004). The Raman spectra of the purified MWCNTs are shown in Figure 4.3. The D-band,

observed around 1340 cm^{-1}, is due to the disorder induced in the walls of multiwall carbon nanotube or the presence of amorphous carbon deposited on the outer surface of the nanotubes (Li et al. 1997). The G-band, around 1590 cm^{-1}, indicates the presence of crystalline graphitic carbon in the MWCNTs. The I_D/I_G ratio was effectively used to evaluate the degree of disorder in the sample prepared. Figure 4.3 shows the Raman spectra of two different batches of purified MWCNTs synthesized. The two different batches of MWCNTs prepared, on Raman analysis shows the value of I_D/I_G ratio as 0.83 and 0.84 respectively, which attribute to the defects introduced during the synthesis and purification process of MWCNTs is consistent in multiple attempts.

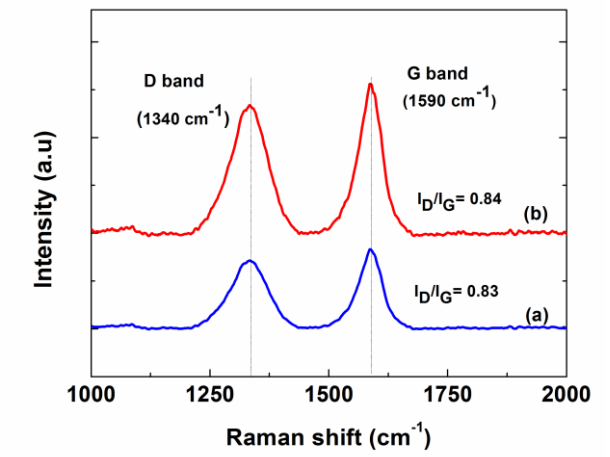

Figure 4.3 Raman spectra of purified MWCNTs.

The purified MWCNTs were characterised using PXRD technique and respective PXRD patterns, are shown in the figure 4.4. The high and low intense peaks at 26.3° and 44.5° can be indexed to (002) and (101) diffraction planes of hexagonal graphite (JCPDS card files, no. 41-1487), respectively. The patterns clearly show that the MWCNTs synthesized are well graphitized and absence of any other extra peak in PXRD spectrum suggest the purity of the MWCNTs.

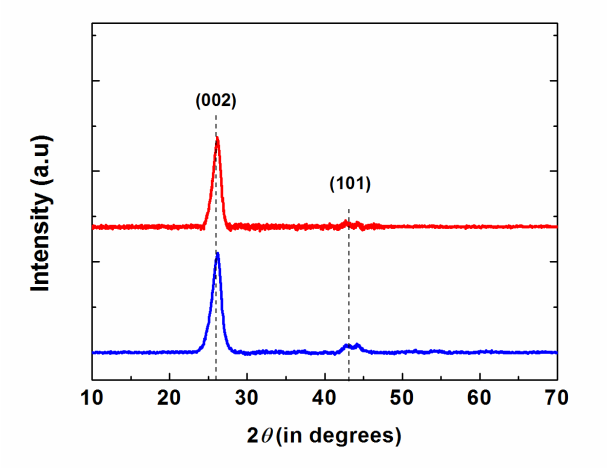

Figure 4.4 PXRD spectra of purified MWCNTs.

4.2.2 The Growth Mechanism of MWCNTs

The catalytic growth of CNTs has been explained based on vapour-liquid-solid (VLS) model. The VLS model consists of the following steps: (i) a carbon source is decomposed on the surface of transition metal nanoparticles, (ii) liquidised metal carbide is formed by diffusion of carbon atoms into the nanoparticles and (iii) after over saturation, the carbon precipitates to form MWCNTs.

Vaporised ferrocene molecules undergo decomposition in the gas phase or on the inner surface of the quartz tube in the reaction zone, iron nanoparticles deposit on the tube wall which acts as an active catalyst. Decomposition of acetylene supplies carbon, which adsorbs on the iron nanoparticles and dissolve to form a miscible alloy. As the carbon saturates on the iron nanoparticle, they start to precipitate to form the MWCNTs. Figure 4.5 shows the supporting TEM image for the carbon nanotube growth model. Initially, they form the graphitic sheets on the catalytic particle (Figure 4.6A and 4.6B). As the graphite sheets lifts off the catalytic particle, a closed tip with the inside hollow is produced (Figure 4.6C and 4.6D). The diameter of the growing tube was limited by size of the catalytic particle. Probably mainly via bulk diffusion, the carbon accumulated on the surface of catalytic particle dissolves inside the tube. As the temperature increases, carbon can arrive at the reaction site of the growing tube with a higher diffusion rate. Consequently, the growth rate of nanotubes increases and the

graphitic sheets build up with a less defect. Therefore, at the higher temperature, the nanotubes can align better during growth (Harris 2007, Wei et al. 2008).

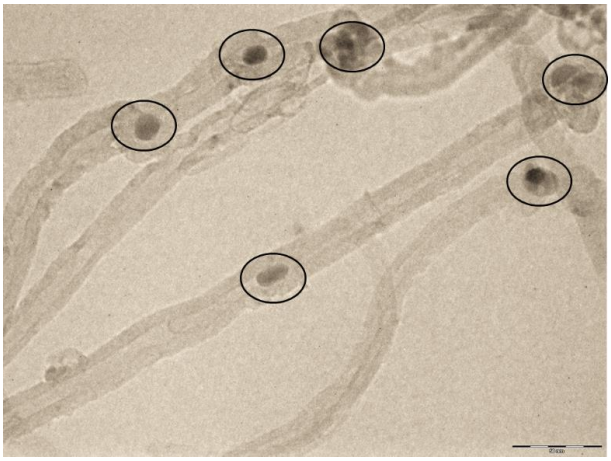

Catalyst particle
at the tip of the grown
carbon nanotube
(circled in the figure)

Figure 4.5 TEM image for the growth model for the carbon nanotube growth.

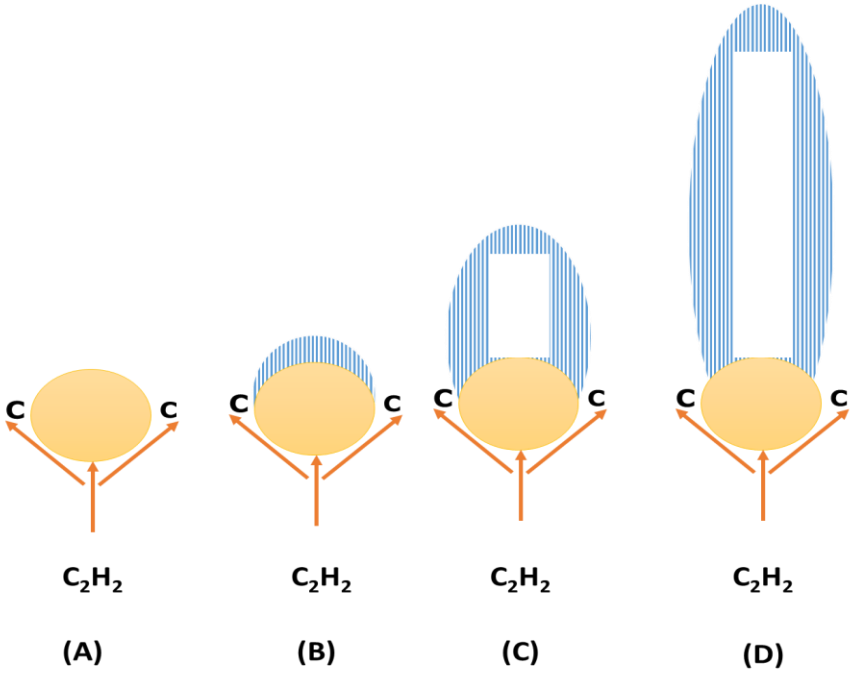

Figure 4.6 Growth model of MWCNTs

The synthesized products contain catalyst particles which were removed by an acid treatment with HCl 5N at 80 °C for 30 minutes. To eliminate the acid, finally the samples were washed with distilled water. The samples were dried in an oven at 100 °C. This was followed by air oxidation to remove the amorphous carbon.

4.3 METAL FORMATES

4.3.1 Characterization of Metal Formate Precursors

A straightforward method for the synthesis of high-quality metal oxide nanoparticles decoration over the surface of MWCNTs in high yields is reported in this work. The metal formate serves as an ideal precursor for the formation of the nano-particles and composite synthesis. Unlike other inorganic salts or oxides, the desired metal nanoparticles are formed directly from the formate, without the usual calcination and reduction steps. In addition, by optimising the experimental conditions, the nanoparticles remain chemically very active, having a small particle size and a narrow size distribution. These metal formates serve as a good metal precursor in composite synthesis with carbon nanomaterials like MWCNTs and reduced graphene oxide. In the present work, three different eco-friendly metal precursors like nickel formate, copper formate and cobalt formate, respectively were synthesized. The synthesized metal formates are confirmed by PXRD analysis. The Figure 4.7A–C represents the PXRD of nickel formate, copper formate and cobalt formate, respectively. The characteristic peaks of these metal formates are represented in each spectrum and respective JCPDS files and nature of the material are listed in the table 4.1.

Table 4.1 The colour and JCPDS reference number for the metal formates synthesized.

Metal formates	Colour	JCPDS card No.	References
Nickel formate	Green	14-0813	Kharat et al. 2002
Copper formate	Light blue	32-0331	Khimchenko et al. 1977
Cobalt formate	Light pink	CCDC 1031566	Khimchenko et al. 1977

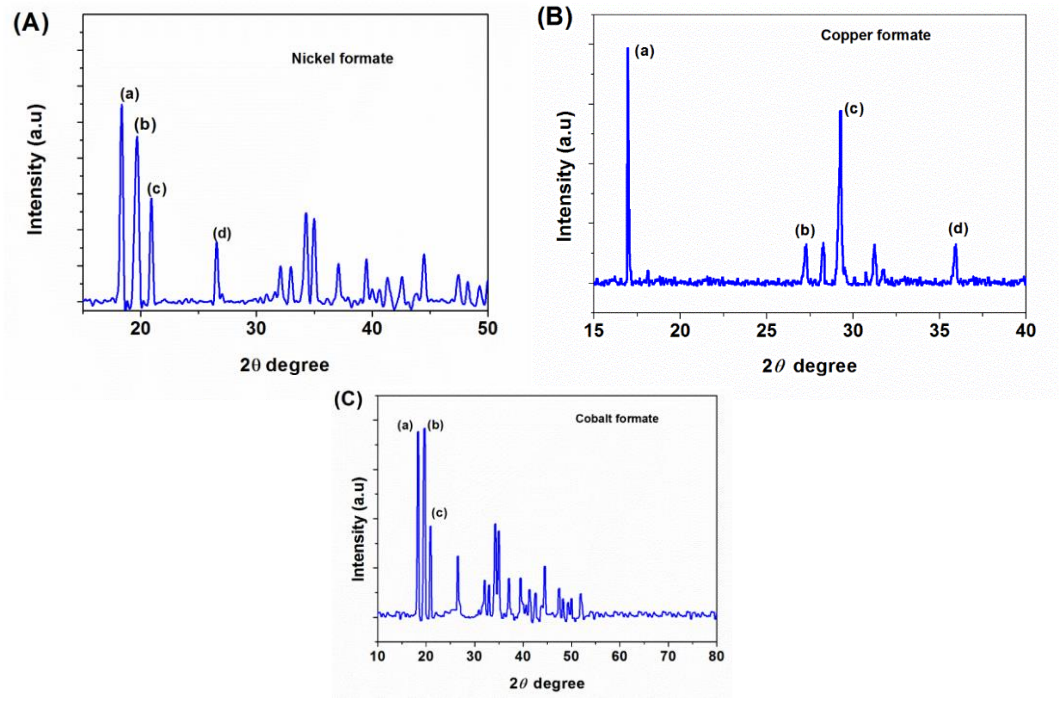

From the above results, it is observed that the characteristic peak of each precursor matches well with the JCPDS and references given respectively. Hence, from these results, the synthesized materials were confirmed as respective metal formates.

Figure 4.7 PXRD spectrum of metal formates (A) Nickel formate, (B) Copper formate and (C) Cobalt formate.

4.3.2 Thermal Decomposition Properties of Metal Formate Precursors

In the solid state, metal formates typically exists in the form of a dihydrate. Measurements by thermal gravimetric analysis (TGA) reveal that these compounds easily decompose at low temperature. Unlike many other metal salts that normally require hydrogen as a reducing agent, metal formates directly decomposes to metallic nanoparticles and gas species by a self-redox reaction. In addition, as these metal formates decompose, number of metal nuclei are formed simultaneously. This type of decomposition mechanism favours the formation of small metal nanoparticles (Khimchenko et al. 1977).

Figure 4.8 (A, B and C) represents the TGA for nickel formate, cobalt formate and copper formate respectively. These metal formates on thermal treatment, dehydration followed by decomposition to metal nanoparticles and the corresponding temperatures are tabulated in Table 4.2. From the results obtained, it is observed that, the nickel formate, cobalt formate and copper formates undergoes dehydration at 140 °C, 130 °C and 110 °C respectively. These intermediates which on further heating to 250 °C, 290 °C and 170 °C, form nickel, cobalt and copper metal/metal oxide nanoparticles respectively.

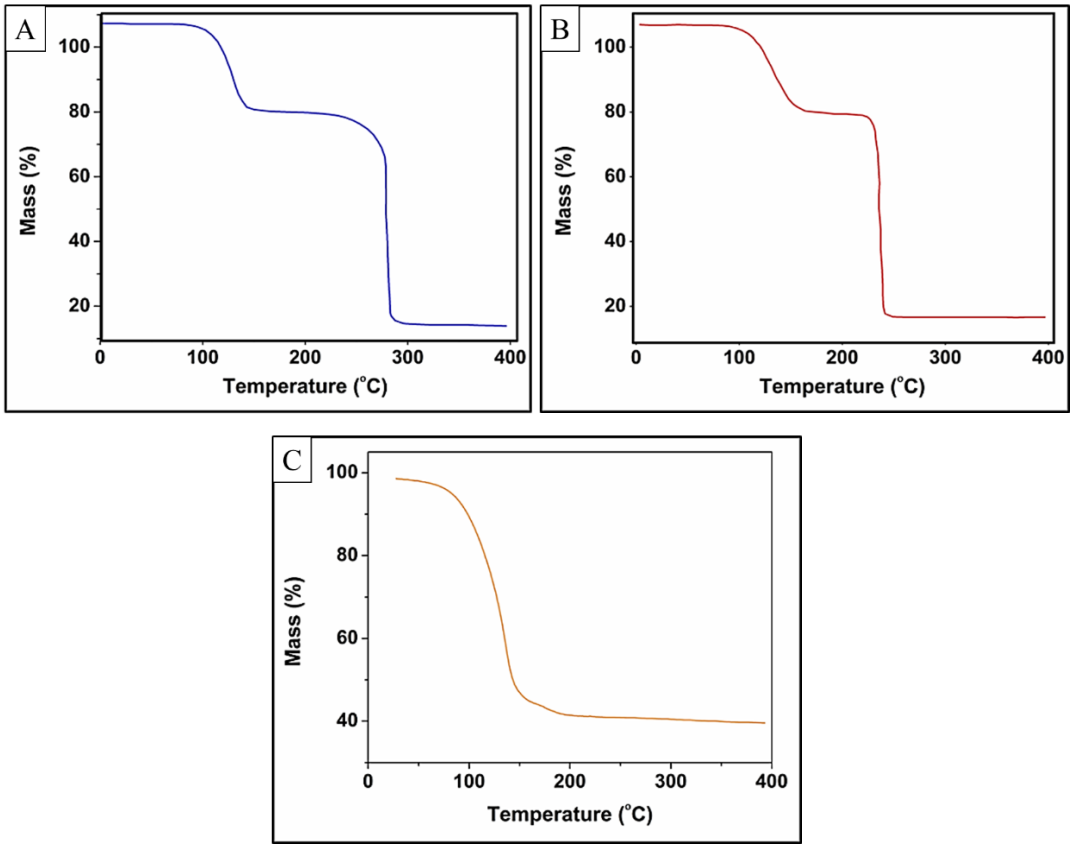

Figure 4.8 TGA profiles of metal formates (A) Nickel formate, (B) Cobalt formate and (C) Copper formate.

The possible mechanism for dehydration and decomposition are represented in equation 4.1, 4.2 and 4.3 for nickel, cobalt and copper formates respectively.

$$Ni(OOCH)_2.2H_2O \xrightarrow{140\,^{\circ}C} Ni(OOCH)_2 \xrightarrow{250\,^{\circ}C} nNi + gases\ species\ (H_2 + CO + CO_2) \quad (4.1)$$

$$Co(OOCH)_2.2H_2O \xrightarrow{130\,^{\circ}C} Co(OOCH)_2 \xrightarrow{290\,^{\circ}C} nCo + gases\ species\ (H_2 + CO + CO_2) \quad (4.2)$$

$$Cu(OOCH)_2.2H_2O \xrightarrow{110\,^{\circ}C} Cu(OOCH)_2 \xrightarrow{170\,^{\circ}C} nCu + gases\ species\ (H_2 + CO + CO_2) \quad (4.3)$$

Table 4.2 The dehydration and thermal decomposition temperatures of all the metal formates

Catalyst precursor	Dehydration temperature (°C)	Thermal decomposition temperature (°C)
Nickel formate	~140	~250
Cobalt formate	~130	~290
Copper formate	~110	~170

Thus, because of low temperature decomposition, impurity free product, eco-friendly and cheap source, metal formate was used as a precursor to decorate the carbon materials in the present research work.

4.4 NICKEL OXIDE MULTIWALLED CARBON NANOTUBE COMPOSITES (NiO-MWCNTs)

4.4.1 Characterization of NiO-MWCNTs composites

The morphology of the MWCNTs and NiO-MWCNTs composites were examined by FESEM and TEM. Figure 4.9 represents the FESEM micrographs of the pure MWCNTs, NiO-MWCNTs and NiO, respectively. An overview of the FESEM images shows that pure MWCNTs are straight and tubular in nature (Figure 4.9 A). On thermal treatment of MWCNTs with the nickel formate, the NiO-NPs generated were uniformly decorated over the surface of MWCNTs with an average particle size of 12 nm which resembles the plant root nodules (Figures 4.9 B and C). Similarly, for further comparison studies pure NiO was synthesized without using MWCNTs. FESEM image of pure NiO shows that particles are granular in nature and with an average particle size of 11 nm and it matches well with the particle size of the NiO observed in NiO-MWCNTs composite (Figure 4.9 D).

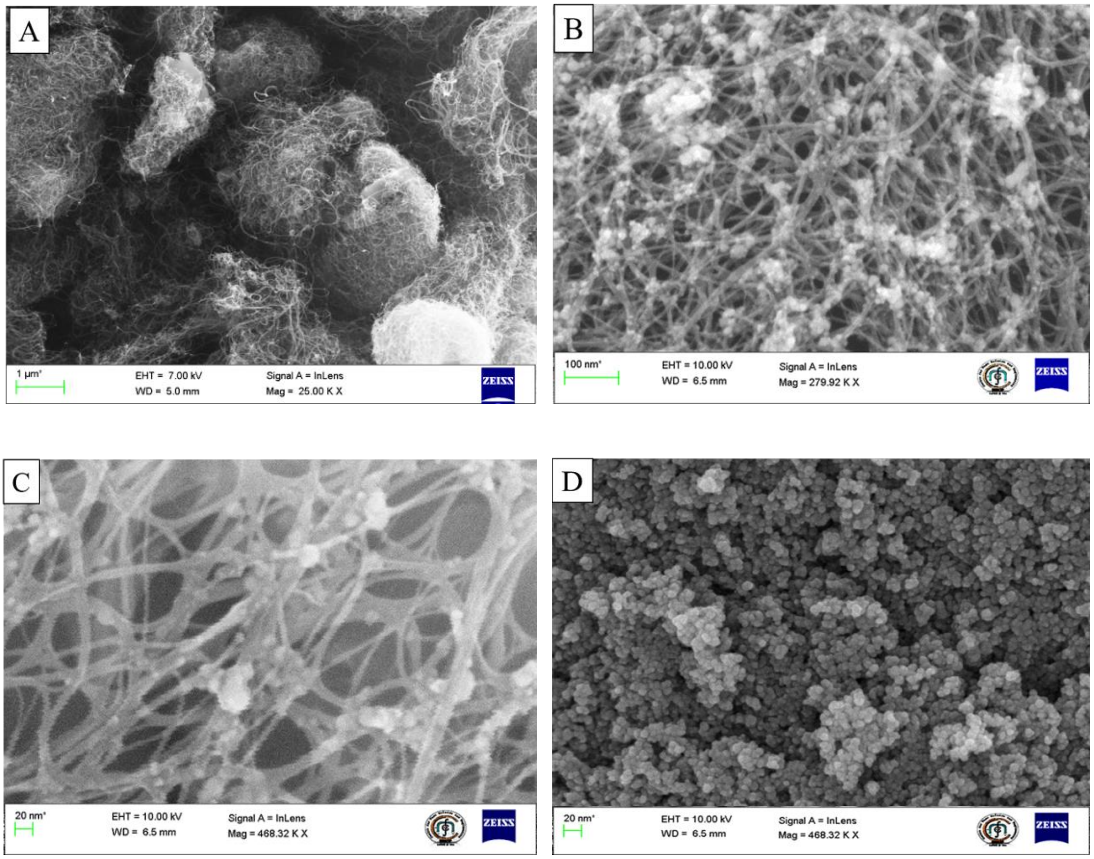

Figure 4.9 FESEM images of (A) purified MWCNTs, (B) NiO-MWCNT composite at 279.92KX magnification, (C) NiO-MWCNT composite at 468.32KX magnification and (D) pure NiO.

To investigate the further morphological features of the NiO-MWCNTs composite TEM results were examined and respective micrographs were shown in Figure 4.10. In the figure 4.10, A and B represents the TEM micrographs of NiO-MWCNTs at 279.92KX and 468.32KX magnification, respectively. From the TEM images, dark stain on the MWCNTs is observed which can be attributed to the NiO-NPs which wrap around the MWCNTs with an average diameter of 12 nm. Similarly, figure 4.10 C, represents the TEM images of pure NiO-NPs. From the figure, it is observed that the NiO particles are granular in nature with an average particle size of 11 nm. The obtained morphological features from FESEM and TEM results matches well with each other which confirms the formation of NiO-MWCNTs nano-composites.

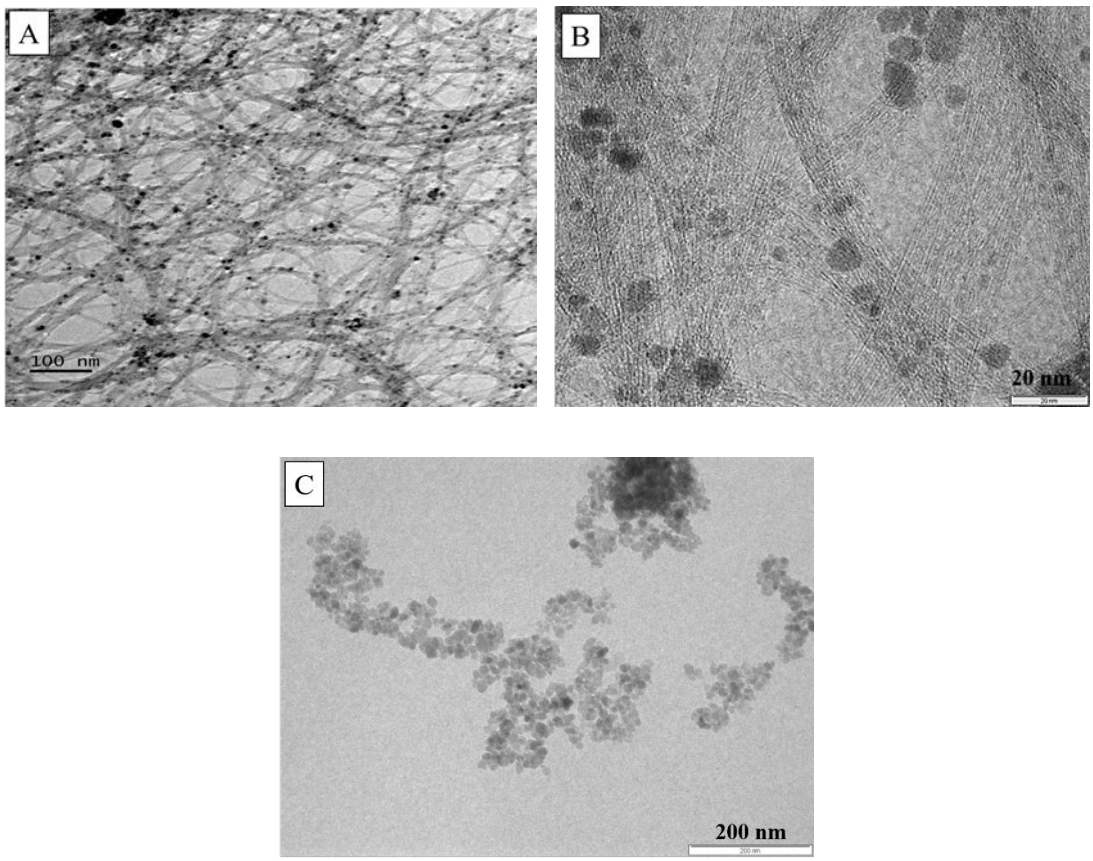

Figure 4.10 TEM images of (A) NiO-MWCNT composite at 279.92KX and magnification, (B) NiO-MWCNT composite at 468.32KX magnification and (C) pure NiO.

The crystallinity of the MWCNTs and its NiO composite were studied using PXRD with Cu Kα radiation (λ = 0.15406 nm) operating at 40 kV, 40 mA with a 2θ scanning rate of 2°/min. Figure 4.11 represents the PXRD pattern of pure MWCNTs (A), in comparison with the NiO (B) and NiO-MWCNT composites (C). For MWCNT, characteristic (002) diffraction peak is observed at 26.3°. In pure NiO-NPs diffraction peaks observed at 37.2°, 43.2° and 62.8° corresponds to the (111), (200) and (220) reflections of cubic lattice form of NiO (JCPDS card no 01-071-1179). In case of NiO-MWCNTs composite, the diffraction peaks show major peaks corresponding to both MWCNTs and pure NiO. The broad diffraction peak for NiO in the composites signifies that the particles are nano-crystalline in nature (Mun et al. 2014). Also, there were no extra peaks observed from other crystal structures in the PXRD spectrum indicating the

high purity of the prepared sample. Hence, these results confirm the formation of the NiO-MWCNTs composites.

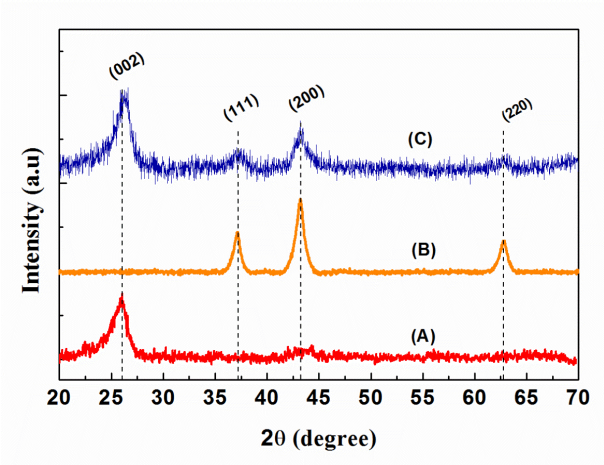

Figure 4.11 PXRD spectra of (A) Purified MWCNTs, (B) Pure NiO and (C) NiO-MWCNT composite.

Raman spectra were recorded to study the MWCNTs (A), Pure NiO-NPs (B) and NiO-MWCNT Composite (C) as shown in figure 4.12. The spectrum for MWCNT showed two typical peaks at 1344 cm^{-1} and 1586 cm^{-1}, which can be assigned to D-band (disorder band) and G-band (graphite band), respectively. The G-band corresponds to the vibration of sp^2 bonded carbon atoms in a graphite layer with an E_{2g} mode of hexagonal graphite and the D-band is associated with vibration of carbon atoms with dangling bonds in the plane terminations of disordered graphite. In the spectrum for NiO-NPs, the small broad peaks were observed at 496 cm^{-1} and 1068 cm^{-1}(Bai et al. 2014). In NiO-MWCNTs characteristic D-band and G-Band were observed along with the NiO characteristic peaks. The NiO-MWCNT composite shows I_D/I_G ratio value 1.5, which is much larger than the pure MWCNTs (0.6). This raise in I_D/I_G ratio value for NiO-MWCNT composite, may be due to the destructive interaction of NiO on the surface of MWCNTs. Hence, from these supporting results we can confirm the formation of NiO-MWCNTs composite.

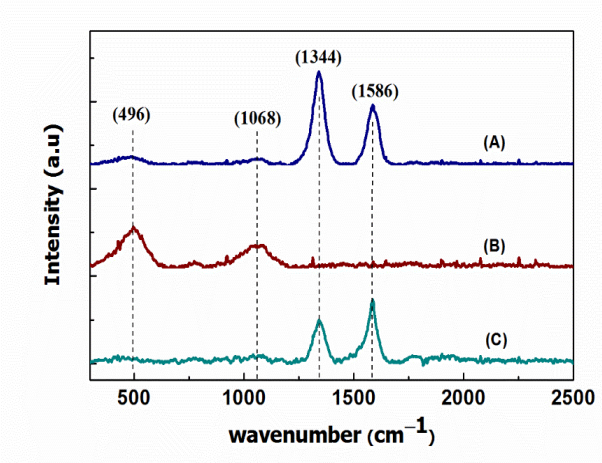

Figure 4.12 Raman spectra of (A) NiO-MWCNTs composite (B) Pure NiO and (C) Purified MWCNTs.

Further, by similar method the different weight ratio of NiO-MWCNTs composites were prepared and characterized. Figures 4.13(A-D) represents the FESEM images of the different wt % ratio of NiO-NPs decorated MWCNTs composites. As the precursor load increases from 5 to 15 %, the nature of NiO-NPs formed on the surface of MWCNTs also differs. The 5% NiO-MWCNTs shows least NiO-NPs decoration on the surface of MWCNT with no agglomeration, whereas 10 % composite shows more dense and uniformly decorated NiO-NPs over the surface of MWCNT with less agglomeration (Figures 4.13 B and C). 15% NiO-MWCNTs composite (Figure 4.13D) shows more agglomerated NiO particles on MWCNTs, which can attribute to the excess precursor load. Hence, from above results, the 10 % NiO-MWCNTs was concluded to be the optimized ratio.

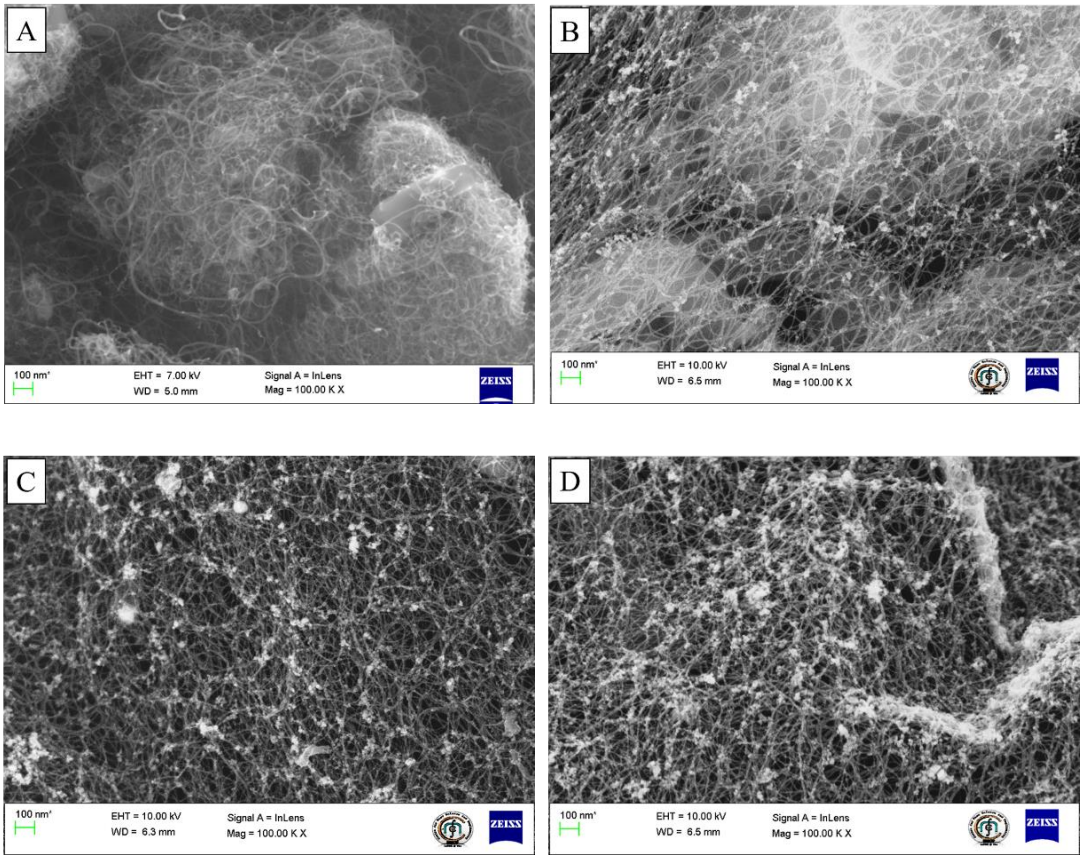

Figure 4.13 FESEM images of (A) Pure MWCNTs (B) 5% NiO-MWCNTs (C) 10% NiO-MWCNTs and (D) 15% NiO-MWCNTs.

Figure 4.14 (A and B) shows the TEM images of the 10% NiO-MWCNTs and 15 % NiO-MWCNT composites. It is observed that in 10% NiO-MWCNT the NiO-NPs are homogenously dispersed on the sidewalls of the MWCNTs without aggregation. The particle size appears to be 2-25 nm with an average particle size of 15 nm. In 15% NiO-MWCNT, although the NiO-NPs are homogenously dispersed, due to the excess precursor load the NiO particles agglomerates and forms macro particle in nature. The results obtained matches well with the FESEM results therefore it may be considered that among the all composites, the 10 % NiO-MWCNTs has optimum NiO to MWCNT ratio.

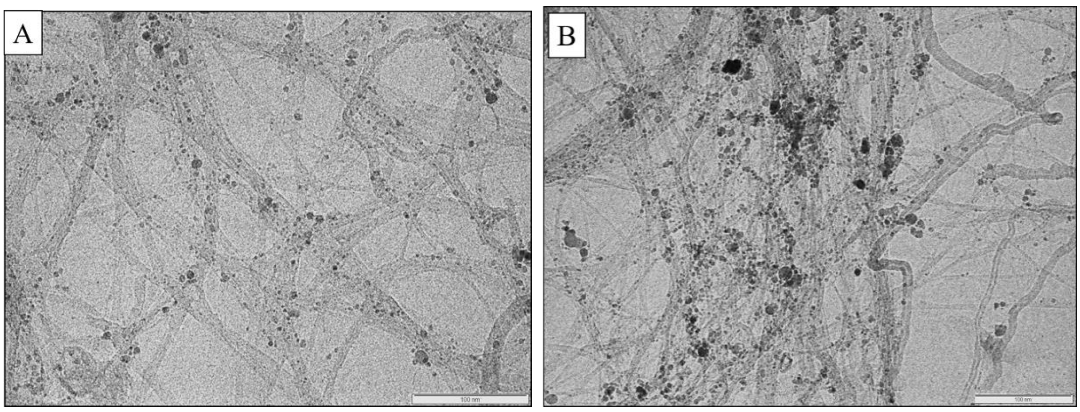

Figure 4.14 TEM images of (A) 10% NiO-MWCNTs (B) 15% NiO-MWCNTs.

The PXRD spectra were recorded to confirm the synthesized different weight percentage of NiO-MWCNTs composites. The Figure 4.15 illustrates the PXRD patterns of a synthesised different weight ratio NiO-MWCNTs composites in comparison with pure MWCNTs and pure NiO-NPs. The strong diffraction peak at 26.3° originates from the (002) plane of hexagonal graphite of MWCNT and the diffraction peaks at 37.2°, 43.2° and 62.8° can be assigned as the crystal planes of (111), (200) and (220) for NiO. These NiO diffraction peaks well matches with the cubic lattice of NiO JCPDS Card Files, No. 01-07-1179 and confirms the composite formation. The NiO diffraction peaks also appear to be broad in nature indicating the formation of nanoparticles. It is also observed that there is no change in phase and crystal structure with increased precursor concentration which confirms the reproducibility of the composites. However, the intensity of NiO peak to the graphite peaks varies with precursor load. In case of different wt.% composites, the intensity of the MWCNTs peak at 26.3° decreases and intensity of NiO peaks increases with raise in NiO ratio, which confirms the prepared different wt.% NiO-MWCNTs composites. The increased intensity order of NiO peaks and decreased intensity of MWCNT peaks for different composites is 5% > 10% > 15%. Thus, the obtained results suggested that, nickel formates can serve as an excellent NiO precursor for the decoration of MWCNTs.

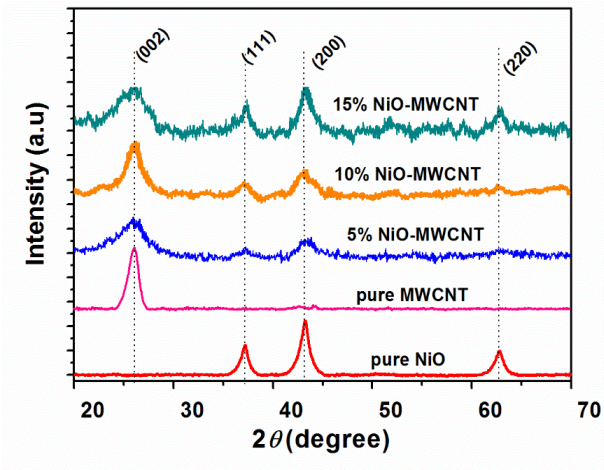

Figure 4.15 PXRD spectra of NiO particles in comparison with purified MWCNTs and 5%, 10% and 15% NiO-MWCNTs composites.

Raman spectra were examined to confirm the successful synthesis of different weight ratio of NiO-MWCNTs. Figure 4.16 represents the Raman spectra of MWCNTs, NiO and different wt.% NiO-MWCNTs composites. The distinctive D and G bands appear at around ~1344 cm^{-1} and ~1588 cm^{-1} for MWCNTs and all NiO-MWCNT composites. From the Raman spectra, it is observed that the intensity of I_D/I_G ratio increases from 1.05 to 1.14, 1.30 and1.43 for MWCNTs, 5% NiO-MWCNT, 10% NiO-MWCNT and 15% NiO-MWCNT composites respectively. As the wt.% of NiO increases in composites, means more NiO particles destructively interacts with the surface of MWCNTs and thus the value of I_D/I_G ratio increases which confirms the formation of different wt.% NiO-MWCNTs composites.

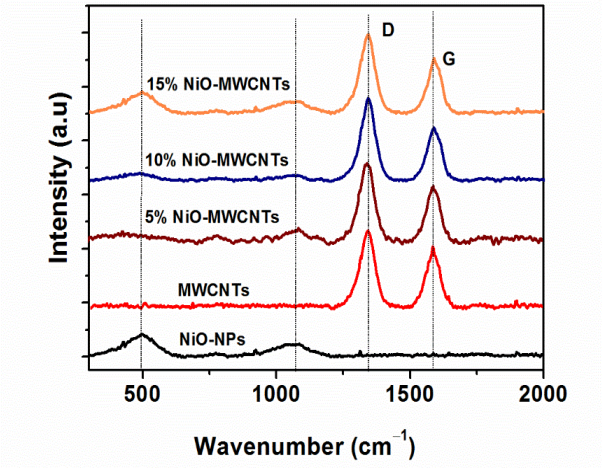

Figure 4.16 Raman spectra of NiO-NPs in comparison with purified MWCNTs and 5%, 10% and 15 % NiO-MWCNTs composites.

4.4.2 Theoretical Simulation Method

To investigate the particle distribution and interaction of metal particles with the MWCNTs, we carried out the theoretical simulation studies. The calculations have been performed using first-principle plane-wave approach, based on the spin-polarized density-functional theory (DFT), in the generalized gradient approximation (GGA), with projector augmented-wave (PAW) pseudo-potentials, as implemented in Vienna Ab-initio Simulation Package (VASP) (Kresse and Hafner 1993). The cut-off energy for the plane-wave expansion was set to be 400 eV. Structure including a NiO-NPs with diameter of 10 Å on a (6,6) carbon nanotube with length of 14.7 Å was embedded in a supercell with periodic boundary conditions. The supercell contains a vacuum of 10Å in the two-direction perpendicular to nanotube axis in order to avoid interaction between neighboring supercells. Using a 1x1x1 k-point mesh, the structures were optimized with force threshold of 0.05 eV/ Å.

4.4.3 Theoretical Simulation Results

From the theoretical simulation studies the geometry of the optimized structure obtained is shown in figure 4.17A. DFT calculations provide charge density of the optimized structure. To visualize the charge, transfer between NiO and nanotube as show in figure 4.17B, the charge density difference in the geometrically optimized

system relative to isolated carbon nanotube and isolated NiO nanoparticle. The charge density difference plot shows redistribution of the charge in carbon nanotube upon adsorption of NiO-NPs. A significant charge accumulation is observed at the interface between the nanotube and the nanoparticle and at the π orbitals of the carbons in the nanotube, while charge depletion appears mainly at sigma bonds of the nanotube. From the isosurface of charge density difference a charge transfer from nanotube to NiO-NPs can be observed.

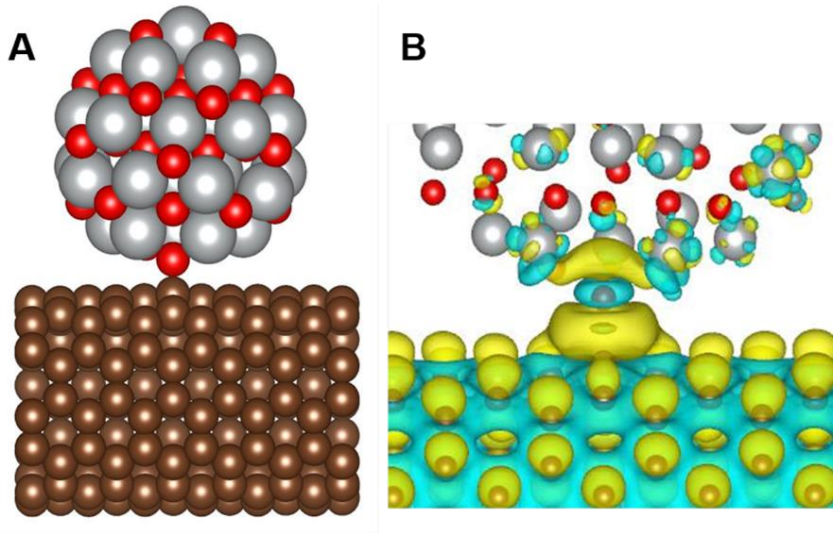

Figure 4.17 (A) Geometrical position of the optimized structure of NiO nanoparticle on (6,6) carbon nanotube and (B) Charge density difference isosurface of NiO adsorbed on nanotube. Charge density difference gives the information about redistribution of charge in the system relative to isolated carbon nanotube and isolated NiO nanoparticle. Yellow and blue indicate charge accumulated region and charge depleted regions, respectively. The isosurface value is $3x10^{-3}$ e/Å. (Color scheme: C= brown, Ni= grey, O=red).

4.4.4 Electrochemical behaviour of NiO-MWCNTs Composite Materials

Generally, nickel-based nanostructures can display an electro-catalytic activity for the detection of glucose. Fleischmann et al. 1971 demonstrated that glucose molecules could be oxidized at a nickel anode in alkaline solution based on the redox couple of Ni^{3+}/Ni^{2+}. Hence, the NiO-MWCNTs modified electrodes were investigated for its electro-catalytic activity towards direct glucose oxidation. In this section, we

constructed the NiO-MWCNT/CPE and NiO-MWCNT/GCE for direct glucose oxidation and examined for glucose sensing. The results obtained from two different types of electrodes were compared and best electrode type was selected to achieve the highest catalytic activity towards glucose sensing.

4.4.5 Cyclic Voltammetry behaviour of NiO-MWCNTs/CPE

Trials conducted on electro-catalytic oxidation of glucose on the modified electrode in different electrolytes such as NaOH solution, acetate and phosphate buffer. It was found that the modified electrode was not showing any response to acetate and phosphate buffer solutions. Hence, NaOH solution was chosen as the electrolyte for the oxidation of glucose. Figure 4.18A shows the CV of bare CPE (a), MWCNT/CPE (b) and NiO-MWCNT/CPE (c). The bare CPE shows no redox peaks and records least current, whereas MWCNT/CPE shows no redox peaks but records four folds higher current than the bare CPE which can be attributed to the high surface area and high electrical conductivity of MWCNTs (Popov 2004). NiO-MWCNT/CPE showed distinct oxidation peak at 0.50 V and reduction peak at 0.44 V due to oxidation of Ni^{2+} to Ni^{3+} and reduction of Ni^{3+} to Ni^{2+} respectively. Figure 4.18B, shows the CVs of the modified electrodes namely, MWCNT/CPE (a and d), NiO/CPE (b and e) and NiO-MWCNT/CPE (c and f) in the presence and absence of glucose. In the absence of glucose there was no current response observed for MWCNT/CPE (a), whereas well-defined quasi-reversible redox peaks were observed for the NiO/CPE (b) and NiO-MWCNT/CPE (d) with anodic peak potential at 0.50 V and the cathodic peak at 0.44 V, which is attributed to the Ni^{3+}/Ni^{2+} redox couple. After the addition of the 1 mM glucose, increase in oxidation and reduction peak current density indicates the NiO can electro-catalyze the direct oxidation of glucose in 0.1 M NaOH solution and similar results were reported on glucose detection using NiO-based materials (Zhang et al. 2010a). Interestingly, the redox peak for NiO-MWCNT/CPE negative shifted anodic peak potential at 0.47 V and the cathodic peak at 0.33 V were observed and current density increases 2.5 folds (e) than the only NiO/CPE (c). The shifts in anodic peak potential to lower potential region may be due to the faster diffusion of glucose at the electrode surface and these results, indicates that NiO-NPs deposited on the MWCNTs exhibits higher electro-catalytic activity towards the direct oxidation of glucose which

is due to the larger surface area and high conductivity for fast electron transfer offered by the MWCNTs which improves the electron transduction.

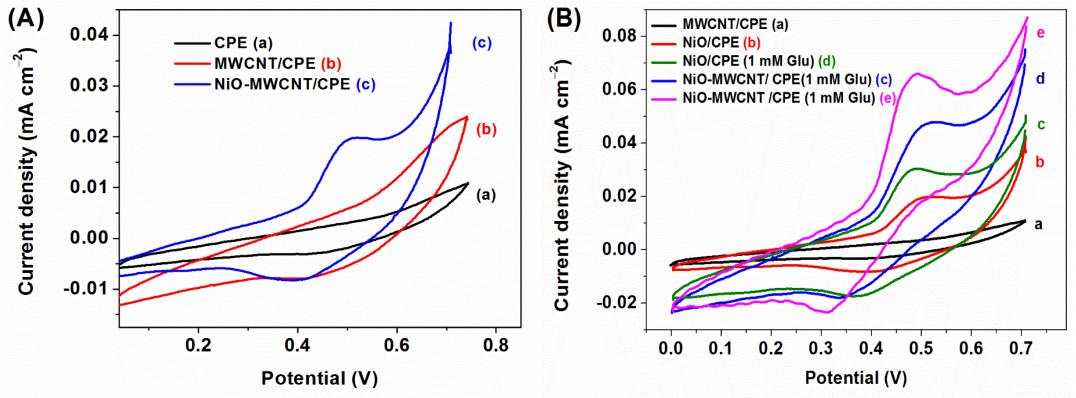

Figure 4.18 (A) CVs of bare CPE, MWCNT/CPE and NiO/CPE at the scan rate of 50 mVs^{-1} in 0.1 M NaOH and (B) CVs of different electrodes in the absence and presence of glucose.

Figure 4.19 displays the cyclic voltammograms of glucose oxidation at the various modified electrodes at 0.5 mM glucose concentration, wherein curve a, b, c and d shows the voltammogram of the NiO/CPE, 5% NiO-MWCNT/CPE, 10% NiO-MWCNT/CPE and 15% NiO-MWCNT/CPE, respectively. The different NiO-MWCNT/CPE constructed show current responses that are approximately 1.1, 2.5 and 1.7 times greater than those in only NiO/CPE (a). This phenomenon indicates that the higher current response is partially due to the high conductivity of the MWCNTs. The MWCNTs based modified electrode, provides more steric structure and platform for more conductive surface area to carry NiO active species. The 5% NiO-MWCNT/CPE (c) shows lesser current than those in 10% and 15% NiO-MWCNT/CPE (d and b) modified electrodes is due to the lesser active site. However, 10% NiO-MWCNT/CPE shows uniquely high net current is due to more reactive site with enhanced surface area and greater conductivity. Slight decrease in response at 15% NiO-MWCNT/CPE may be due to the agglomerated NiO particles which decreases the conductivity and active surface area as well. Hence, from the obtained experimental results, 10% NiO-MWCNT/CPE showed enhanced electro-catalytic activity for glucose oxidation.

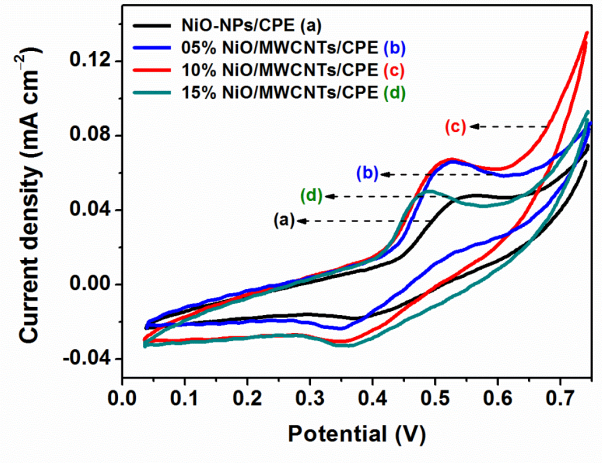

Figure 4.19 CVs of NiO/CPE in comparison with 5, 10 and 15% NiO-MWCNTs/CPE in the presence of 0.5 mM glucose at a scan rate of 50 mV s^{-1} in 0.1 M NaOH solution.

The plausible mechanism for oxidation of glucose by NiO-based materials could be represented by the following reactions (Zhao et al. 2007, Wang et al. 2012b).

$$NiO + OH^- \rightarrow Ni(OH)_2 \quad (4.4)$$

$$Ni(OH)_2 + OH^- \rightleftharpoons NiO(OH) + H_2O + e^- \quad (4.5)$$

$$NiO(OH) + glucose \rightarrow Ni(OH)_2 + glucolactone \quad (4.6)$$

When the electrochemical reaction produces Ni^{2+} species while consumes Ni^{3+}, on the other hand, the produced Ni^{2+} can be further oxidized to Ni^{3+} at electrode surface as depicted in equations 4.5 and 4.6. As a result, the change in concentrations of Ni^{2+} and Ni^{3+} species cause the increase in the anodic peak current and decrease of the cathodic peak current. The change in redox peak current density after glucose addition is believed to be due to the fact that the Ni^{+2}/Ni^{+3} redox couple serves a double function of the electronic medium and catalyst, synchronously (Zhao et al. 2007).

The optimum concentration of NaOH solution for the voltammetric detection of glucose at the 10% NiO-MWCNT/CPE modified electrode was investigated using different concentrations ranging from 0.05 to 0.3 M. From the figure 4.20, it is observed that the anodic peak *(E_{pa})* shift negatively with a rise in NaOH concentration indicating that the hydroxyl ions (OH^-) are directly involved in electrochemical oxidation process

and the potential value achieved the best response in 0.2 M NaOH solution. However, when the NaOH concentration exceeded 0.3 M, the glucose oxidation peaks current observed to decrease instead, since much high concentration of OH^- can block the further electro-adsorption of glucose anion (Chen et al. 2010). Therefore, 0.2 M of NaOH aqueous solution was considered to be optimized concentration.

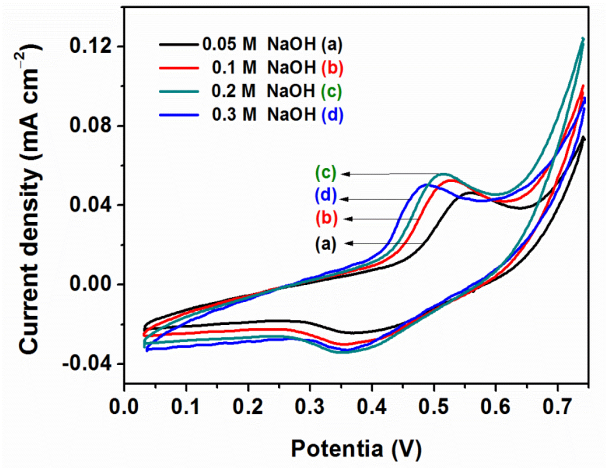

Figure 4.20 CVs of 10% NiO-MWCNT/CPE with different NaOH concentrations.

The valuable information concerning the electrode reaction mechanism (rate-determining step) may be acquired from the relationship between the peak current and scan rate (v). The scan rate influence was studied on 10% NiO-MWCNT/CPE using CV experiment. From the figure 4.21A, it can be observed that the peak current increases with increasing scan rate from 25–200 mV s^{-1}. The anodic and cathodic peak current were found linear to square root of scan rate with a regression equation of I_{pa} (mA) = 0.0107ν –0.0084 and I_{pc} (mA) = -0.0058 ν +0.0111 with correlation coefficient 0.9983 and 0.9867, respectively (Figure 4.21B). When the scan rate increases, the redox potentials (E_{pa} and E_{pc}) shift slightly indicating a surface-controlled quasi-reversible process for the electrode reaction of NiO on the surface of 10% NiO-MWCNT/CPE. Similarly, figure 4.21C shows the linear relationship between the peak potential (E_p) and the logarithm of scan rate ($log\ v$) at 1.0 mM glucose in 0.2 M NaOH, where two straight lines are obtained and the linear regression were calculated as E_{pa}(V)=0.0549logν + 0.4047 and E_{pc}=0.011logν +0.2887 with correlation co-efficient 0.9604 and 0.8196, respectively.

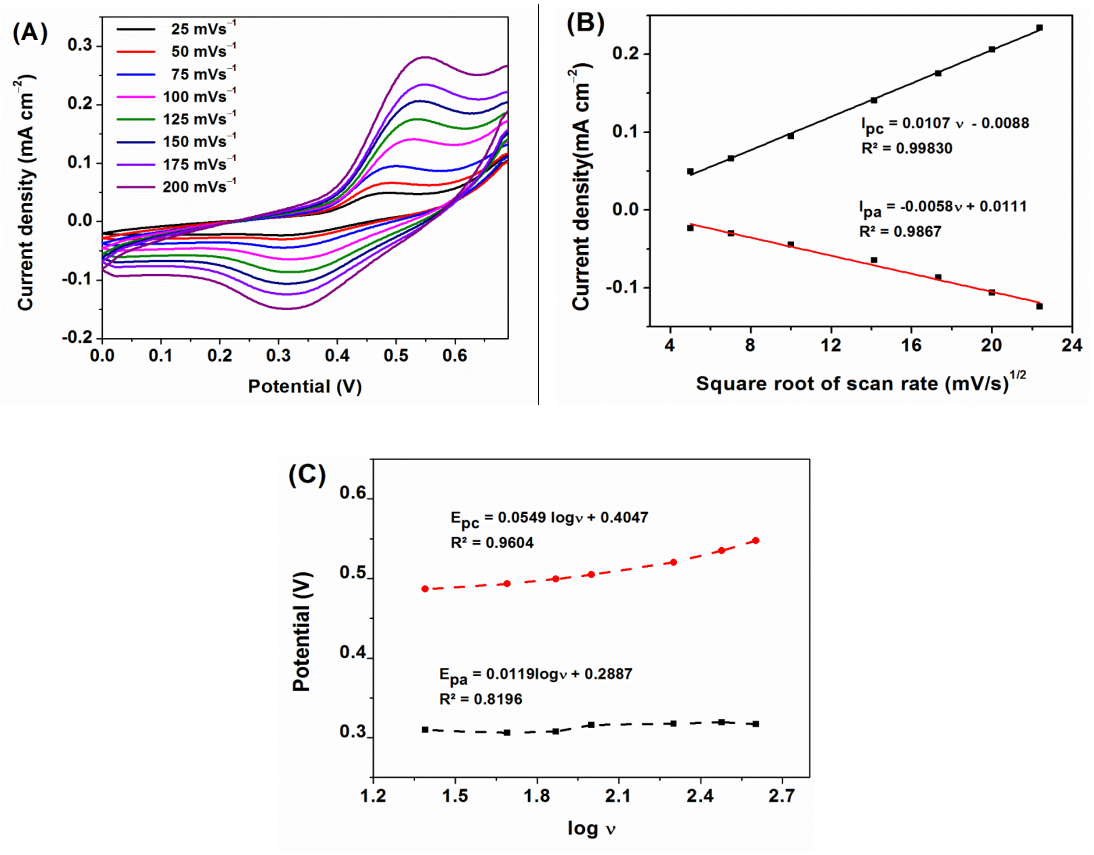

Figure 4.21 (A) CVs of 10% NiO-MWCNT/CPE electrode at different scan rates from 25 to 200 mV s^{-1} in 0.2 M NaOH with 0.5 mM glucose, (B) plot of peak current (I_P) vs. square root of scan rate ($\sqrt{\nu}$) and (C) plot of peak potential (E_P)vs. logarithm of scan rate ($log\ \nu$).

The kinetic parameters of charge transfer coefficient (α) and apparent charge transfer rate constant (Ks) were calculated using Laviron's equation 4.7 (Laviron 1979).

$$\log K_s = \alpha \log(1-\alpha) + (1-\alpha) log\alpha - log\frac{RT}{nF\vartheta} - \frac{(1-\alpha)\alpha nF\Delta E_P}{2.3RT} \quad (4.7)$$

where α is the electron transfer coefficient, n is the number of electrons, ΔE_p is the peak-to-peak separation redox peaks, n is the scan rate, R *is gas constant* (8.314 J mol^{-1} K^{-1}), T is the temperature (298K), ν is scan rate and F is the Faraday's constant (96,493 C mol^{-1}). The value of αn was calculated to be 0.47, given $0.3 < \alpha < 0.7$, it could be concluded that $n = 1$ and $\alpha = 0.47$. So, the redox reaction was a single electron transfer process and then the value of K_S calculated to be 0.64 s^{-1}. It is

assumed that, the increased efficiency of the direct electron transfer is due to increase in effective surface area and also synergistic effect of NiO-NPs and MWCNTs nanocomposite on the electrode surface.

The surface coverage of electroactive substance (Γ^*) of 10% NiO-MWCNT/CPE was calculated as 1.5629×10^{-6} mol $cm^{-2,}$ using the Faraday's law [Q = nFAΓ*], where *Q* is the integration charge of the reduction peak (0.010556 C), *A* is the area of the electrode (0.07 cm^{-2}), *n* is the number of electrons transferred and *F* is the Faraday constant. The average value of Γ^* calculated was larger than Ni-Co/rGO/GCE (8.99×10^{-8} mol cm^{-2}) (Wang et al. 2013). These results could be attributed to the large specific surface area of the 10% NiO-MWCNT/CPE.

4.4.6 Chronoamperometry response of NiO-MWCNTs/CPE towards Glucose

Since cyclic voltammetry is not sensitive to low concentration measurements, the chronoamperometric technique we employed to detect glucose. Figure 4.22 represents the chronoamperometry response of the NiO-MWCNTs/CPE in 0.2M NaOH solution. Figure 4.22A shows a typical current-time plot of the NiO-MWCNT/CPE electrode on successive additions of 10.0 μM of glucose at different working potential. The constant stirring (350 rpm) was provided to achieve an instant homogeneous glucose concentration. With the stepwise addition of glucose, the chronoamperometric response also shows a step-like increase in current. A significant well defined, stable and rapid current change was observed with successive addition of 10.0 μM of glucose and achieving the steady state current in less than 3 s (Figure 4.22B). The proposed sensor exhibits higher sensitivity in an applied potential of 0.5 V when compared with that of the 0.2 V, 0.3 V and 0.4 V. However, the higher noise is observed at 0.5 V which may be due to the adsorption of the intermediate species onto the electrode surface with increased concentration and longer reaction time. At the different applied potential, chronoamperometric current versus total glucose concentrations and the corresponding calibration curve are shown in (Figure 4.22C). Figure 4.22A shows that at 0.5 V, the sensor shows highest current response with respect to glucose addition and this potential matches well with the oxidative peak potential from the CV results (Figure 4.18B, curve e). These results can attribute to the highest catalytic activity of the

10 % NiO-MWCNTs/CPE sensor at 0.5 V in 0.2 M NaOH solution towards glucose oxidation. Hence, 10 % NiO-MWCNTs/CPE was further investigated for glucose detection at an applied potential of 0.5 V in 0.2 M NaOH solution upon the successive addition of 0.5 mM glucose (Figure 4.22D). The chronoamperometric current versus time and respective calibration curve are shown in figure 4.22E. The results show that the sensor at optimised conditions can detect upto 14 mM glucose concentrations with excellent sensitivity and limit of detection (LOD). From the obtained results, the sensitivity, detection limit, response time and regression value were determined at different applied potentials and are tabulated in table 4.3.

Table 4.3 Analytical performance of the proposed NiO-MWCNT/CPE electrode.

Sl. No	Applied potential (V)	Sensitivity ($\mu A\ mM^{-1}cm^{-2}$)	LOD (μM)	Response time (s)	Regression value (R^2)
1	0.2	898	36	3	0.9866
2	0.3	2837	70	2	0.9707
3	0.4	3733	23	4	0.9946
4	0.5	6527	23	3	0.9952

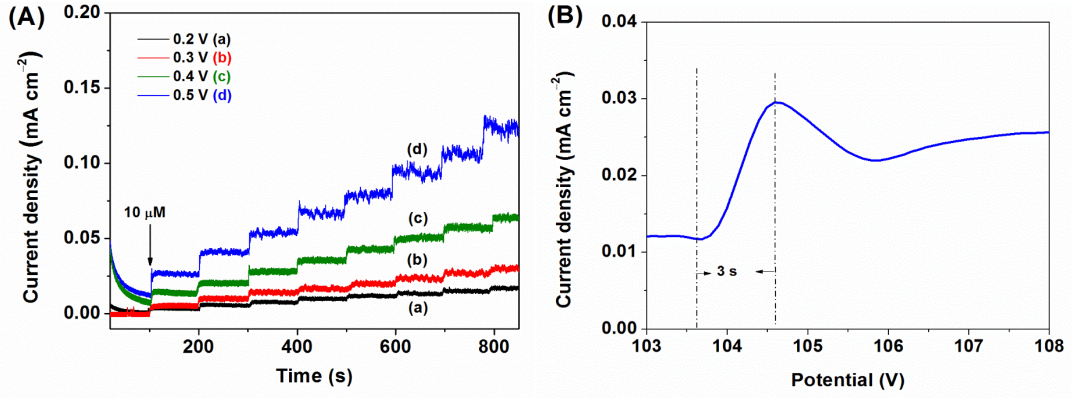

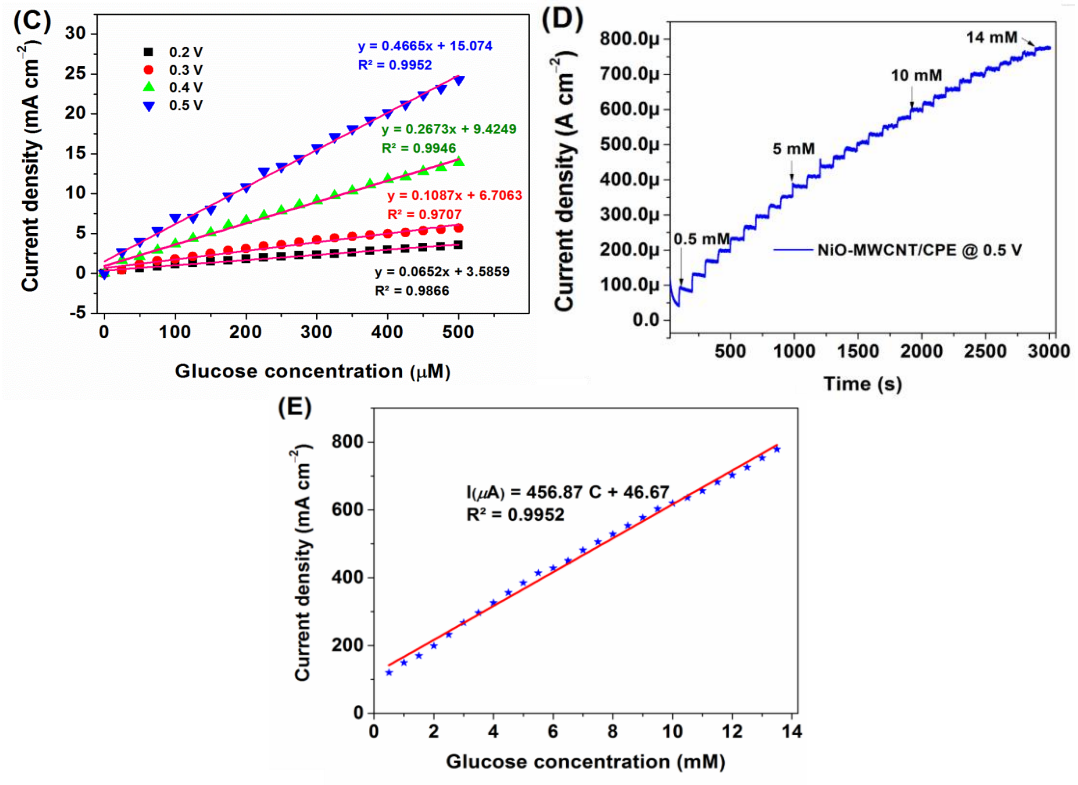

Figure 4.22 (A) Chronoamperometric responses of NiO-MWCNT/CPE electrode upon the successive addition of 10 µM glucose, (B) Time response graph for 10% NiO-MWCNTs/CPE at 0.5 V, (C) the chronoamperometric current plotted vs. total glucose concentration and their corresponding linear calibration curves, (D) chronoamperometric responses of NiO-MWCNT/CPE electrode upon the successive addition of 0.5 mM glucose and (E) the chronoamperometric current plotted vs. total glucose concentration and their corresponding linear calibration curves (0.5 mM -14 mM).

From the table 4.3, it is observed that, 10 % NiO-MWCNTs/CPE shows the highest sensitivity of 6527 µA mM^{-1} cm^{-2} at 0.5 V with the detection limit of 23 µM which is greater than the other applied potential sensitivity of 3733 µA $mM^{-1}cm^{-2}$, 2837 µA $mM^{-1}cm^{-2}$, 898 µA $mM^{-1}cm^{-2}$ with the LOD of 23, 70, 36 mM of glucose at an applied potential of 0.4 V, 0.3 V and 0.2 V respectively. Overall, from these experimental results, it is observed that 10 % NiO-MWCNTs/CPE sensor shows the

greater electro-catalytic activity at an applied potential of 0.5 V. Hence, further interference and stability studies were performed at applied potential of 0.5 V.

4.4.7 Reproducibility, Stability and Anti-interference property of 10% NiO-MWCNTs/CPE

The interference effect of DA, UA, Gly, AA and Trp towards the determination of glucose, which commonly co-exists with glucose in human blood serum (HBS) was investigated. The effect of interference was studied by recording the chronoamperometry response for the above said molecules of concentration 2 mM at an applied potential of 0.5 V as shown in figure 4.23A. There is no distinct current response observed with the addition of 0.2 mM DA, UA, Gly, AA and Trp. On the contrary, a significant current response with the addition of 2 mM glucose appeared. Hence, the current response of common interfering biomolecules caused negligible interference to the response of glucose at 10 % NiO-MWCNT/CPE. The long-term stability of the sensor was evaluated by measuring chronoamperometric current responses to 2 mM L^{-1} glucose for 30 days period (Figure 4.23B). The results show that the 10 % NiO-MWCNT/CPE retained 90% of its initial current response to glucose which could be mainly ascribed to the chemical stability of NiO/MWCNTs where I is the current response at first day and I_0 is the current recorded at subsequent days. The proposed sensor was compared for its sensitivity, limit of detection and for its linear range with the previously reported work as shown in table 4.4. However, the sensor shows high sensitivity of 6527 μA mM^{-1} cm^{-2} which is much higher than any other CNT based non-enzymatic sensor reported previously (Table 4.4). Hence, these results demonstrate that 10 % NiO-MWCNTs composite is a potential material for the fabrication of the non-enzymatic glucose sensor.

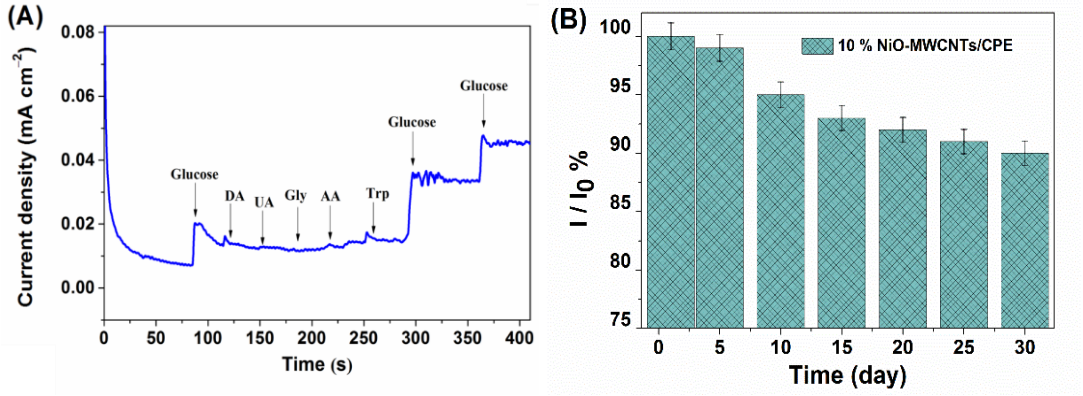

Figure 4.23 (A) Chronoamperometric response of the NiO-MWCNT/CPE electrode on successive addition of 2 mM of glucose, DA, UA, UA, Gly, AA and Trp into 0.2 M NaOH solution and (B) Stability plot for NiO-CNT/CPE sensor stored over three weeks in 0.2 M NaOH with 2 mM glucose at 0.5 V.

For practical application, 10% NiO-MWCNT/CPE was investigated to determine the glucose concentration in HBS. HBS was injected into 10 mL of 0.2 M NaOH solution at an applied potential of +0.5 V under constant stirring. The electrode current recorded was correlated with the glucose concentration calibration curve (Figure 4.22 E) and the values obtained were compared with the results obtained using a commercial glucose meter and the measured values are tabulated in Table 4.5. The results show that accuracy of the electrode is > 95 % with the Relative Standard Deviation (RSD) less than 5 % for all the samples. Hence, these results suggest that the proposed sensor can be used to estimate accurate amount of glucose in HBS.

Table 4.4 Comparison of analytical performance of proposed NiO-MWCNT/CPE electrode with reported MWCNTs based non-enzymatic glucose sensors.

Type of electrode	**Linear range (mM)**	**Detection limit (μM)**	**Detection potential (V)**	**Sensitivity ($\mu A\ mM^{-1}\ cm^{-2}$)**
NiO/MWCNTs/Ta (Hsieh et al. 2007)	7.00	2.00	0.50	1.77
CS-GA-GOx-Nafion-PtPd–MWCNT (Chen et al. 2012)	14.00	31.00	0.60	112
Ni-MWCNT (Sun et al. 2012)	17.50	0.89	0.60	67.20
MnO_2/MWNTs (Chen et al. 2008)	28.00	N.A.	0.30	34.19
Pt–Pb/CNTs (Cui et al. 2007)	0.50	1.80	0.30	18.00
Cu nanocluster/MWCNT (Kang et al. 2007)	4.50	0.21	0.65	17.76
Cu/Au/CNT (Lu et al. 2012)	0.50	0.30	0.65	NA
NiO-MWCNT/CPE (Present work)	0.50	36.00	0.20	898.00
NiO-MWCNT/CPE (Present work)	0.50	70.00	0.30	2837.00
NiO-MWCNT/CPE (Present work)	0.50	23.00	0.40	3733.00
NiO-MWCNT/CPE (Present work**)**	**14.00**	**23.00**	**0.50**	**6527.00**

Table 4.5 The detection of glucose in human blood serum.

Sample	Glucose (mM) (Proposed sensor)	RSD* (%) (N = 4)	Glucose (mM) (commercial glucose sensor)	Actual Glucose Concentration (mM)	Accuracy (%)
1	5.8	4.0	5.5	5.6	96.5
2	4.5	4.8	4.4	4.5	100.0
3	7.0	2.2	7.1	7.2	97.3
4	4.8	2.9	4.6	4.6	95.7
5	6.7	5.2	6.6	6.5	97.0

* Average of four trials

4.5 NiO-MWCNTs/GLASSY CARBON ELECTRODE FOR NON-ENZYMATIC GLUCOSE SENSING

In electrochemical sensor application, the most promising and generally used electrode is glassy carbon electrode (GCE). Glass-like carbon, often called glassy carbon or vitreous carbon, is a non-graphitizing, or non-graphitizable, carbon which combines glassy and ceramic properties with those of graphite. The most important properties are high temperature resistance, hardness (7 Mohs), low density, low electrical resistance, low friction, low thermal resistance, extreme resistance to chemical attack and impermeability to gases and liquids. Due to these special properties and easy-to-modify the surface by our choice of materials, it is widely used in many electrochemical applications. Herein, the electro-catalytic properties of the NiO-MWCNTs modified GCE towards direct glucose oxidation was studied and results obtained were compared with the results obtained from NiO-MWCNTs/CPE is reported.

4.5.1 CV behaviour of NiO-MWCNTs/GCE towards Glucose Sensing

Different composites NiO-MWCNTs modified GCE were fabricated namely, 5%, 10%, 15% NiO-MWCNT/GCE for 5%, 10% and 15% NiO-MWCNTs composites, respectively. CV responses of glucose on various NiO-MWCNTs/GCE modified electrodes are shown in figure 4.24 and results were compared with the results of 10% NiO-MWCNTs/CPE modified electrode. Clearly, the 5%, 10% and 15% NiO-MWCNT/GCE electrodes show direct oxidation of glucose similar to the NiO-MWCNTs/CPE. However, the 5% (a) and 10% NiO-MWCNT/GCE (b) shows the significant raise in redox current density than 10% NiO-MWCNTs/CPE (d), which may be due to the high conductivity and higher surface area offered by the GCE. At the same time the 15% NiO-MWCNT/GCE (peak c) shows lesser current response, which may be due to the agglomerated NiO particles in the composites that reduces the activity of the materials. These redox peaks obtained can be ascribed to the irreversible oxidation of glucose which is similar to the redox process from NiO-MWCNTs/CPE described in the section 4.4.5. This phenomenon indicates that glucose can be electro-catalytically oxidized by the hybrid composite and the GCE plays important role in electron transfer from the catalysed product.

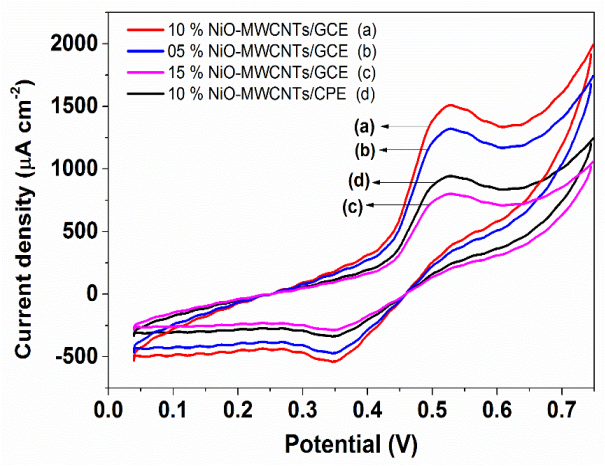

Figure 4.24 CV response for different NiO-MWCNTs composite electrodes in 0.1 M NaOH solution at the scan rate of 50 mVs^{-1}.

4.5.2 Chronoamperometric behaviour of NiO-MWCNTs/GCE towards Glucose Sensing

Since cyclic voltammetry is not sensitive to low concentration measurement, chronoamperometric technique was employed to detect glucose. To find out the optimal wt.% ratio of composites, the modified NiO-MWCNTs/GCE were investigated towards glucose sensing at an applied potential of 0.5 V in 0.1 M NaOH solution as shown in figure 4.25A. The results show that the 10% NiO-MWCNTs/GCE records five and three folds higher current response than 5% and 15% NiO-MWCNTs/GCE respectively. These results obtained were very similar to the results obtained in case of NiO-MWCNTs/CPE electrodes, which can be attributed to the catalytic activity of NiO-NPs distributed on the walls of MWCNTs. However, the current density recorded by the GCE modified electrode were higher than the CPE, which is due to enhanced properties like high conductivity and higher surface area offered by the GCE. Figure 4.25B represents the current response time for 10% NiO-MWCNTs/GCE where in current response reaches > 90% in less than 3 s which suggests the faster electron transfer properties and easy diffusion of glucose to electrode surface. Further to find the optimal conditions for the chronoamperometric detection of glucose, the effect of applied potential on the current response of the 10% NiO-MWCNTs/GCE was investigated.

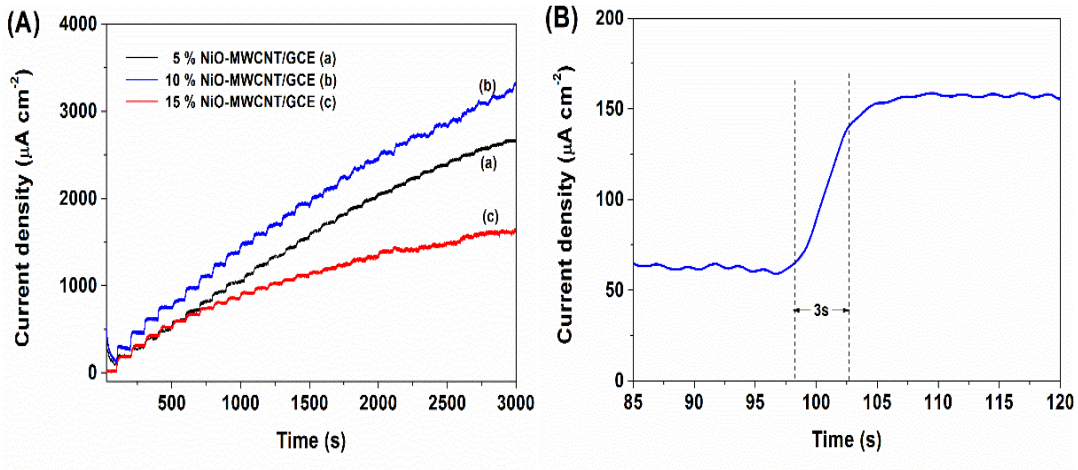

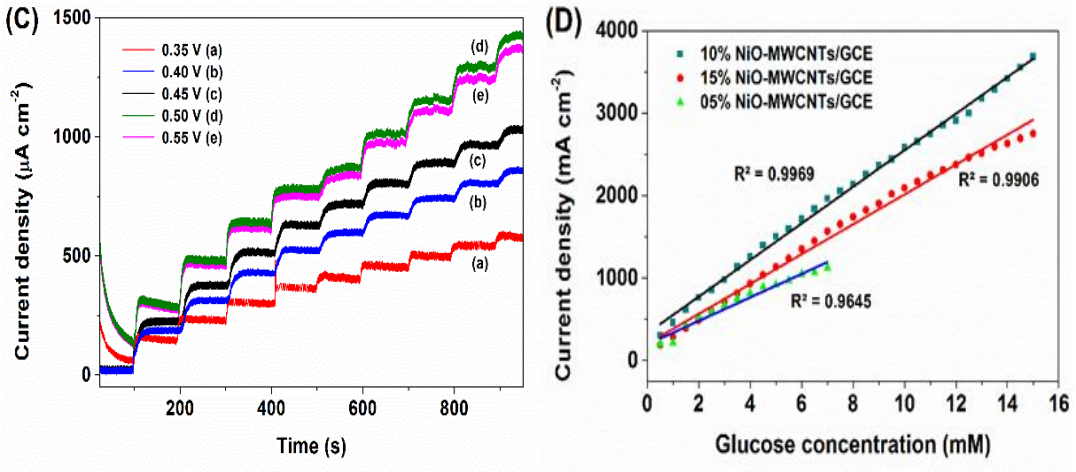

Figure 4.25 (A) CA response of 5, 10 and 15% NiO-MWCNTs/GCE at 0.5 V in 0.1 M NaOH solution upon the successive addition of 0.5 mM glucose (B) Response time plot for 10% NiO-MWCNTs/GCE, (C) Current verses time (i-t) graph for 10% NiO-MWCNTs/GCE at different working potential and (D) Current vs. glucose concentration plot of 5, 10 and 15% NiO-MWCNTs/GCE.

Chronoamperometric curves of 10% NiO-MWCNTs/GCE in 0.1 M NaOH solution with successive addition of 0.1 mM glucose at applied potentials of 0.35, 0.40, 0.45, 0.50 and 0.55 V were recorded (Figure 4.25C). The signal-to-background ratio increases with the potential in range from 0.35 to 0.50 V and then decays after that potential. For a high sensitivity, a constant potential of 0.50 V was selected as the optimal detection potential. The chronoamperometric currents versus total glucose concentrations and the corresponding calibration curve of current versus glucose concentration are presented in figure 4.25D. In the figure, curve a, b and c represents the linear fit calibration curves for 5%, 10% and 15% NiO-MWCNTs/GCE, respectively. At an applied potential 50 mVs^{-1} and 0.1 M NaOH solution with the addition of 0.5 mM glucose at each interval, the 5% and 10% NiO-MWCNTs/GCE shows linear response range up to 15 mM glucose concentration with the regression equation being Ipa (μA) = 27.588 + 0.7596c (μM) and Ipa (μA) = 21.447 + 0.2680c (μM), with linear regression coefficient (R^2) of 0.9967 and 0.9967 respectively. However, at similar conditions 15% NiO-MWCNTs/GCE shows linear response range up to 7 mM glucose concentration with the regression equation *Ipa* (μA) = 27.588 + 0.7596c (μM) and corresponding linear regression coefficient (R^2) value found to be

0.996. The sensitivity for these electrode sensors were found to be 7068 $\mu Acm^{-2}mM^{-1}$, 4580 $\mu Acm^{-2}mM^{-1}$ and 2528 $\mu Acm^{-2}mM^{-1}$ for 10%, 5% and 15% NiO-MWCNTs/GCE and corresponding LOD was found to be 0.5 μM, 14 μM and 80 μM, respectively. The obtained sensor results were compared with the latest reports of non-enzymatic glucose sensors and tabulated in Table 4.6. From the table, it is clear that the sensitivity of the proposed sensor is higher than most of the previous studies.

4.5.3 Selectivity, Reproducibility and Stability of 10% NiO-MWCNT/GCE

Selectivity is another important parameter for a glucose sensor. We tested the glucose specificity for 10% NiO-MWCNTs/GCE by comparing its sensitivity towards glucose versus other potentially interfering analytes, namely AA, UA, D-lactose, sucrose, Trp and D-fructose, which generally co-exists with glucose in the human body (Figure 4.26A). Given that the normal physiological level of glucose is substantially higher than the analytes. We studied the chronoamperometric response of the sensor by adding 2 mM of glucose and other interference at the scan rate of 0.5 V. Negligible current response was observed for these analytes, comparing to glucose addition. The results indicate excellent specificity of the 10% NiO-MWCNTs/GCE arrayed sensor.

The stability of the 10% NiO-MWCNTs/GCE sensor is investigated over a 40-day period. The oxidation current of glucose exhibits a sharp drop to about 85% of the initial response after 3 weeks due to the absence of some NiO-NPs. However, the current response remains relatively stable throughout the rest of the 40-day period, implying a long-term stability of the sensor (Figure 4.26B).

Table 4.6 Analytical performance comparison of proposed NiO-MWCNT/GCE with reported MWCNT based non-enzymatic glucose sensors.

Type of electrode	Linear range (up to mM)	Detection limit (µM)	Detection potential (V)	Sensitivity ($\mu A\ mM^{-1}\ cm^{-2}$)
NiO/MWCNTs/Ta Hsieh et al. 2007	7.0	2.0	0.50	1.77
CS-GA-GOx-Nafion-PtPd–MWCNT Chen et al. 2012	14.0	31.0	0.60	112.00
Ni-multi-wall CNT Sun et al. 2012	17.5	0.89	0.60	67.20
MnO_2/MWNTs Chen et al. 2008	28.0	N.A.	0.30	34.19
Pt–Pb/CNTs Cui et al. 2007	0.5	1.8	0.30	18.00
Cu /MWCNTs Kang et al. 2007	4.5	0.21	0.65	17.76
Cu/Au/CNT Lu et al. 2012	0.5	0.3	0.65	NA
NiO-MWCNT/CPE (**section 4.4 result**)	14.0	23.0	0.50	6527.00
NiO-MWCNT/GCE (Present work)	**15.0**	**0.5**	**0.50**	**7068.00**

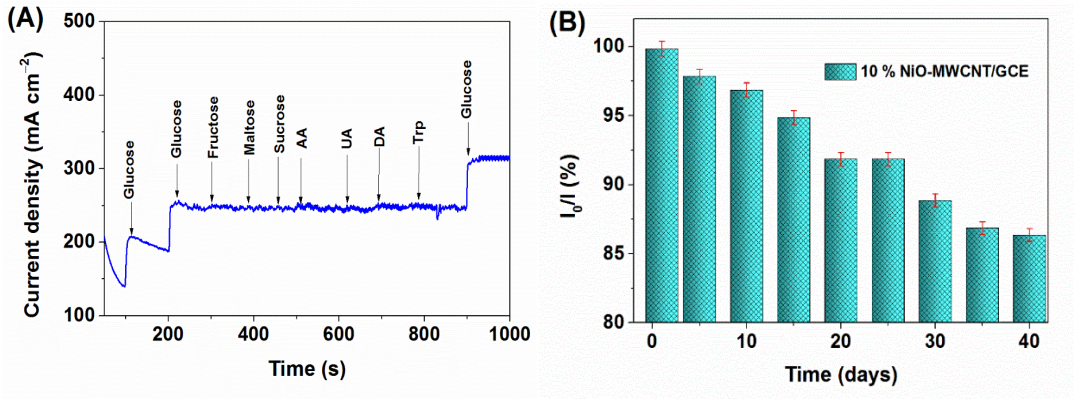

Figure 4.26 (A) Chronoamperometric response of the 10% NiO-MWCNT/GCE electrode on successive addition of 2 mM of glucose, fructose, maltose, sucrose, DA, UA, UA, AA and Trp into 0.1 M NaOH solution and (B) Stability plot for 10% NiO-CNT/CPE sensor stored over three weeks in 0.1 M NaOH with 2 mM glucose at 0.5 V.

Finally, as a real application, the 10% NiO-MWCNTs/GCE was further employed to detect glucose in human blood serum. HBS was injected into 5 mL of 0.1 M NaOH and the measurement was conducted at an applied potential of +0.5 V. The measured current change was correlated with the glucose concentration according to the calibration curve in figure 4.25D and then compared with the values obtained using a commercial glucose meter. As shown in Table 4.7, good accuracy along with the high precision (low RSD) demonstrates the reliability of 10% NiO-MWCNTs/GCE based non-enzymatic glucose sensor for the detection of HBS.

Table 4.7 The detection of glucose concentration in HBS at an applied potential of +0.5 V vs. commercial glucometer.

Sample	Glucose concentration (mM) from our glucose sensor	RSD* (%) (N = 5)	Glucose Conc. (mM) from commercial glucose meter	Actual Glucose Concentration (mM)	Accuracy (%)
1	6.36	5.1	6.3	6.30	99.9
2	6.37	6.5	6.5	6.40	99.5
3	6.68	5.5	6.5	7.00	95.4
4	6.50	4.7	6.4	6.40	98.5
5	7.66	4.6	7.8	7.20	92.7

The obtained results like sensitivity, detection limit, linear range and working potential of the fabricated sensor was compared with the previously reported sensors are tabulated in the Table 4.6. From the tabulated results, it is observed that 10% NiO-MWCNT/GCE sensor has highest sensitivity than any other reported sensors and works at low potential of 0.5 V. Apart from this, sensor also shows competitively low detection limit and linear range. Hence, easy fabrication procedure, fast response, high catalytic activity and good specificity favour the 10% NiO-MWCNTs/GCE as a potential electrode material for non-enzymatic glucose sensors fabrication.

4.5.4 Comparison of NiO-MWCNTs based CPE and GCE towards Glucose Sensing

To finalise the best type of electrode (CPE or GCE) towards glucose sensing, results obtained from NiO-MWCNTs/CPE and NiO-MWCNTs/GCE were compared. The three-different wt.% materials like 5%, 10% and 15% NiO-MWCNTs composite materials on CPE and GCE modified electrodes show similar behaviour. Among these three materials 10% NiO-MWCNTs shows best sensing features in both type of

electrode. Hence, in this section we are comparing the results of 10% NiO-MWNCTs CPE and 10% NiO-MWNCTs/GCE for glucose sensing are tabulated in table 4.8.

Table 4.8 Glucose sensing results comparison for 10% NiO-MWNCTs/CPE and 10% NiO-MWNCTs/GCE.

Sl. No.	Parameters	10% NiO-MWNCTs/ CPE	10% NiO-MWNCTs/GCE
1.	**Electrolyte**	0.2 M NaOH	**0.1 M NaOH**
2.	**Scan rate**	50 mV s^{-1}	50 mV s^{-1}
3.	**CV oxidative peak potential**	0.5 V	0.5 V
4.	**CA working potential**	0.5 V	0.5 V
5.	**Response time**	0.3 s	0.3 s
6.	**Sensitivity**	6540 mA cm^{-1} mM^{-1}	**7068 mA cm^{-1} mM^{-1}**
7.	**LOD**	12.0 μM	**0.5 μM**
8.	**Selectivity**	Yes	Yes
9.	**Stability**	30 days (> 80% response retain)	**40 days (> 85% response retain)**

From the tabulated results, it is observed that the sensitivity, electrolyte concentration, LOD and stability of the 10% NiO-MWCNTs/GCE is greater than NiO-MWCNTs/CPE. Due to its easy electrode fabrication and lesser electrode material required to construct the modified electrodes the GCE has several advantages over CPE. Though, the CPE modified sensor also shows good response towards glucose sensing, because of its fabrication method, like use of inert silicon oil as a binder, mechanical mixing and possibility of maximum electrode material appear on the surface is minimal.

Hence, lesser catalytic activity can be expected in CPE modified electrode in comparison with the GCE modified electrode. Therefore, GCE modified electrodes were used in our further studies.

4.6 COPPER OXIDE MULTI-WALLED CARBON NANOTUBE COMPOSITES (CuO-MWCNTs)

4.6.1 Characterization of CuO-MWCNTs Composites

The surface morphology of the synthesized CuO-MWCNTs composite was examined using FESEM and TEM analysis. Figure 4.27 represents the FESEM image of the purified MWCNTs in comparison with the CuO-MWCNTs, pure CuO particles (Figure 4.27 A, B and C) and corresponding particle size distribution histograms (Figure 4.27 D, E and F) respectively. An overview of the FESEM result shows that the sidewalls and tips of the unmodified MWCNTs are clean and relatively smooth indicating the purity of MWCNTs (Figure 4.27A) with an average diameter of 5.16 nm for MWCNT (Figure 4.27D). However, these pure MWCNTs which on decoration with CuO-NPs via solvent-free thermal decomposition of copper formate precursor, the surface of the MWCNTs gets rough and thicker, due to several granular CuO-NPs (Figure 4.27B) with an average particle size of 7.4 nm (Figure 4.27E) attached to the surface of the MWCNTs. For comparison studies, the pure CuO particles (Figure 4.27C) were synthesized by similar method and appears to be granular in nature with an average particle size of 7.5 nm (Figure 4.27F). The similar size and shape of CuO-NPs observed in both pure CuO and CuO-MWCNT composite can be attributed to the stable and consistent CuO-NPs synthesis.

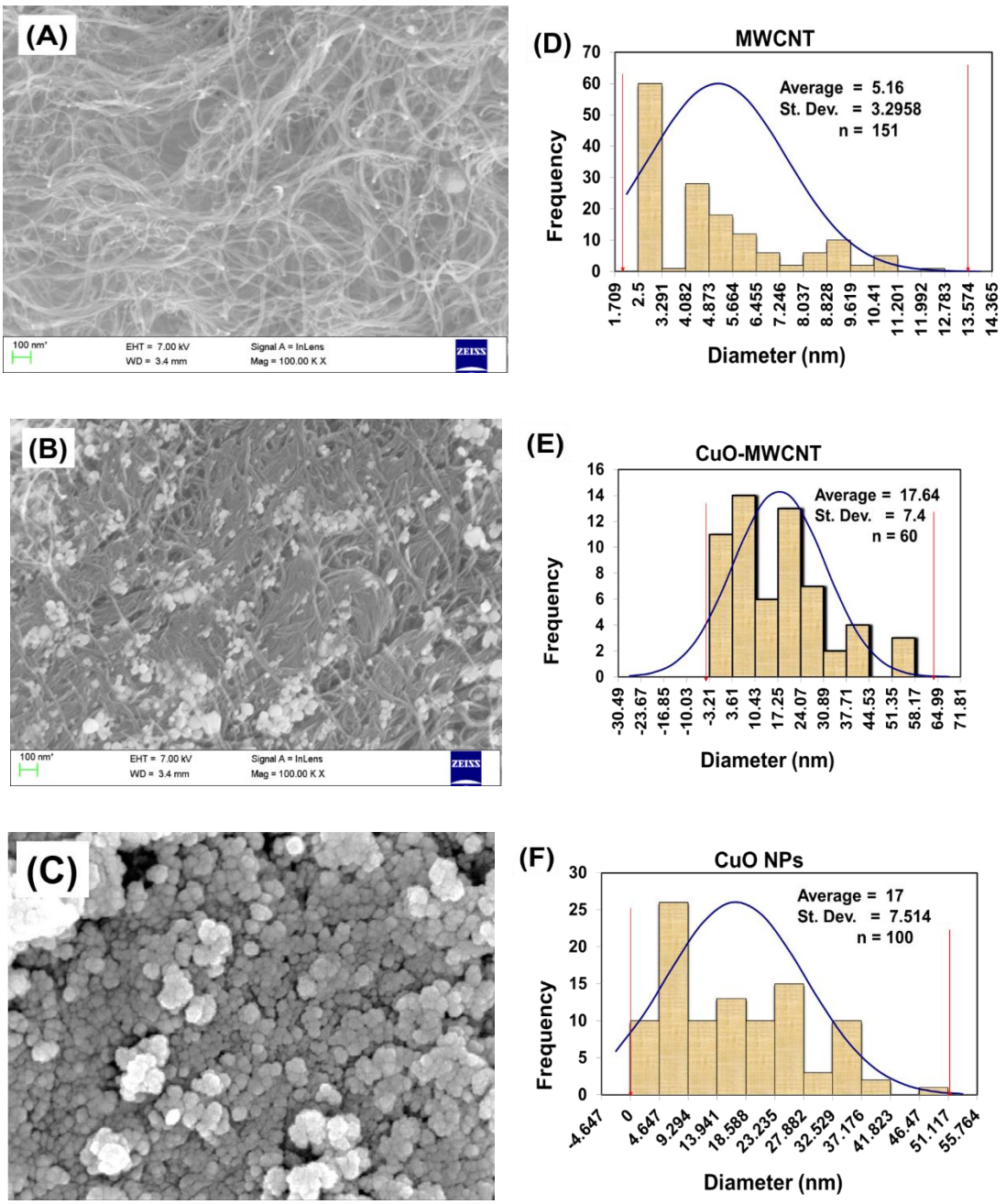

Figure 4.27 FESEM images of (A) unmodified pure MWCNTs, (C) CuO-MWCNT composite, (E) pure CuO-NPs and their respective particle size distribution histogram (B) MWCNTs, (D) CuO-MWCNT composite and (F) pure CuO-NPs.

Further, the morphology of the synthesized CuO-MWCNTs composite sample was confirmed by TEM analysis. Figure 4.28 represents the TEM image of the 10% CuO-MWCNTs composite. The TEM micrograph shows that dark stain on the MWCNTs surface which is attributed to the CuO-NPs wrapping around the MWCNTs

with an average particle size of 7 nm and these results resembles well with the FESEM results.

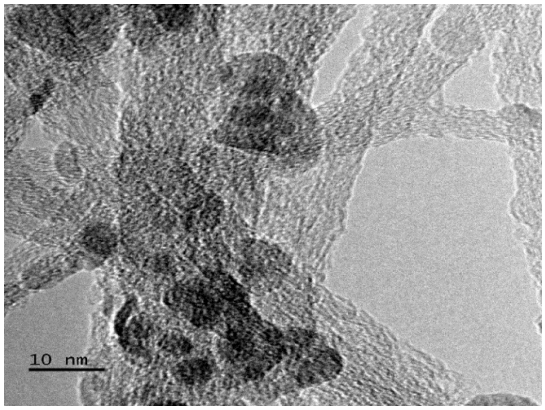

Figure 4.28 TEM micrograph of 10% CuO-MWCNTs composite.

Energy dispersive X-ray (EDXA) analysis was carried out to confirm the elemental compositions. Figure 4.29 depicts the EDXA spectrum of the CuO-MWCNTs composites. The spectrum reveals that the synthesized composite material consists of elements like carbon, oxygen, copper only and the corresponding weight percentage and elemental ratio (atomic %) were tabulated in the inset table of figure 4.29. These results confirm the formation of the CuO-MWCNTs composites. No other elemental peak was observed in the EDX spectrum which indicates the purity of the composite.

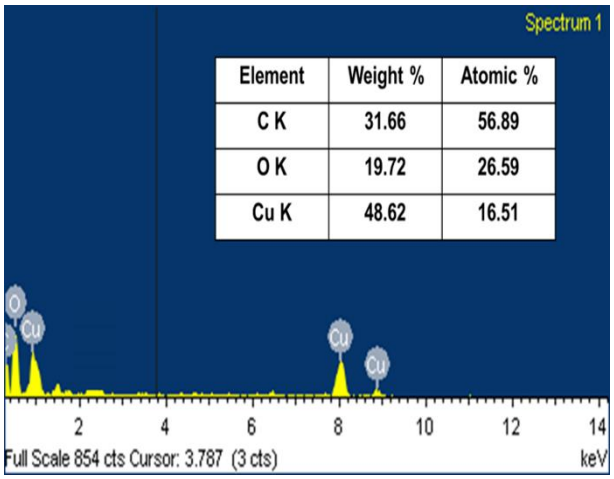

Figure 4.29 EDXA spectrum of CuO-MWCNT composites. (Inset: table consisting percentage component of each element present in the EDXA spectrum).

The samples were further characterized by PXRD technique. Figure 4.30 depicts the PXRD spectrum of MWCNTs, CuO and CuO-MWCNT nanocomposites. The PXRD pattern shows the distinct CuO characteristic diffraction peaks for CuO particles and CuO-MWCNT composite at 32.5°, 35.5°, 38.9°, 48.7°,54.4°, 58.3°,61.5°, 66.2° and 68.1°, which can be indexed to the (110), (-111), (111), (-202), (020), (202), (-113), (-311) and (220) planes of the monoclinic tenorite CuO structure (JCPDS card no. 005-0661) (Wu et al. 2002). Besides this, there is a diffraction peak at 26.3° in a MWCNTs and CuO-MWCNT composite which is attributed to the (002) phase of the CNTs (Kim et al. 2012). The well-defined characteristic peaks corresponding to the MWCNT and CuO-NPs observed in the composite confirms the prepared CuO-MWCNT composite. No other peaks in PXRD spectra suggest high purity of the prepared samples. The above results confirm the preparation of CuO-NPs and CuO-MWCNT composite.

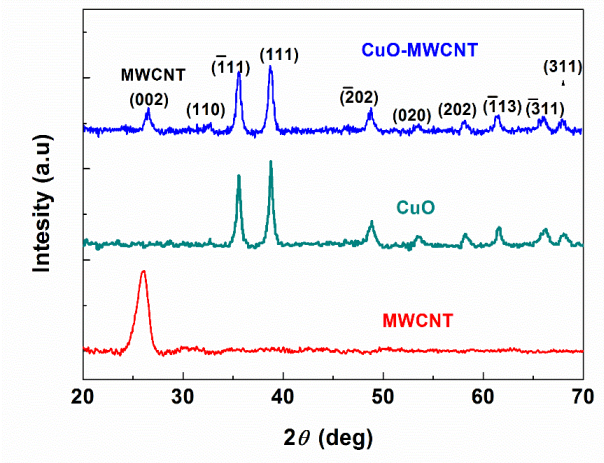

Figure 4.30 PXRD spectra of unmodified pure MWCNTs, CuO and CuO-MWCNTs.

Raman spectra was analysed to study the defects in the MWCNTs before and after the composite synthesis. Figure 4.31 illustrates the Raman spectra of MWCNTs and CuO-MWCNTs, where in the characteristic peaks of MWCNTs such as, D-band and G-band are observed at 1590 cm^{-1} and 1346 cm^{-1}, respectively. The G-band appears from the vibrations of the sp^2 bonded carbon atoms of two-dimensional hexagonal lattice in graphite and D-band peak corresponds to the defects introduced in

the structure during composite synthesis (Kim et al. 2014). Generally, value of (I_D/I_G) indicates the quality of the MWCNTs (Dillon et al. 2004, He et al. 2007). In this case, increase in I_D/I_G ratio from 0.83 to 1.43 for MWCNTs and CuO-MWCNTs nanocomposites was observed. The significant raise in I_D/I_G value suggests that the more defects were introduced to the smooth surfaced MWCNTs, which may be due to the destructive interaction of the CuO-NPs with the surface of MWCNTs. Hence, from the obtained results the formation of composite can be confirmed.

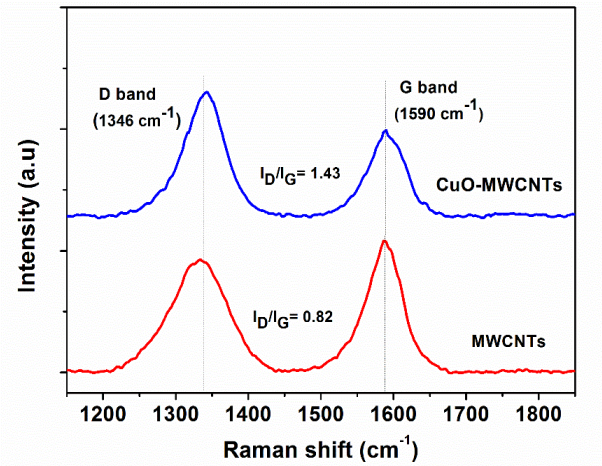

Figure 4.31 Raman spectra of purified MWCNT and CuO-MWCNTs composite.

To obtain the optimized composite ratio with high catalytic activity, we further synthesized the CuO-MWCNT with different weight ratio by varying the copper precursor load during composite synthesis. Figure 4.32 represents the FESEM images of different weight ratio of CuO-MWCNTs composites synthesized. The overview of the FESEM results shows that as the precursor load increases from 5% to 20%, the nature of CuO-NPs formed on the surface of MWCNTs also differs. The 5% CuO-MWCNT (Figure 4.32A) shows uniform distribution of CuO-NPs with an average particle size of 8 nm. However, the greater surface area of the MWCNTs are vacant sites without any CuO particles, which may be due to the lesser precursor load. Similarly, in case of 10% CuO-MWCNTs (Figure 4.32B) shows the uniform distribution of CuO-NPs with an average particle size of 7.5 nm and no vacant site on the surface of MWCNTs. This confirms the optimized ratio to synthesize the CuO-MWCNTs composites. Figure 4.32 (C and D) represents the 15% and 20% CuO-

MWCNTs, where in which the CuO particles were decorated uniformly on the surface of MWCNTs. However, due to the excess precursor load the CuO particles formed got agglomerated and expected to possess lesser catalytic activity. An overview of these analysis shows that, agglomeration is more in case of 20% sample compared with the 15% as expected. Hence, from the FESEM results it is observed that, among all the different ratio of CuO-MWCNTs composites, the 10% CuO-MWCNTs composite shows maximum and uniform CuO-NPs decorated on MWCNTs surface with least or no agglomerated particles and hence is considered as optimized ratio.

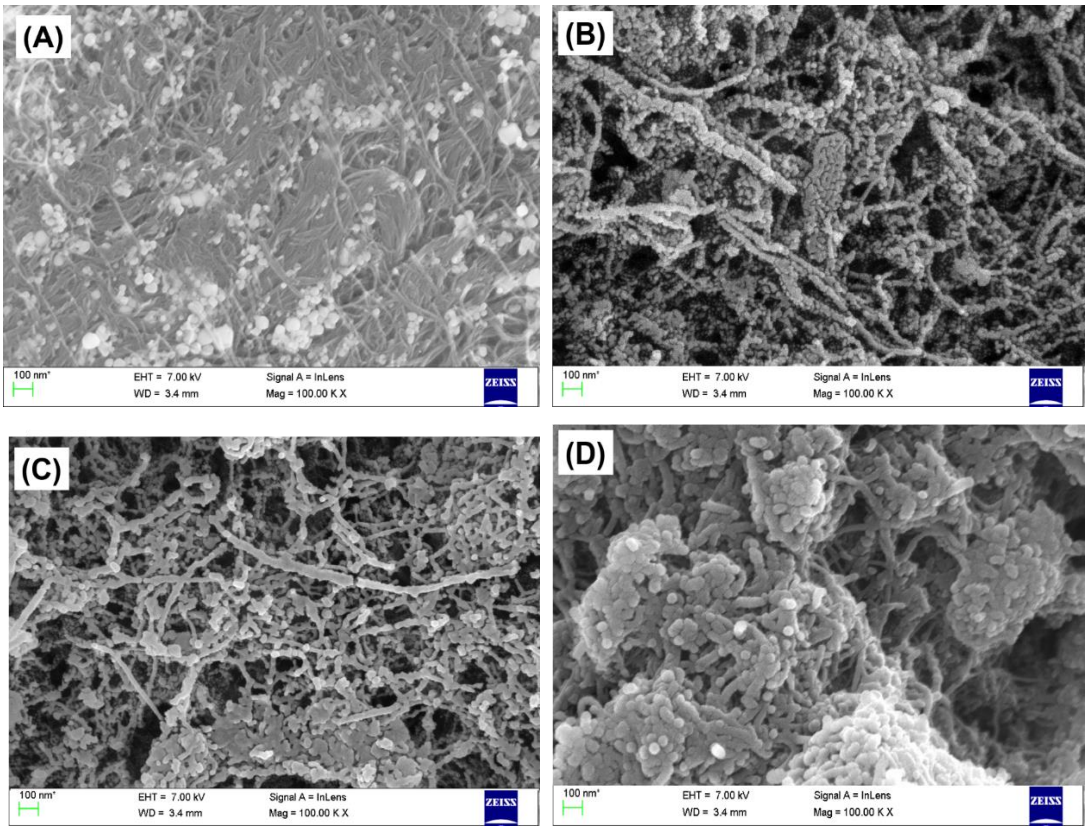

Figure 4.32 FESEM images of (A) 5% CuO-MWCNTs, (B) 10% CuO-MWCNTs, (C) 15% CuO-MWCNTs and (D) 20% CuO-MWCNTs.

Further these different wt.% composite prepared were confirmed by PXRD analysis. Figure 4.33 represents the PXRD pattern for different wt.% composites such as (a) 5% CuO-MWCNTs, (b) 10% CuO-MWCNTs, (c) 15% CuO-MWCNTs and (d) 20% CuO-MWCNTs respectively. An overview of the PXRD spectrum shows, well defined diffraction peak at 26.3° which originates from the (002) plane of hexagonal

graphite and the diffraction peaks at 32.5°, 35.5°, 38.9°, 48.7°, 54.4°, 58.3°, 61.5°, 66.2° and 68.1°, which can be indexed to the (110), (-111), (111), (-202), (020), (202), (-113), (-311) and (220) planes of the monoclinic tenorite CuO structure with the JCPDS card no. 005-0661. It is also observed that with the raise in precursor load (from 5% to 20%) it leads to decrease in intensity of the (002) reflection of carbon diffraction peak at 26.3°, suggesting the formation of different wt.% of CuO-MWCNTs composite materials.

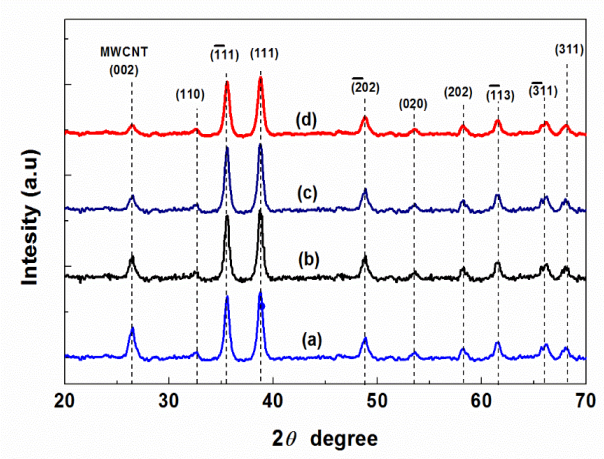

Figure 4.33 PXRD spectrum of (a) 5% CuO-MWCNT (b) 10% CuO-MWCNT (c) 15% CuO-MWCNT and (d) 20% CuO-MWCNT.

In addition, Raman spectra were also analyzed to confirm the different wt.% composite formation. Figure 4.34 represents Raman spectra for different wt.% composite such as 5% CuO-MWCNTs (a), 10% CuO-MWCNTs (b), 15% CuO-MWCNTs (c) and 20% CuO-MWCNTs (d), respectively. From the obtained Raman spectra, it is observed that, with the rise in precursor load the intensity of I_D/I_G ratio also increases from 1.09 (5% CuO-MWCNT) to 1.2 (10% CuO-MWCNT), 1.36 (15% CuO-MWCNT) and 1.5 (20% CuO-MWCNT). This increase in I_D/I_G ratio for composite can be attributed to the destructive interaction of CuO-NPs with the surface of MWCNTs. In composites, with increase in precursor load larger surface get interacted with the copper and more defects were introduced. Thus, higher I_D/I_G value obtained in case of 20% CuO-MWCNTs in comparison with the 5%, 10% and 15 % CuO-MWCNTs. These results confirm the prepared different wt.% of CuO-MWCNTs composite.

Hence, from all the above characterization techniques, it is observed that the products formed are consistent, with uniformly distributed NPs over the surface of MWCNTs, which supports the use of metal formate as precursor for composite synthesis.

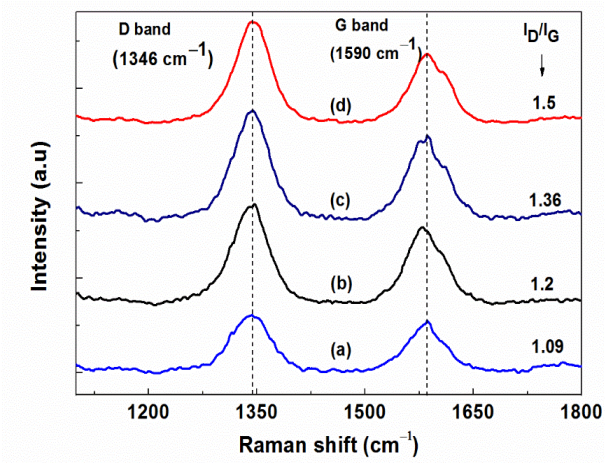

Figure 4.34 Raman spectrum of (a) 5% CuO-MWCNTs, (b) 10% CuO-MWCNTs, (c) 15% CuO-MWCNTs and (d) 20% CuO-MWCNTs.

4.6.2 Cyclic Voltammetry behaviour of CuO-MWCNT/GCE Modified Electrodes towards Glucose Sensing

The electro-catalytic activities of the pure MWCNTs electrode (MWCNT/GCE), CuO electrode (CuO/GCE) and the CuO-MWCNTs electrode (CuO-MWCNT/GCE) were investigated using CV in 0.2 M NaOH solution with and without 2.0 mM glucose at 50 mV s^{-1}, as shown in figure 4.35 (A and B). In the presence of 2 mM glucose the MWCNT/GCE shows the enhanced current as compared to cyclic voltagram without addition of glucose (Figure 4.35A). Similarly, in the absence of glucose, the CuO/GCE and CuO-MWCNT/GCE shows low current response (Figure 4.35B, curve d and f). However, in the presence of 2.0 mM glucose, the MWCNTs/GCE records only a negligible response, but a significant increase in current, with well-defined oxidation peak observed at +0.35 V and +0.48 V for CuO/GCE and CuO-MWCNT/GCE, respectively (Figure 4.35B, curve g), which is due to the Cu^{2+}/Cu^{3+} redox couple (Wu et al. 2010, Alizadeh and Mirzagholipur 2014). However, upon addition of 2.0 mM glucose, a significant increase in anodic current signal, corresponding to the irreversible glucose oxidation, was observed in the potential range

of 0.30–0.65 V. This increase of current suggests the significant catalytic activity of CuO-MWCNT/GCE towards glucose oxidation. Substantial higher current recorded for CuO-MWCNT/GCE electrode than the CuO/GCE electrode in response to the glucose oxidation (Figure 4.35B), can be attributed to the larger surface area provided by MWCNTs and the higher electro-catalytic active sites owing to the CuO nanostructures. All these results illustrate that the electro-catalytic performance towards the oxidation of glucose has been greatly improved due to the synergetic effect of CuO and MWCNTs.

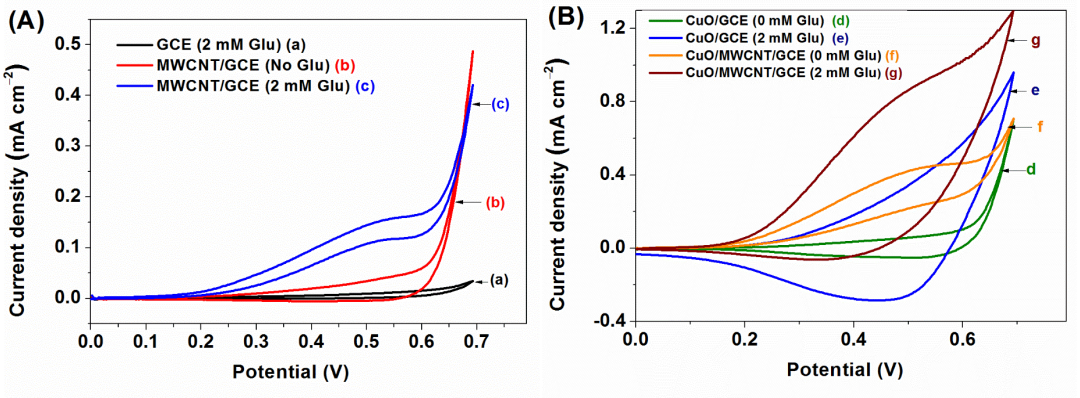

Figure 4.35 (A) Cyclic voltammograms of bare GCE (curve a), MWCNT/GCE (curve b and c), (B) Cyclic voltammograms of CuO/GCE (d, e) and CuO-MWCNT/GCE (f, g) in the absence and presence of 2.0 mM glucose in 0.2 M NaOH. Scan rate: 50 mV s^{-1}.

The plausible mechanism for oxidation of glucose by CuO-based materials could be represented by the following reactions.

$$CuO + OH^- \rightarrow CuOOH + e^- \; (Cu(II) \rightarrow Cu(III)) \qquad (4.8)$$

$$CuOOH + glucose \rightarrow CuO + Glucolactone \; (Cu(III) \rightarrow Cu(II)) \qquad (4.9)$$

First, Cu^{2+} could be electro-oxidized to Cu^{3+} in 0.2 M NaOH solution where the release of electron resulted in the formation of oxidation peak current (Eq. (4.8). Then, glucose ($C_6H_{12}O_6$) could be oxidized to glucolactone by Cu^{3+} which itself reduces to Cu^{2+} (Eq. 4.9) at the same time. Hence, the presence of glucose could lead to an increase in current (Wu et al. 2010, Alizadeh and Mirzagholipur 2014).

Further, the effect of scan rate was investigated for glucose oxidation at CuO-MWCNT/GCE at different scan rate ranging from 25 mV s^{-1} to 200 mV s^{-1} with 2 mM glucose concentration in 0.2 M NaOH using CV as illustrated in the figure 4.36. From the figure 4.36A, it is observed that, anodic peak current (I_{pa}) increases with increasing scan rates, which is due to the glucose oxidation. However, the anodic peak current (I_{pa}) is found to be proportional to the square root of the scan rate (Figure 4.36B) and the linear relationship between *Ipa* and square root of scan rate (ν) was found to be *Ipa* (mV) = 0.3311ν -1.408 with linear regression value R^2=0.9947. Hence, these results illustrate that the electrochemical kinetics are diffusion controlled and it can be an ideal case for the quantitative analysis in practical application.

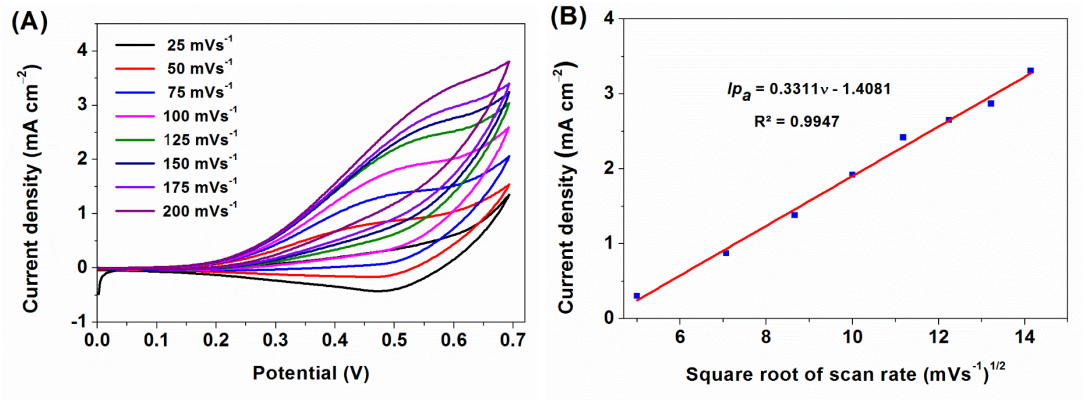

Figure 4.36 (A) Cyclic voltammograms of CuO-MWCNT/GCE at different scan rates from 25 mV s^{-1} to 200 mV s^{-1} in 0.2 M NaOH with 2.0 mM glucose and (B) Variation of anodic current peak with the square root of scan rate.

The surface coverage of the electrode (Γ*) was evaluated from the area under the cathodic peak of the CV (Q) for the CuO-MWCNT/GCE (68.4940 µC) and CuO/GCE (0.7668979 µC) electrodes. This is defined by the Faraday's law [$Q=nFA\Gamma$*], where Q is the integration charge of the reduction peak, A is the area of the electrode (0.07 cm^{-2}), n is the number of electrons transferred and F is the Faraday constant (Sharifi et al. 2014). The surface coverage value of (Γ*) was found to be of 1.014×10^{-8} mol cm^{-2} and 1.135×10^{-10} mol cm^{-2} for CuO-MWCNT/GCE and CuO/GCE respectively. These results suggest that, in the presence of MWCNTs the CuO-NPs significantly enhances electrode peak current in the CuO-MWCNT/GCE,

electrode in comparison with the CuO/GCE, which can be attributed to the large specific surface area offered by the MWCNT.

The Laviron's equation was used to calculate the kinetic parameters of charge transfer coefficient (α) and apparent charge transfer rate constant (*Ks*) by measuring the variation of peak potential with scan rate by using Eqn. (4.7) (Wang et al. 2013).

$$\log k_s = \alpha \log(1-\alpha) + (1-\alpha)\log \alpha - \log \frac{RT}{nF\vartheta} - \frac{(1-\alpha)\alpha\, nF\Delta Ep}{2.3RT} \quad (4.7)$$

where α is the electron transfer coefficient, n is the number of electrons, ΔEp is the peak-to-peak separation of redox peaks, ν is the scan rate, R is gas constant (8.314 J mol^{-1} K^{-1}), T is the temperature (298 K) and F is the Faraday's constant (96,493 C mol^{-1}). The value of αn was calculated to be 0.52, given $0.3 < \alpha < 0.7$ (Laviron 1979), it could be concluded that n =1 and α = 0.52. The electron transfer rate constant (*ks*) of CuO-MWCNT/GCE is calculated as 1.31 s^{-1}, indicating fast electron transfer kinetics. This increase in efficiency and faster direct electron transfer can be attributed to the larger active surface area offered by the synergistic effect of CuO-NPs and MWCNTs in nanocomposite.

4.6.3 Chronoamperometry response of CuO-MWCNT/GCE towards Glucose Sensing

The chronoamperometric responses of the fabricated electrodes were recorded to further investigate the electro-catalytic activity towards the direct glucose oxidation. Due to the well-known fact that the detection potential strongly affects the chronoamperometric response of a biosensor, we systematically investigated the optimal applied potential to obtain maximum catalytic current. Figure 4.37A shows the chronoamperometric responses measured to investigate the electro-catalytic activity of CuO-MWCNT/GCE towards drop wise addition of 0.1 mM glucose under different applied potentials from +0.2 V to +0.6 V in 0.2 M NaOH. As observed from figure 4.37A, the current response was very low at potentials lesser than 0.3 V and it is increased to about four-fold at +0.40 V while it reached the maximal value at +0.6 V. However, at 0.6 V, the current recorded was unstable and more of noise was observed

which may be due to oxidization of unwanted species or intermediate interfering species at high potentials. Hence, 0.5 V was selected as an optimal applied potential for further chronoamperometric studies which matches well with the peak anodic oxidation potential (Figure 4.35B) obtained from CV measurement.

The chronoamperometric responses of as constructed electrodes like MWCNT/GCE, CuO/GCE and CuO-MWCNT/GCE for successive addition of 0.5 mM glucose at 100 s intervals in 0.2 M NaOH at optimal potential of +0.5 V are compared in figure 4.37B. At 0.5 V, MWCNT/GCE shows no current response with the glucose addition, whereas a well-defined, significantly larger current response was recorded for CuO/GCE and CuO-MWCNT/GCE. From the figure 4.37B it is also observed that current response recorded for CuO-MWCNT/GCE is three-fold (46 %) greater than that of the CuO/GCE with the incremental addition of glucose (0.5 mM) and reaches the 95% of the steady-state current less than ~4 s (Figure 4.37C) indicating that the composite sample efficiently enhances the catalytic oxidation of glucose than the individual. Further the calibration curve plotted for the electrochemical responses recorded at CuO-MWCNT/GCE electrode towards glucose concentration range is shown in figure 4.37D. The sensor shows a sensitivity of 3530.47 μA mM^{-1} cm^{-2} and a detection limit of 0.3 μM for the linear range up to 18 mM glucose concentration with a correlation coefficient of R^2=0.9946 which is much higher than the many other reported sensors. The proposed sensor was compared with the previously reported nanomaterial based enzyme-free glucose sensors as shown in Table 4.9. As it can be seen from the table, the CuO-MWCNT sensor shows highly enhanced sensitivity and low limit of detection due to the excellent catalytic activity of CuO-NPs and the electrical network formed through self-assembled CuO-NPs distributing on the surface of MWCNT, which not only can keep the intrinsic electrical conductivity but also facilitates faster glucose oxidation. This is due to the synergetic effect of the CuO and MWCNTs, which facilitates larger active surface area and high catalytic activity towards glucose oxidation. Therefore, the CuO-MWCNT composite material is promising for fabrication of enzyme-free glucose sensor.

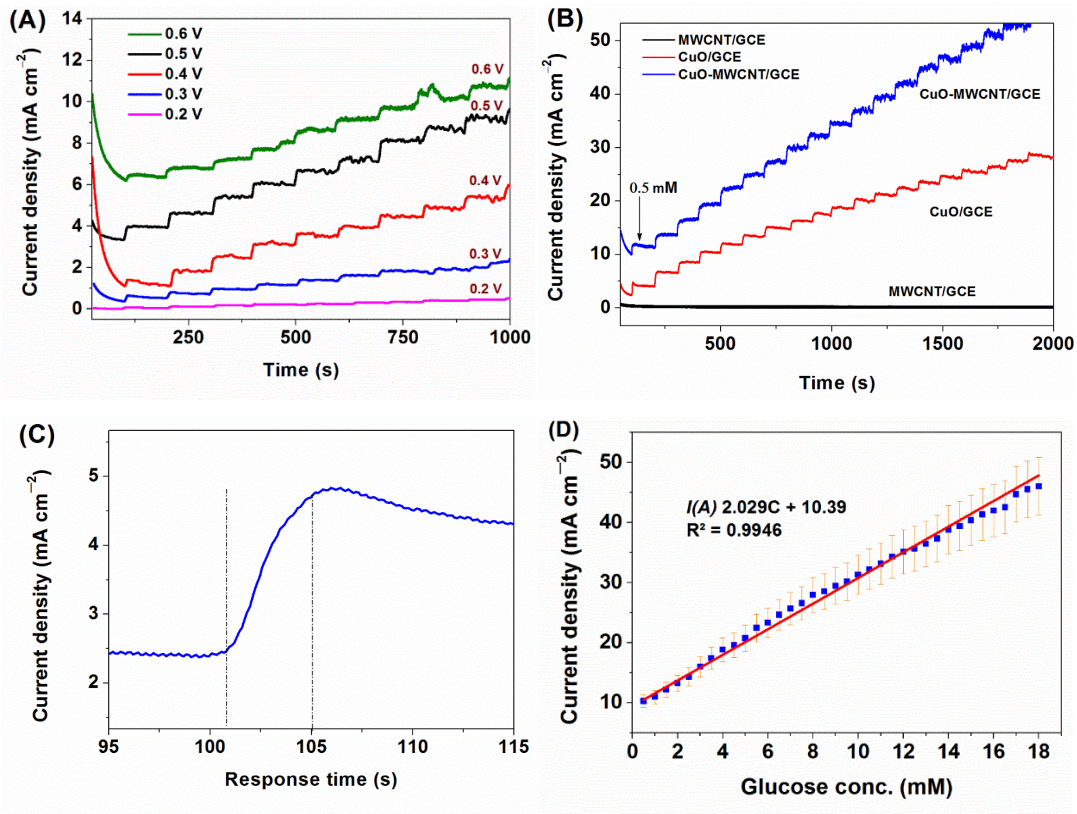

Figure 4.37 (A) Chronoamperometric responses of CuO-MWCNT/GCE at different potentials in 0.2 M NaOH with a dropwise addition of 0.1 mM glucose at 100 s intervals, (B) Current–time responses at +0.5 V with an increasing glucose concentration of 0.5 mM per 100 s for the MWCNTs/GCE, CuO/GCE and CuO-MWCNTs/GCE (C) Response time curve for CuO-MWCNTs/GCE addition of 0.5 mM of glucose and (D)The dependence of the current response vs. glucose concentration at CuO-MWCNTs/GCE. Error bars indicate standard deviations of three measurements.

Table 4.9 Comparison of analytical performance of proposed CuO-MWCNT/GCE electrode with reported MWCNT based non-enzymatic glucose sensors.

Electrode type	Sensitivity ($\mu A\ mM^{-1}\ cm^{-2}$)	Linear range (mM)	LOD (µM)	Working potential (V)
Gold nanoparticles electrode (Jena and Raj 2006)	179.0	8.0	0.05	+0.16
Cu nanocluster /MWCNTs/GCE (Kang et al. 2007**)**	254.0	4.5	0.21	+0.65
Gold nanowire array electrode (Cherevko and Chung 2009)	309.0	10.0	50.0	−0.40
CuONR-graphite electrode (Wang et al. 2010)	371.4	8.0	4.0	+0.60
CuO NS electrode (Reitz et al. 2008)	404.5	2.6	1.0	+0.60
Ni-CNF paste electrode (Liu et al. 2009)	420.4	2.5	1.0	+0.60
SA-CNT thin films with Cu-NPs electrode (Li et al. 2009)	602.0	1.8	0.1	+0.55
Ni NW array electrode (Lu et al. 2009)	1043.0	7.0	0.1	+0.55
CuO-MWCNTs array Electrode (Yang et al. 2010a)	2190.0	4.0	0.8	+0.55
CuO-MWCNT/GCE (Present work)	**3530.0**	**18.0**	**0.3**	**+0.50**

4.6.4 Selectivity, Stability and Reproducibility of the CuO-MWCNT/GCE

Many biomolecules like fructose, lactose, maltose, AA and DA, etc., are generally the potentially interfering ions with human blood glucose and these may also get easily oxidized at the applied potential. Therefore, it is necessary to investigate if such interfering species could generate current responses that corresponding to glucose. Hence, for the CuO-MWCNT/GCE sensor, the interference effect was tested chronoamperometrically at +0.5 V as shown in figure 4.38A. It is observed from the figure 4.38A that current response obtained for 2 mM concentration of above said interfering species were less than 4% of that obtained for 2 mM glucose. Hence, these results indicate that CuO-MWCNT/GCE sensor is highly specific to glucose even in the presence of many common interference electro-active molecules. The long-term stability of the sensor was also investigated to evaluate the performance of the sensor by measuring its current response to glucose over three weeks during which only 15% loss in the current signal was observed (Figure 4.38B), suggesting greater stability of the sensor. Reproducibility of the sensor was also investigated for five similar electrodes with RSD of less than 5.0% suggesting the accuracy of the method (Figure 4.38C). The sensor was measured for its current response ten times for a single electrode upon the addition of 0.5 mM glucose in 0.2 M NaOH shows excellent reproducibility with RSD less than 4% (Figure 4.38D). These results suggest that proposed sensor has a high selectivity, greater stability and excellent reproducibility which makes the CuO-MWCNT composite a potential material for practical use in glucose sensor fabrication.

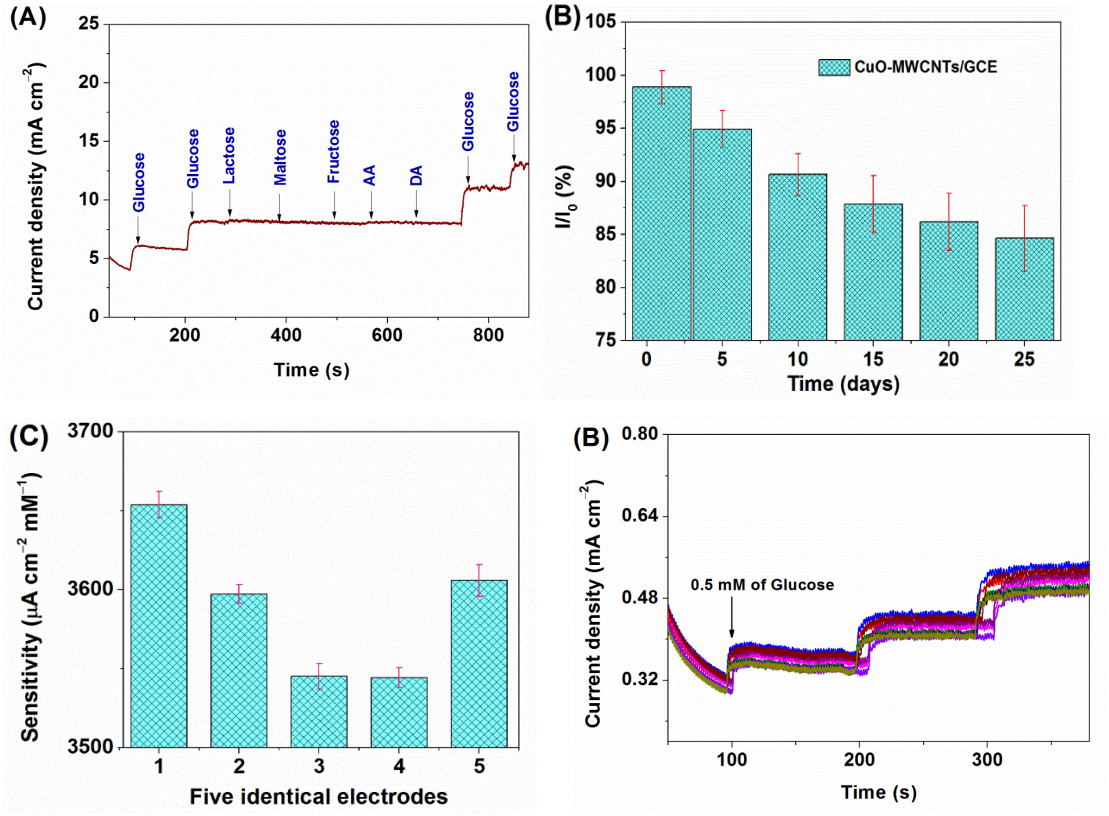

Figure 4.38 (A)Interference test of the sensor in 0.2 M NaOH at +0.50 V with 2.0 mM glucose and other interferons as indicated, (B) Stability of the sensor stored at ambient conditions over three weeks using 0.2 M NaOH with 2.0 mM glucose at +0.50 V, (C) The sensitivity of the five identical sensors (Average of three trails) and (D) the current response measured ten times for a CuO-MWCNT/GCE with the addition of 0.5 mM glucose in 0.2 M NaOH.

As a real application, the CuO-MWCNT/GCE was applied to the determination of glucose concentration in HBS. HBS was injected into 10 mL of 0.2 M NaOH at an applied potential of +0.5 V. The measured current change was correlated with the glucose concentration according to the calibration curve in figure 4.37D and then compared with the value obtained using a commercial glucose meter. As shown in Table 4.10, a good accuracy along with the high precision (RSD) demonstrates the reliability of CuO-MWCNTs in the application of enzyme-free glucose sensing. Hence, these results suggest that the proposed CuO-MWCNT composite is a potential material for the fabrication of enzyme-free glucose sensors.

Table 4.10 The detection of glucose concentration in HBS at an applied potential of +0.5 V.

Sample	Glucose (mM) (Proposed sensor)	RSD* (%) (*N* = 4)	Glucose (mM) (commercial glucose sensor)	Actual glucose Conc. added(Mm)	Accuracy %
1	4.8	4.5	4.9	5.0	96.0
2	5.6	6.2	5.5	5.4	96.3
3	7.2	4.7	7.0	7.0	97.1
4	6.6	4.5	6.7	6.6	100.0

*** Average of four trials**

4.7 SELF-ASSEMBLY SYNTHESIS OF Co_3O_4/MWCNTS COMPOSITES: AN EFFICIENT ENZYME-FREE GLUCOSE SENSOR

4.7.1 Morphologies and Structural Characterization

The prepared Co_3O_4-MWCNT composite were examined for their morphological, chemical compositional and structural aspects by using different analytical techniques. The surface morphology of the synthesized Co_3O_4-MWCNTs composite was characterized using FESEM and TEM analysis. Figure 4.39(A-C) represents the FESEM images of the pure MWCNTs, Co_3O_4/MWCNT composite and Co_3O_4, respectively. An overview of FESEM images shows that purified MWCNTs (Figure 4.39A) appear like a mesh on which Co_3O_4 NPs were decorated and these Co_3O_4-NPs also appear to wrap around the MWCNTs (Figure 4.39B). Co_3O_4 particles

synthesized using similar method appears to be granular particles in nature (Figure 4.39C). From these FESEM result, it is observed that Co_3O_4 NPs and its MWCNTs composites are similar in shape and size.

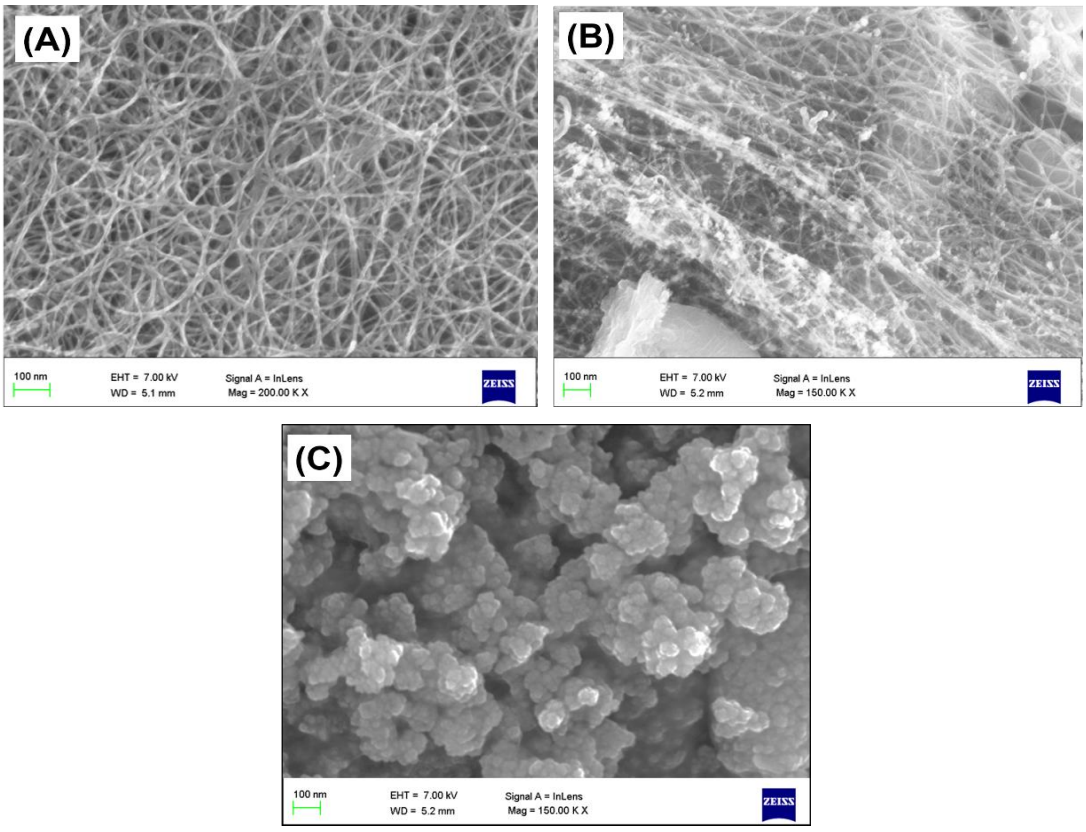

Figure 4.39 FESEM images of (A) pure MWCNT, (B) Co_3O_4-MWCNT composite and (C) Co_3O_4 NPs.

The TEM micrograph of synthesized carbon nanotubes were examined for further study of morphology as shown in figure 4.40. Result shows that carbon nanotubes were multiwall in nature and there were no impurities on the surface of the MWCNTs suggesting high purity of the synthesized sample (Figure 4.40A). Size distribution histogram of MWCNTs show average diameter of 8.09 nm and length of few microns (Figure 4.40B). However, the TEM micrograph of MWCNTs-Co_3O_4 composite shows dark spherical stain on the surface of the MWCNTs with an average size of 3 nm (Figure 4.40 C and D), which can be attributed to the self-assembled Co_3O_4-NPs on the surface of MWCNTs. The TEM micrograph of Co_3O_4-NPs synthesized appears to be granular in shape with average particle size of about 6.7 nm

(Figure 4.40E and F), which clearly suggested the formation of the Co_3O_4-NPs. Hence, from the morphological studies it can be concluded that Co_3O_4-NPs were uniformly decorated on the surface of the MWCNT.

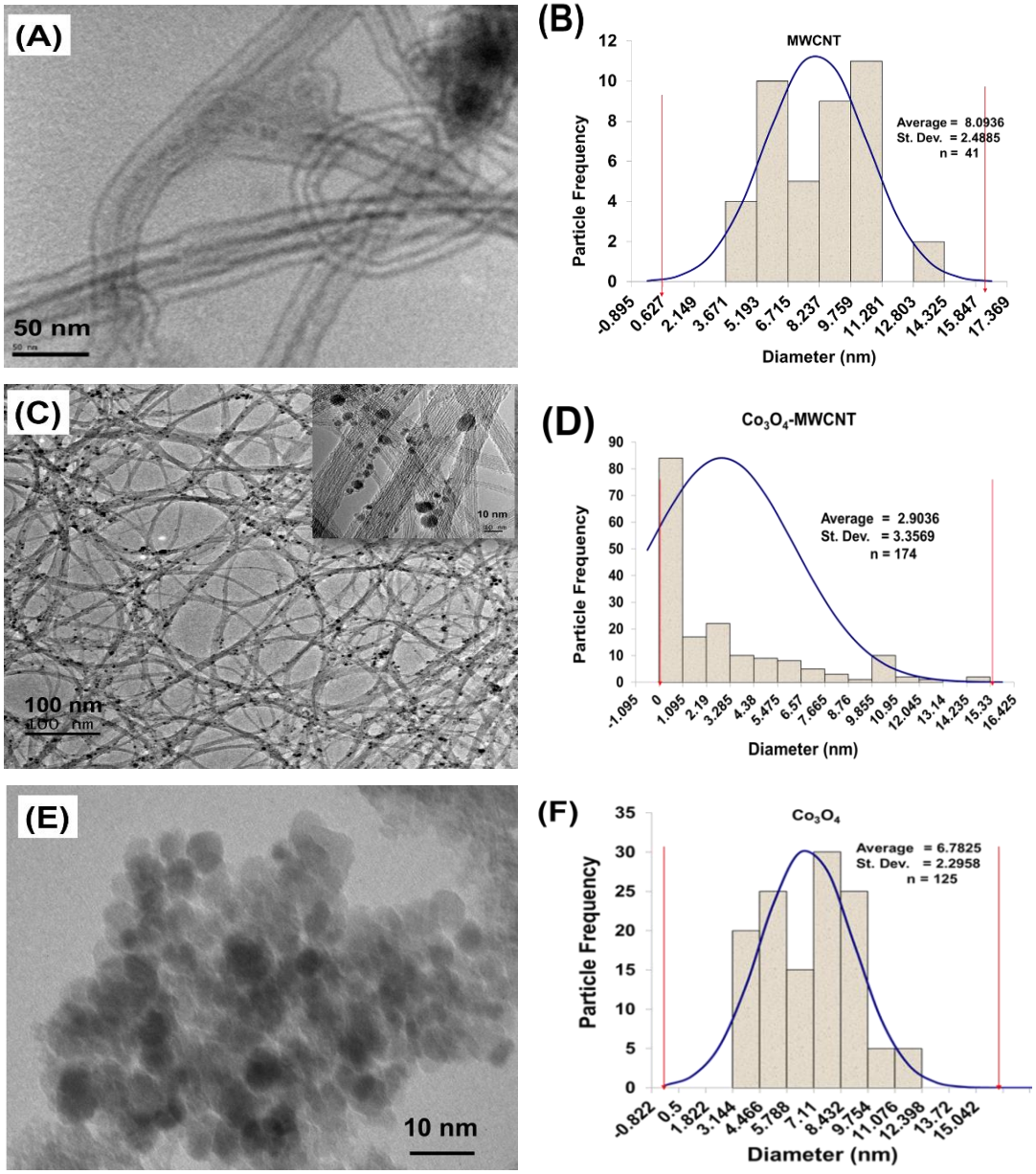

Figure 4.40 TEM images of (A) pure MWCNT, (C) Co_3O_4-MWCNT composite (inset: with higher magnification TEM image), (E) Co_3O_4 and size distribution histograms with Gaussian fits for (B) MWCNT (D) Co_3O_4-MWCNT composite and (F) Co_3O_4 NPs.

The samples were further examined by PXRD and results are shown in the figure 4.41. These results exhibit different diffraction peaks associated with MWCNT and Co_3O_4. The diffraction pattern of Co_3O_4-MWCNT shows the characteristic peaks of cubic Co_3O_4 and the peaks at 18.9°, 31.2°, 36.83°, 38.5°, 44.8°, 55.6°, 59.3° and 65.2° corresponding to (111), (220), (311), (222), (400), (422), (511) and (440) crystal planes (JCPDS no. 009-0148) along with diffraction peak at 26.3° representing (002) crystal plane of MWCNTs. However, decrease in relative intensity of the Co_3O_4 diffraction peaks in composite sample is due to the amorphous nature of the MWCNTs. These results suggest that the obtained product is a mixture of Co_3O_4 and MWCNT and there were no other peaks in the spectrum indicating the high purity of sample.

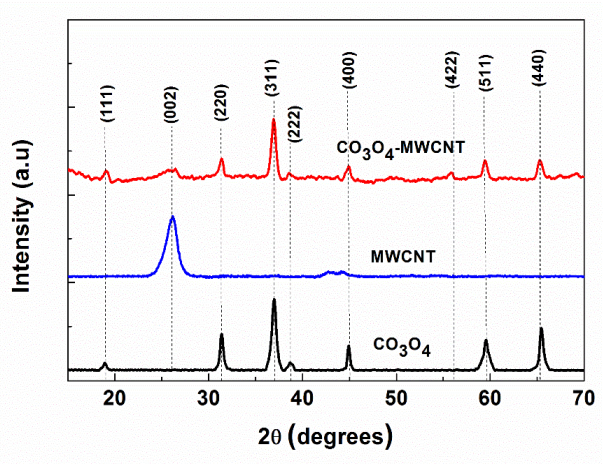

Figure 4.41 PXRD spectra of Co_3O_4 NPs, pure MWCNTs and Co_3O_4-MWCNT composites.

Raman spectra of Co_3O_4-MWCNT composite revealing successful assembly of the Co_3O_4 on MWCNTs are shown in the figure 4.42. The Raman spectra shows two characteristic peaks at ~1337 cm^{-1} and ~1586 cm^{-1} corresponding to D-band and G-band of MWCNTs respectively in both MWCNT and Co_3O_4-MWCNTs composite. The I_D/I_G ratio was effectively used to evaluate the degree of disorder in the sample. Increase in I_D/I_G ratio from 0.81 to 1.21 for MWCNT and Co_3O_4-MWCNT, suggests the defects introduced in the composite sample due to the destructive interaction of Co with the MWCNTs. The peaks at 483 cm^{-1}, 525 cm^{-1} and 694 cm^{-1} for the composites are attributed to the Co_3O_4 which matches well with the spectrum recorded for pure

Co_3O_4 (Jena and Raj 2006, Liu et al. 2009). The above results confirm the formation of composites.

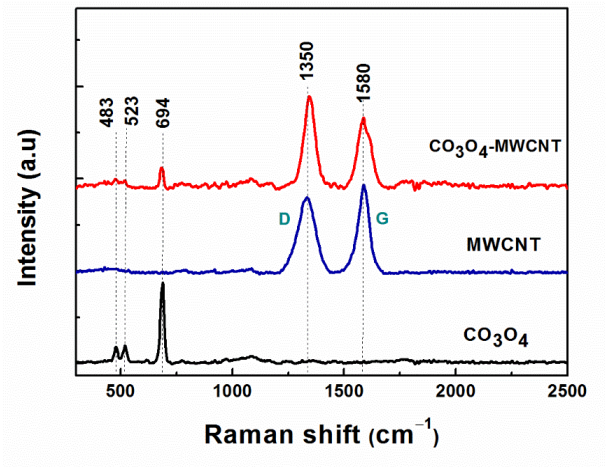

Figure 4.42 Raman spectra of Co_3O_4 NPs, pure MWCNTs and Co_3O_4-MWCNT composites.

Different weight ratio of Co_3O_4-MWCNTs composites were synthesized and examined for their morphology by using FESEM analysis. Figure 4.43(A-D) represents the FESEM images of 5%, 10%, 15% and 20% Co_3O_4-MWCNTs respectively. As we can see from the figure, with the rise in the precursor load, the more Co_3O_4 particles decorated on the surface of the MWCNTs. The uniform distribution of Co_3O_4-NPs was observed in case of 5% and 10% composites, but 5% Co_3O_4-MWCNTs composite shows lesser Co_3O_4 NPs distributed on the surface of MWCNTs with many vacant sites without any surface change which may be due to the less precursor load (Figure 4.42A). However, in case of 15% and 20% Co_3O_4-MWCNTs composite, dense and agglomerated particles are observed, which may be due to the excess precursor load (Figure 4.42B and C). Among all the Co_3O_4-MWCNTs composites, the 10% Co_3O_4-MWCNTs (Figure 4.42B) composite shows maximum decoration with least or no vacant site and agglomerated particle. Hence, 10 % Co_3O_4-MWCNTs composite is considered as the best optimised ratio with an average particle size of 10 nm Co_3O_4-NP uniformly decorated on the surface and walls of the MWCNTs.

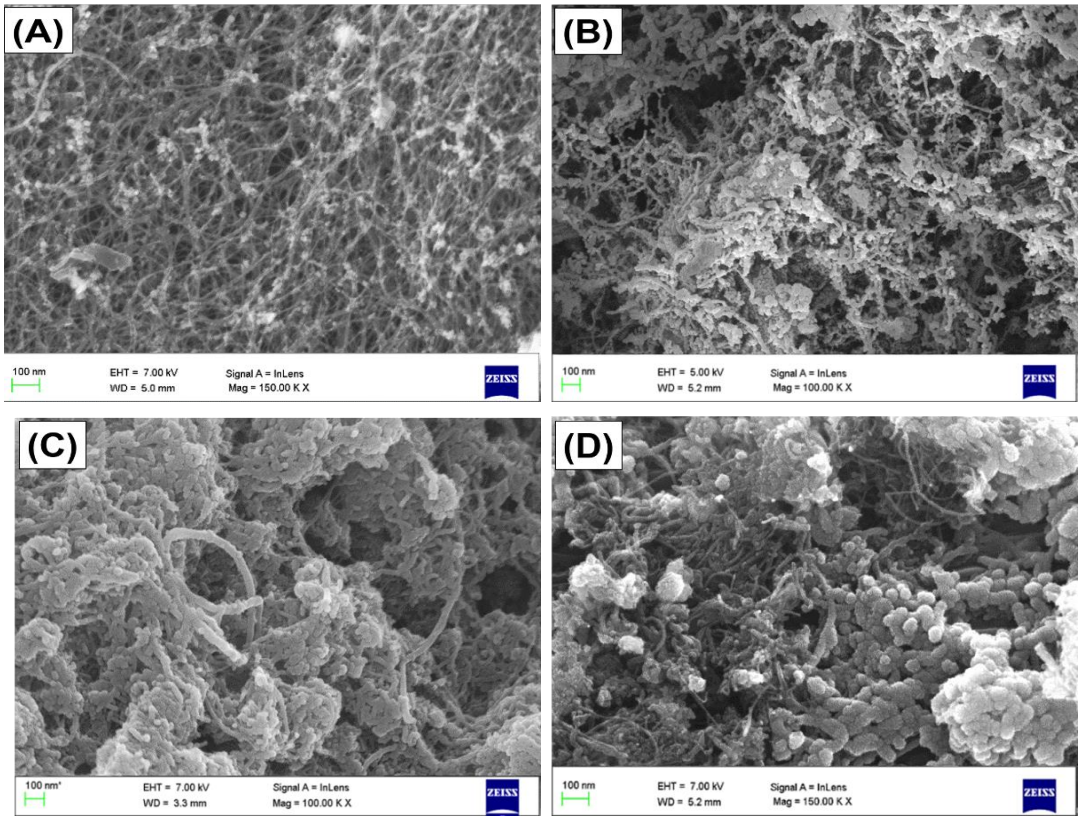

Figure 4.43 FESEM images of (A) 5% Co_3O_4-MWCNT, (B) 10% Co_3O_4-MWCNT, (C) 15% Co_3O_4-MWCNT and (D) 20% Co_3O_4-MWCNT.

To further confirm the synthesized different composite materials, we examined for PXRD and Raman analysis. Figure 4.44 shows the PXRD spectrum of the different wt.% ratio of Co_3O_4-MWCNTs composites synthesized. It is observed that as the Co_3O_4 ratio increases from 5% to 20%, the crystallinity of the composites also increases and the corresponding carbon peak at 26.3° decreases as expected (a-d). The decrease in intensity of the MWCNTs peak from 5% to 20% composites is due to lowered fraction of MWCNTs in composite whereas, increase in Co_3O_4 particles which interact with the surface of the MWCNTs contributes to crystallinity of the composites which is evident by well-defined Co_3O_4 characteristics peaks. Hence in 5% and 10% Co_3O_4-MWCNTs, noisier PXRD pattern was recorded in comparison with 15% and 20% Co_3O_4-MWCNTs composites. It is also observed that there is no significant change in phase and crystal structure with increased precursor concentration. However, intensity ratio of the Co_3O_4 to the graphite peaks varies with precursor load. The PXRD pattern

recorded for different composite shows Co_3O_4 planes, which were well-defined and corresponds to the JCPDS card No. 009-0148. These obtained results matches-well with the FESEM data and hence, confirms the formation of different wt.% Co_3O_4-MWCNTs composites.

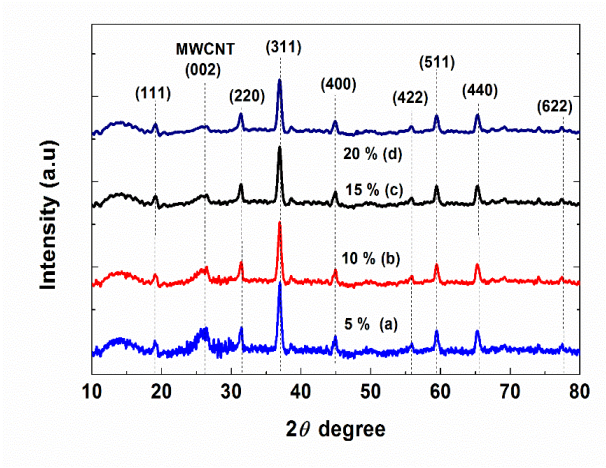

Figure 4.44 PXRD spectrum of (a) 5% Co_3O_4-MWCNTs, (b) 10% Co_3O_4-MWCNTs, (c) 15% Co_3O_4-MWCNTs and (d) 20% Co_3O_4-MWCNTs.

Raman spectra recorded to confirm the prepared different wt.% Co_3O_4-MWCNTs composites are shown in the Figure 4.45. In the figure pattern a, b, c and d corresponds to the Raman pattern of 5%, 10%, 15%, and 20% Co_3O_4-MWCNTs composites respectively. From Raman results, we observed defects present on the surface of MWCNTs during composite synthesis. From the figure 4.45, it is also observed that the distinctive D and G bands appear at around ~1350 cm^{-1} and ~1580 cm^{-1} for MWCNTs and all Co_3O_4-MWCNTs composites. From the Raman spectra, it is also observed that the intensity of I_D/I_G ratio increases from 1.1 (5% Co_3O_4-MWCNTs) to 1.30 (10% Co_3O_4-MWCNTs), 1.48 (15% Co_3O_4-MWCNTs) and 1.57 (20% Co_3O_4-MWCNTs). As the wt.% of Co_3O_4 increases, the value of I_D/I_G ratio also increases which is due to the destructive interaction of Co_3O_4 NPs with the surface of MWCNTs. The above results obtained matches well with the FESEM, PXRD results and hence confirms the formation of different wt.% Co_3O_4-MWCNTs composites.

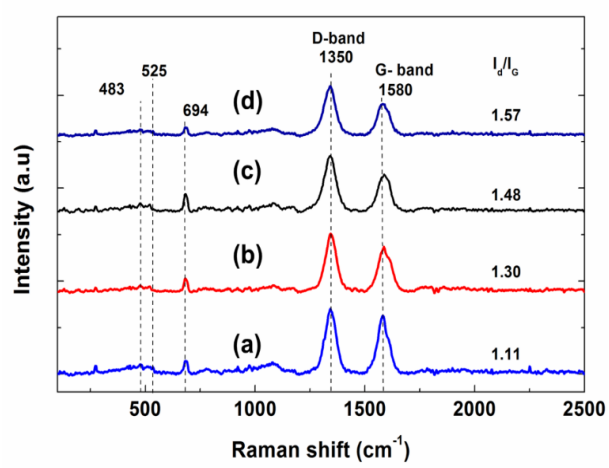

Figure 4.45 Raman spectrum of (A) 5% Co_3O_4-MWCNT, (B) 10% Co_3O_4-MWCNT, (C) 15% Co_3O_4-MWCNT and (D) 20% Co_3O_4-MWCNT.

4.7.2 Cyclic Voltammetry behaviour of the Co_3O_4-MWCNT/GCE

The CVs of the Co_3O_4/GCE and Co_3O_4-MWCNT/GCE composite were investigated for the direct oxidation of glucose in both alkaline solution (0.2 M NaOH) and neutral phosphate buffer solution (0.1 M, pH 7.0) in the range from −0.4 V to 0.7 V (Figure 4.46A). There was no oxidation or reduction peak seen in the phosphate buffer solution (inset Figure 4.46A), while two pairs of well-defined redox peaks were obtained in NaOH solution. This redox peaks formed suggests that the OH^- participates in the electrochemical redox reaction of Co_3O_4. From the figure 4.46B, as labelled pair of redox peaks I/II can be ascribed to the reversible transformation between Co_3O_4 and CoOOH while another pair of redox peaks III/IV can be assigned to further transition between CoOOH and CoO_2 (Meng et al. 2011, Lee et al. 2012). These two reversible redox reactions can be illustrated as in Eqs. (4.10) and (4.11)

$$Co_3O_4 + OH^- + H_2O \rightleftharpoons 3CoOOH + e^- \qquad (4.10)$$

$$CoOOH + OH^- \rightleftharpoons CoO_2 + H_2O + e^- \qquad (4.11)$$

The direct catalytic oxidation of glucose at the Co_3O_4/GCE and Co_3O_4-MWCNT/GCE was first examined in 0.2 M NaOH. Figure 4.46B represents CVs in the absence and presence of 2 mM glucose for Co_3O_4/GCE (curve a and c) and the Co_3O_4-

MWCNT/GCE (curves b and d), respectively. The Co_3O_4/GCE and Co_3O_4-MWCNT/GCE exhibited oxidation peak for Co3O4 starting at +0.20 and CoOOH at +0.55 V and CoOOH and CoO_2 are formed respectively. These results suggest that the direct catalytic oxidation of glucose in 0.2 M NaOH solution was referred to CoOOH and CoO_2. From the figure 4.46B it also observed that with the addition of glucose, Co_3O_4-MWCNT/GCE shows notable increase in the redox peak current but negligible in case of Co_3O_4/GCE. These results can be attributed to the synergistic effect of Co_3O_4 and MWCNTs which make the substrate a better platform for electron transfer between Co_3O_4 NPs and GCE. This increase in current with increased glucose concentration is due to the direct catalytic activity of the Co_3O_4-MWCNTs toward glucose. In addition, peak III (CoOOH → CoO_2) which causes the electro-oxidation of glucose is mainly mediated in a NaOH solution, hence the peak III potential was applied for subsequent chronoamperometric detection. It is also well known that glucose can be oxidized to produce gluconolactone through 2-electron electrochemical reaction. Therefore, the possible mechanism of glucose electrochemical oxidation reaction catalysed by CoO_2 at peak III (+0.55 V) can be illustrated as following Eq. 4.12.

$$2CoO_2 + C_6H_{12}O_6\,(glucose) \rightarrow 2CoOOH + C_6H_{10}O_6\,(gluconolactone) + 2e^- \qquad (4.12)$$

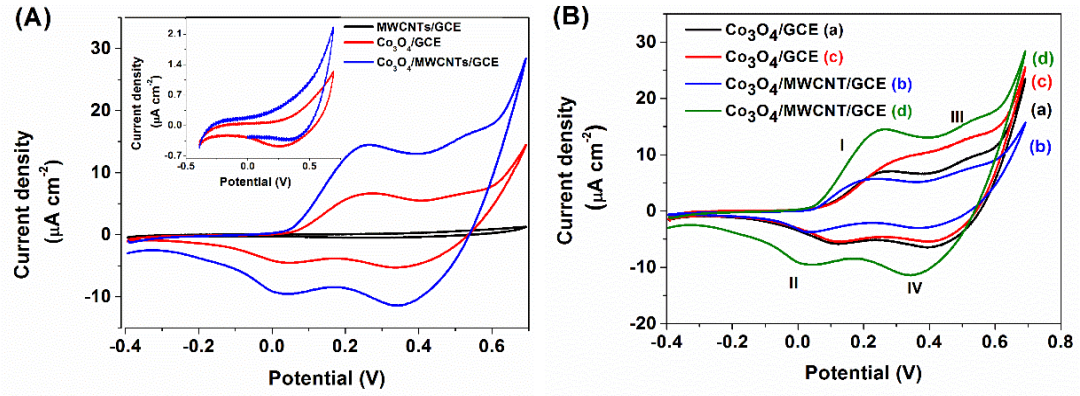

Figure 4.46 (A) Cyclic voltammograms of Co_3O_4/GCE and Co_3O_4-MWCNT/GCE in the 0.2 M NaOH and 0.1 M phosphate buffer solution (inset figure 4.44A) and (B) Cyclic voltammograms of Co_3O_4/GCE and Co_3O_4-MWCNT/GCE in the absence (a, b) and presence (c, d) of 2.0 mM glucose in 0.2 M NaOH. Scan rate: 50 mV s^{-1}.

The information about electrochemical mechanism can be obtained from the relation between peak current and scan rate. Hence the effect of scan rate on electrochemical oxidation of glucose on Co_3O_4-MWCNT/GCE was also investigated. Figure 4.47A shows the cyclic voltammograms of Co_3O_4-MWCNT/GCE with 2 mM glucose at different scan rates ranging from 10 to 200 mV s^{-1}. From the obtained results, it is observed that anodic and cathodic peak currents increased with increasing scan rate. From the figure 4.47B the anodic and cathodic peak currents are linearly correlated to the square root of scan rate (mV $s^{-1})^{1/2}$ and the corresponding linear regression equations with the linear correlation coefficient values are as follows

(i) I_{pa} (A) = 1.6871ν −2.099 (mV $s^{-1})^{1/2}$, (R^2 = 0.9942),

(ii) I_{pc}(A) = −1.7078ν −3.572 (mV $s^{-1})^{1/2}$, (R^2 = 0.9946),

iii) I_{pa} (A) = 2.767ν −5.9153 (mV $s^{-1})^{1/2}$, (R^2 = 0.998) and

(iv) I_{pc} (A) =−1.6681ν −1.9275 (mV $s^{-1})^{1/2}$, (R^2 = 0.9954).

The studies show that synergistic effect of Co_3O_4-NPs and MWCNTs effectively electro-catalyse the direct glucose oxidation. The results indicate that the electrochemical kinetics is diffusion-controlled and it can be ideal for quantitative analysis in practical applications.

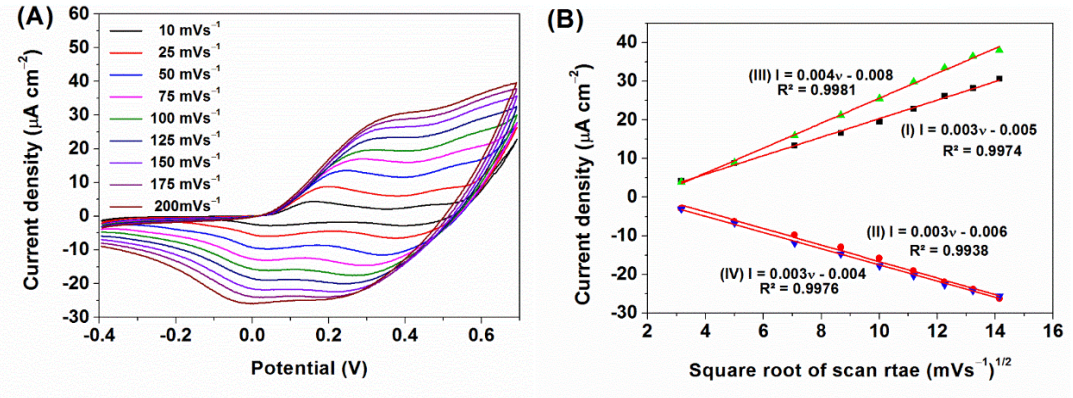

Figure 4.47 (A) Cyclic voltammograms of Co_3O_4-MWCNT/GCE at different scan rates from 10 mV s^{-1} to 200 mV s^{-1} in 0.2 M NaOH with 2.0 mM glucose and (B) plot of peak current density vs. square root of scan rate.

4.7.3 Chronoamperometry response of the Co_3O_4-MWCNT/GCE

Since cyclic voltammetry has the limitations to low concentration measurements, chronoamperometry response was investigated to detect the glucose. The chronoamperometry was executed by successive addition of 50 μM glucose into 10 mL of 0.2 M NaOH solution at constant intervals. To investigate the best optimal applied potential, chronoamperometry was carried out at different applied potentials such as 0.5, 0.55 and 0.6 V to yield the excellent electrochemical properties (Figure 4.48A). From these results, it is seen that the signal-to-background ratio increases with the potential range from 0.5 to 0.6 V and observed that current response recorded for 0.55 V is greater than the other applied potentials and which is supported from the CV results, where ~0.55 V, the CoOOH oxidation peak potential was observed. Hence, 0.55 V was chosen as an optimal applied potential for the further chronoamperometry investigation. Using these optimal conditions, the chronoamperometry of the modified GCE electrodes was examined. From the figure 4.48B it can be seen that current response recorded for Co_3O_4-MWCNT/GCE (curve a) is 40% greater than the Co_3O_4/GCE (curve b) with the incremental addition of glucose (50 μM) and reaches the 95% of the steady-state current within 5s (Figure 4.48C) indicating the Co_3O_4-MWCNT composites efficiently catalyse glucose oxidation. The calibration curve for the electrochemical responses of the Co_3O_4-MWCNT/GCE electrode to glucose concentration is shown in figure 4.48D. From the slope of the calibration curve, the sensitivity of the sensor was found to be 5089.1 μA $mM^{-1}cm^{-2}$ for a linear glucose concentration range from 0.05 mM to 12 mM with a linear coefficient of $R^2 = 0.988$. From the calculations, the LOD of the sensor was found to be 10.42 μM. The sensors were also compared with the previously reported nanomaterial based enzyme-free glucose sensors and are shown in Table 4.11. As it can be seen from the table, the fabricated electrode shows highly enhanced sensitivity and LOD due to the excellent catalytic activity of Co_3O_4-NPs and the electrical network formed through self-assembled Co_3O_4-NPs distributing on the surface of MWCNT, which not only can keep their intrinsic excellent electrical conductivity but also facilitates easy access of Co_3O_4-NPs to glucose oxidation. Therefore, the direct electrochemical glucose oxidation can be greatly enhanced with the use of Co_3O_4-MWCNT composites.

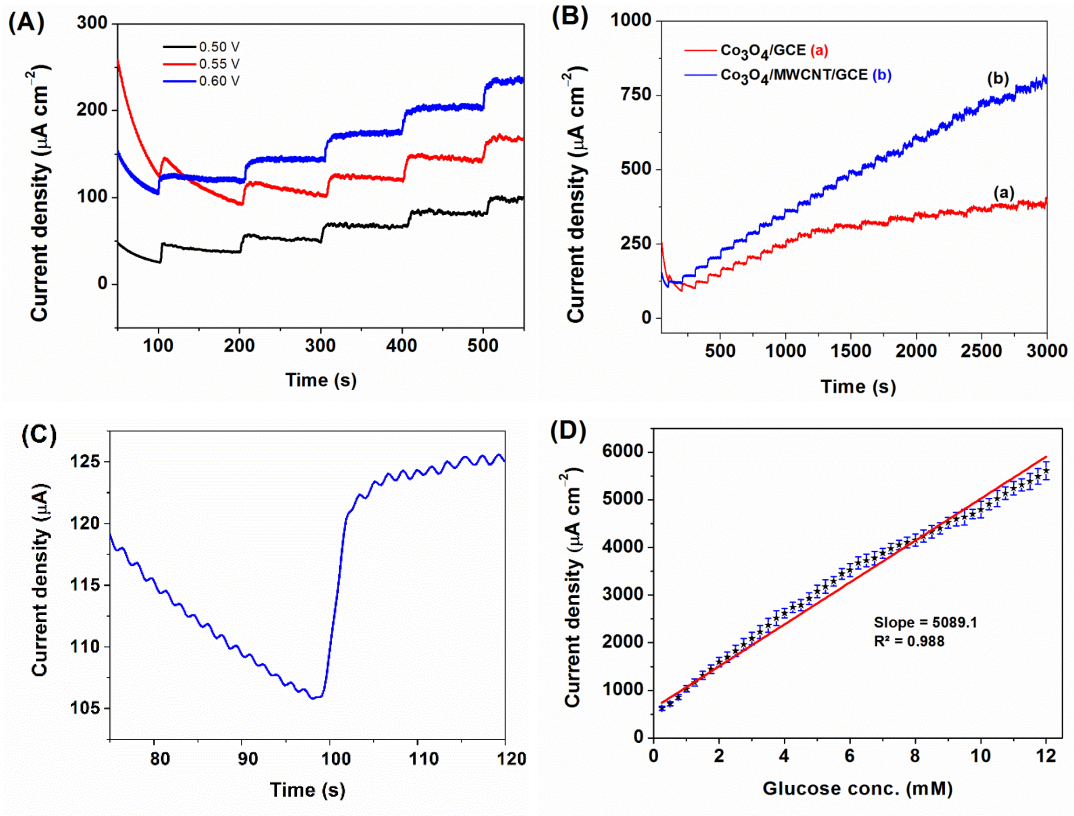

Figure 4.48 (A) Chronoamperometric responses of Co_3O_4-MWCNT/GCE at different potentials in 0.2 M NaOH with a dropwise addition of 50 μM glucose at every 50 s, (B) Current–time responses at 0.55 V with an increasing glucose concentration (50 μM) per 100 s for Co_3O_4-MWCNT/GCE, (C) Response time measurement using i-t curve and (D) The current density response vs. glucose concentration at Co_3O_4-MWCNT/GCE.

Table 4.11 Comparison of non-enzymatic glucose sensing performance based on different electrode materials of transition metal compounds with Co_3O_4-MWCNT-GCE.

Electrode	Sensitivity ($\mu AmM^{-1} cm^{-2}$)	Linear range (mM)	LOD (µM)	Applied Potential (V)
Co_3O_4 nanofibers (Heller and Feldman 2010)	36.2	2.04	0.97	+0.60
CuO nanospheres Reitz et al. 2008	404.5	2.6	1.0	+0.60
Ni NPs -CNF paste electrode (Liu et al. 2009)	420.4	2.5	1.0	+0.55
CuO nanofibers (Wang et al. 2009b)	431.3	2.5	0.8	+0.40
SA-CNT thin films with Cu NPs (Li et al. 2009)	602.0	1.8	0.1	+0.60
Ni nanowire arrays (NiNWAs) (Lu et al. 2009)	1043.0	7.0	0.1	+0.55
CuxO flowers (Li et al. 2010)	1620.0	6.0	49	+0.50
CuO–MWCNTs array electrode (Yang et al. 2010a)	2190.0	4.0	0.8	+0.55
IrO_2/ PbO_2-carbon microelectrodes (Gorski and Kennedy 1997)	-	20.0	50.0	+0.75
Co_3O_4-MWCNT /GCE (Present work)	**5089.1**	**12.0**	**10.4**	**+0.55**

4.7.4 Selectivity, Stability and Reproducibility of the Co_3O_4-MWCNT/GCE

The biomolecules like fructose, sucrose, maltose, AA, DA and UA are potentially interfering ions with human blood glucose and these may also get easily oxidized at the applied potential on the sensor electrode. Hence these interference biomolecules were also tested chronoamperometrically at +0.55 V along with glucose using Co_3O_4-MWCNT/GCE in 0.2 M NaOH solution (Figure 4.49). From the figure, it can be seen that response obtained for 2 mM concentration of Fructose, maltose, sucrose, AA, DA and UA were less than 5% of that obtained for 2 mM glucose which indicates the remarkable selectivity of the sensor for glucose detection in the presence of commonly interfering electro active molecules.

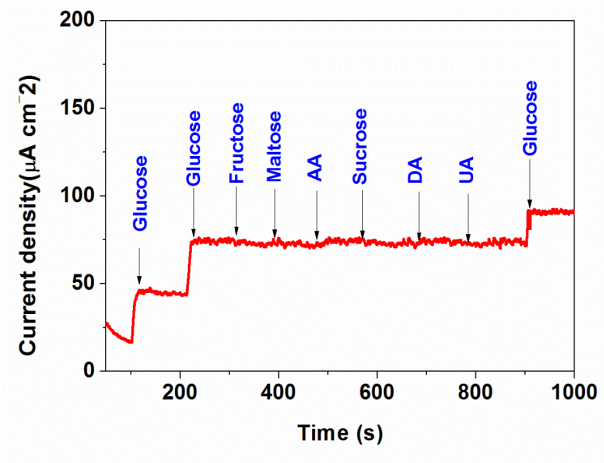

Figure 4.49 Interference response of the sensor in 0.2 M NaOH at +0.55 V with 2 mM glucose and other interference as indicated.

Long term stability experiments were investigated to evaluate the performance of the Co_3O_4-MWCNT/GCE non-enzymatic sensor, as shown in figure 4.50A. The sensor shows the current response to glucose over a period of three weeks (five identical electrodes), during which 85% current was retained. However, when sensor was not in use it was stored at lab atmosphere. These results suggest that the Co_3O_4-MWCNT/GCE electrode possessed a good stability. The reproducibility was examined for ten identically constructed electrodes at 50 μM of glucose concentration shows 4.1% of RSD suggesting excellent reproducibility (Figure 4.50B). From these results,

it may be confirmed that the Co_3O_4-MWCNT/GCE has a greater stability and reproducibility that makes it applicable for practical use.

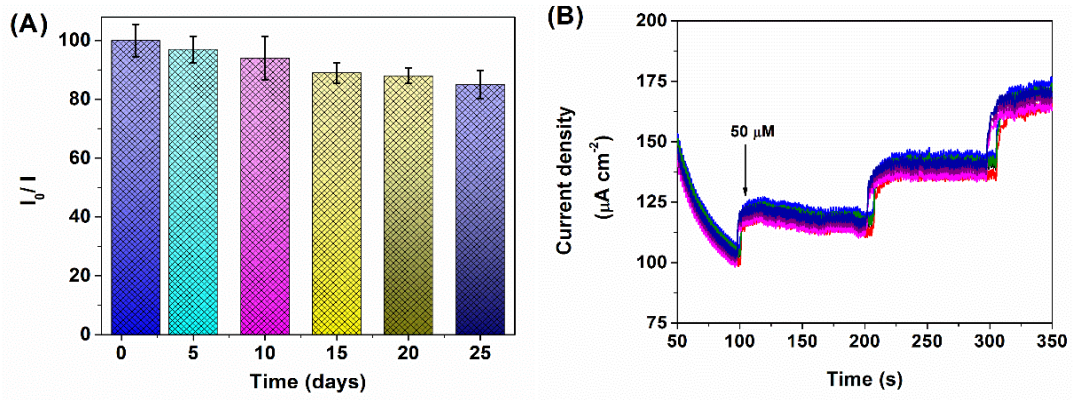

Figure 4.50 (A) Stability of the sensor stored at ambient conditions over three weeks using 0.2 M NaOH with 2.0 mM glucose at +0.55 V and (B) i-t response for stability check using ten identical Co_3O_4-MWCNT/GCEs.

For real application, the Co_3O_4-MWCNT/GCE was tested for the determination of glucose concentration in human blood serum. Blood serum without any pre-treatments were injected into 5 mL of 0.2 M NaOH at an applied potential of +0.55 V. The measured current change was correlated with the glucose concentration according to the calibration curve in figure 4.48D and then compared with the value obtained using a commercial glucose meter as shown in the table 4.12. The results show that the RSD less than 7%. Hence, these results suggest that, the Co_3O_4-MWCNT/GCE composite as a potential material for the fabrication of enzyme-free glucose sensors.

Table 4.12 The detection of glucose in human blood serum

Sample	**Glucose (mM)**	**RSD* (%) (N = 5)**	**Glucose (mM) (Commercial glucose meter)**	**Actual glucose Conc. added(Mm)**	**Accuracy %**
1	6.1	4.4 %	6.3	6.0	98.3
2	4.6	4.8 %	4.9	4.8	95.8
3	4.5	5.2 %	4.6	4.5	100.0
4	5.1	4.7%	5.2	5.0	98.0

Self-assembled uniformly decorated cobalt oxide nanoparticles over MWCNTs were successfully synthesized by simple solvent free thermal decomposition of cobalt formate. The synthesized composite was employed to fabricate enzyme-free glucose sensor for the detection of glucose. The results of cyclic voltammetry, chronoamperometry revealed that uniformly dispersed cobalt oxide on multi-walled carbon nanotubes possessed attractive electrochemical properties such as high sensitivity, low detection limit, good selectivity, greater stability and excellent reproducibility. These improved performances are ascribed to the synergistic effect of Co_3O_4 and MWCNTs. Thus, the Co_3O_4-MWCNT composite is expected to be a promising material for the fabrication of enzyme-free glucose sensors.

4.8 NICKEL-OXIDE MULTIWALL CARBON-NANOTUBE/REDUCED GRAPHENE OXIDE TERNARY COMPOSITE NON-ENZYMATIC GLUCOSE SENSOR

4.8.1 Material Characterization

In general, electrochemical response of any material to be employed as sensing matrix is highly subjective to its surface morphology. In this section, MWCNTs, rGO and their composites with NiO are being used as electrochemical biosensors for the detection of glucose. The surface morphology of the as-synthesized materials and their hybrid composites were studied using electron microscopy. An overview of FESEM images of MWCNTs, rGO, MWCNTs-rGO, NiO-MWCNTs-rGO, NiO-MWCNTs, NiO-rGO and pure NiO are shown in figure 4.51(A-G). These FESEM micrographs shows that the CNTs and rGO synthesized from the CVD method are multiwall CNTs (Figure 4.51A) and few layered rGO sheets (Figure 4.51B) respectively. When these materials are mechanically mixed using mortar and pestle, uniform and homogenous hybrid of MWCNT-rGO were obtained which are depicted in figure 4.51C. Further the figure 4.51(D-F) shows the FESEM micrographs of the NiO-MWCNT-rGO, NiO-MWCNT and NiO-rGO composites, respectively. These figures show that, the thermal decomposition of nickel formate precursor results in uniformly decorated NiO-MWCNT-rGO composites. Finally, for comparison, pure NiO-NPs were prepared similarly without using rGO and MWCNT (Figure 4.51G). These NiO-NPs correlates well with the size and morphology of the NiO-NPs decorated in the composite. These results suggest the reproducible synthetic method for the preparation of NiO-NPs by the thermal decomposition of nickel formate.

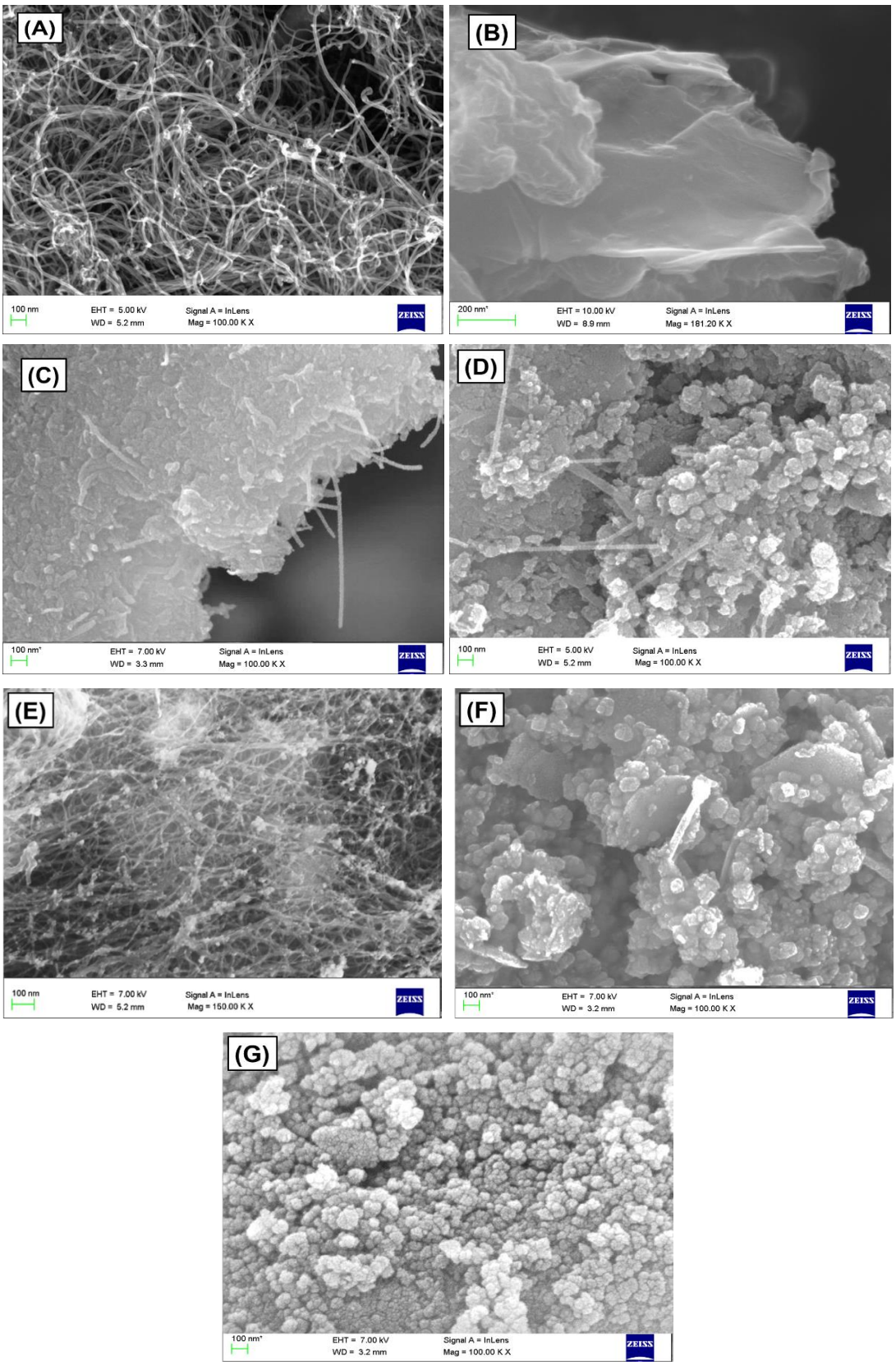
(A)
100 nm
EHT = 5.00 kV
WD = 5.2 mm
Signal A = InLens
Mag = 100.00 K X
(B)
200 nm
EHT = 10.00 kV
WD = 8.9 mm
Signal A = InLens
Mag = 181.20 K X
(C)
100 nm
EHT = 7.00 kV
WD = 3.3 mm
Signal A = InLens
Mag = 100.00 K X
(D)
100 nm
EHT = 5.00 kV
WD = 5.2 mm
Signal A = InLens
Mag = 100.00 K X
(E)
100 nm
EHT = 7.00 kV
WD = 5.2 mm
Signal A = InLens
Mag = 150.00 K X
(F)
100 nm
EHT = 7.00 kV
WD = 3.2 mm
Signal A = InLens
Mag = 100.00 K X
(G)
100 nm
EHT = 7.00 kV
WD = 3.2 mm
Signal A = InLens
Mag = 100.00 K X

Figure 4.51 FESEM images of synthesized materials. (A) pure MWCNT, (B) rGO, (C) rGO-MWCNT composite (D) NiO-MWCNT-rGO composite, (E) NiO-MWCNT composite, (F) NiO- rGO composite and (G) pure NiO-NPs.

Figure 4.52 shows the FESEM images of NiO-MWCNT-rGO composites synthesized from different weight ratios of nickel formate precursor load, namely (A) 10% NiO-MWCNTs-rGO, (B) 20% NiO-MWCNTs-rGOE, (C) 30% NiO-MWCNTs-rGO and (D) 40% NiO-MWCNTs-rGO for 10, 20, 30 and 40 wt.% precursor load respectively. It is clearly observed that, as the precursor load increase from 10 to 40 wt.%, the size of NiO-NPs morphology on the surface of MWCNTs-rGO changes from nanoparticles to micro particles due to agglomeration. However, it is known that the NPs tend to have high surface area which leads to higher catalytic activity. Among these synthesized composite, 20% NiO-MWCNTs-rGO (Figure 4.52B) has uniformly distributed NiO-NPs with least agglomeration, hence it is considered as optimised ratio.

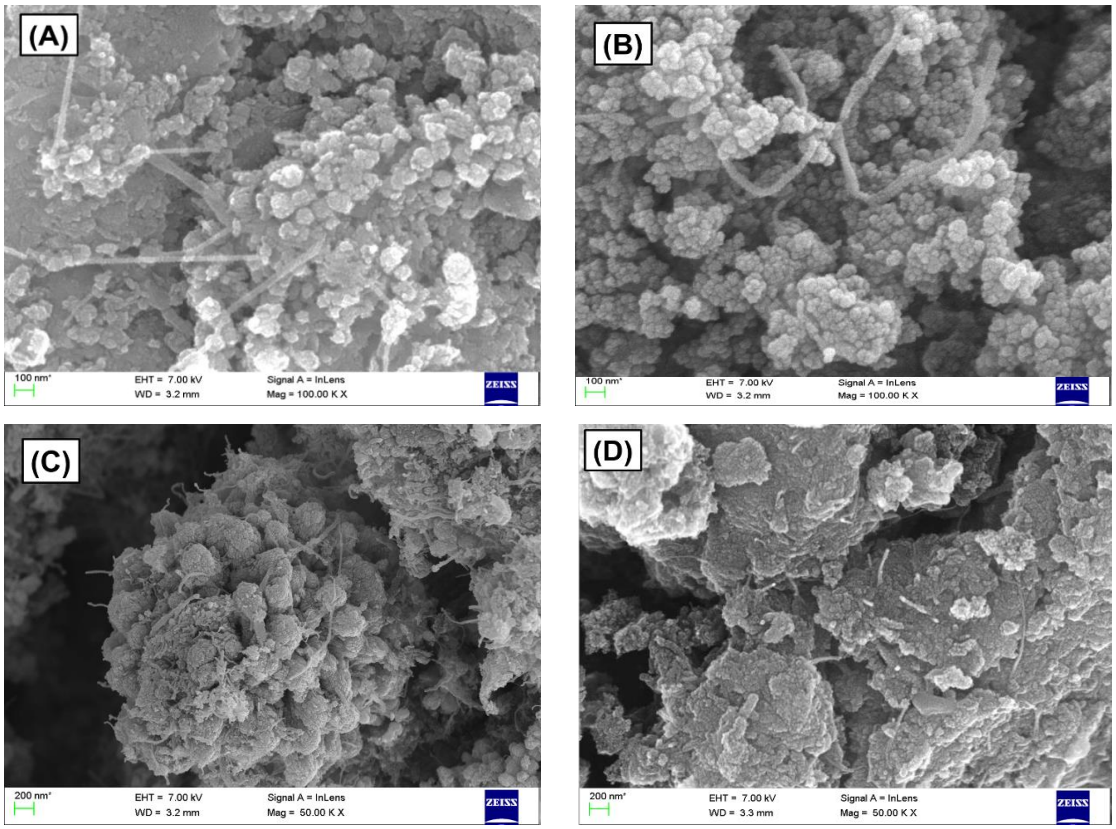

Figure 4.52 FESEM images of (A) 10 wt.% NiO-MWCNT-rGO, (B) 20 wt.% NiO-MWCNT-rGO, (C) 30 % wt NiO-MWCNT-rGO and (D) 40 wt.% NiO-MWCNT-rGO.

Figure 4.53 depicts the TEM micrographs of prepared samples. MWCNT (Figure 4.53A) and few layered rGO sheets (Figure 4.53B) on mechanical mixing gives homogenous hybrid of MWCNT-rGO which is shown in figure 4.53C. Further, thermal treatment of MWCNT, rGO and MWCNT-rGO composite with nickel formate results in NiO-MWCNTs (Figure 4.53D), NiO-rGO (Figure 4.53E) and NiO-MWCNTs-rGO (Figure 4.53F) respectively. For comparison, pure NiO-NPs (Figure 4.53G) synthesized by a similar method are granular in nature with an average particle size of ~7 nm. It is observed that the NiO-NPs are uniformly distributed in the composite.

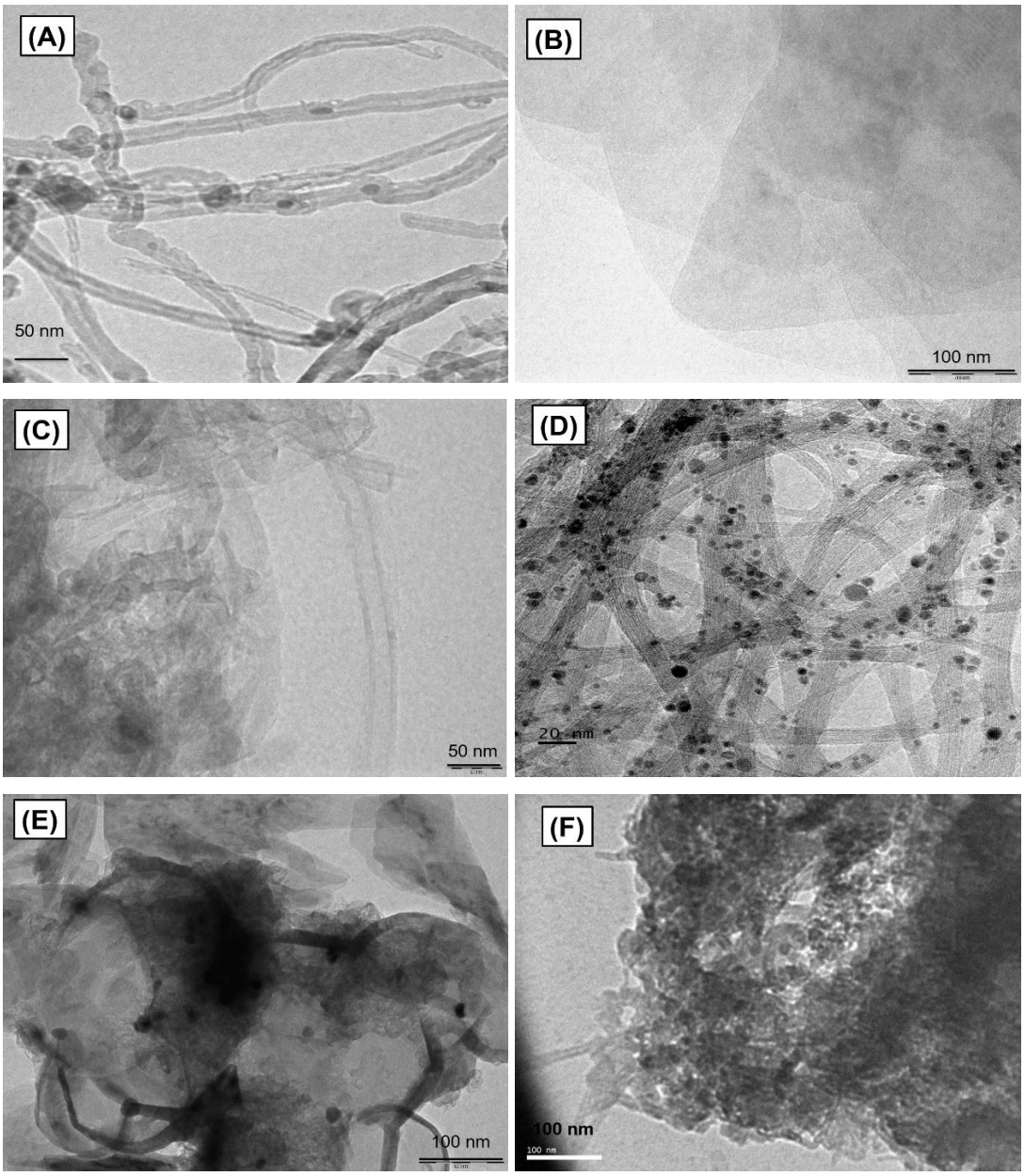

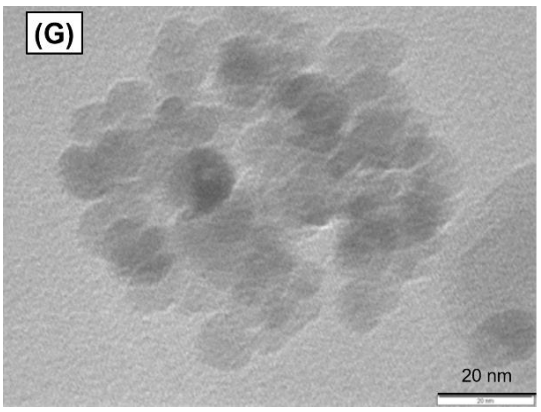

Figure 4.53 TEM images of synthesized materials, (A) pure MWCNT, (B) rGO, (C) rGO-MWCNT composite, (D) NiO-MWCNT composite, (E) NiO-rGO composite, (F) NiO-MWCNT-rGO composite and (G) pure NiO-NPs.

In the PXRD spectra (Figure 4.54), the NiO-MWCNTs-rGO composite sample has been compared with that of the starting materials. PXRD spectra display the corresponding planes for graphite flake (a), GO (b), MWCNTs (c), MWCNTs-GO hybrid mixture (d), MWCNTs-rGO (e), NiO (f) and NiO-MWCNTs-rGO (g) respectively. The diffraction peak observed at $2\Theta = 26.3°$ in (Figure 4.54 (a) and (c)) can be indexed to (002) peak of graphitic carbon in flake graphite sheets and MWCNT (JCPDS 008-0415) (Li et al. 2015). This graphite on conversion to GO (b) by Hummer's method shows (002) broad graphite peak at 11°. This broadening in the peak can be attributed to the oxygen containing functional groups intercalation. For MWCNTs-GO hybrid sample, two (002) diffraction peaks appear at 11° and 26.3° in the PXRD spectrum (d), which corresponds to GO and MWCNT respectively. In thermally treated composite (e), a broad diffraction peak appear at 26.3°, which may be due to the complete conversion of GO to rGO which incidently coincides with (002) diffraction peak of MWNCT. In addition, NiO-MWCNTs-rGO hybrid sample (g) shows peaks at 37.25, 44.28, 62.91, 75.40 and 79.37° (rhombohedral, JCPDS No 00-044-1159), which are corresponding to (101), (012), (104), (113) and (202) rhombohedral planes of NiO-NPs along with (002) peak of MWCNT-rGO hybrid at 26.3°. Similarly, pure NiO synthesized from similar method shows the PXRD pattern (f) that matches well with the rhombohedral crystal lattice (JCPDS No. 00-044-1159), which is same as NiO crystal planes of NiO-MWCNTs-rGO hybrid. Hence, these

results indicate complete reduction of nickel formate precursor to NiO-NPs and their successful decoration over graphene and MWCNT.

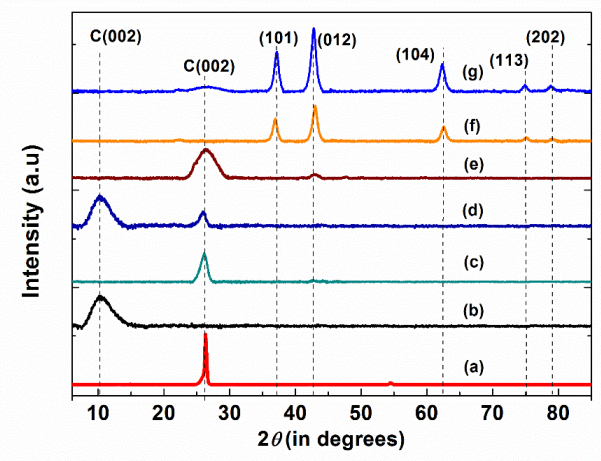

Figure 4.54 PXRD spectra of graphite flake (a), GO (b), MWCNTs (c), MWCNT-GO (d), MWCNT-rGO (e), NiO (f) and 20% NiO-MWCNTs-rGO (g).

Figure 4.55 shows the typical Raman spectra of raw graphite flake (a), GO (b), MWCNTs (c), MWCNT-GO (d), MWCNT-rGO (e), NiO (f) and NiO-MWCNTs-rGO (g) respectively. The distinctive D, G (as described earlier) and 2D bands ~1350 cm^{-1}, 1590 cm^{-1} and 2700 cm^{-1} are observed in all samples except for pure NiO-NPs. The 2D band at ~2700 cm^{-1} originates from a double resonance process (Shahriary et al. 2015, Singh et al. 2015). Further, the value of I_D/I_G are effectively used to evaluate the degree of disorder in these samples and the corresponding I_D/I_G values are tabulated in Table 4.13 (Saito et al. 2011). Graphite exhibits a prominent G-band peak at 1581 cm^{-1} (a). After extensive oxidation, the G band of GO is broadened and blue-shifted to 1595 cm^{-1} and a D band appears at 1348 cm^{-1}(b) with an I_D/I_G value of about 0.76. In case of MWCNT (c) the value I_D/I_G is observed to be 0.65 corresponding to smooth surface with least structural defects. When MWCNTs and GO are mixed together, the value of I_D/I_G for MWCNTs-GO hybrid (d) has been raised to 0.75 than the individual MWCNT and GO, which can be attributed to the more defects introduced during mechanical mixing process. Similarly, MWCNT-rGO hybrid (e) composite have I_D/I_G value 0.87. Though the conjugated sp^2 carbon of rGO and MWCNT is re-established, the size of the re-established rGO and MWCNT network is usually smaller than the original,

resulting in the increase of I_D/I_G ratio (Bai et al. 2014). Therefore, the increase of I_D/I_G ratio from 0.81 to 0.87 is reasonable. The Raman spectrum of NiO-MWCNT-rGO (g), shows greater raise in I_D/I_G value to 1.5, which is due to the destructive interaction of the NiO on the surface of MWCNT and GO. Raman spectrum of pure NiO-NPs (f) consists of peaks at 747 cm^{-1} and 1078 cm^{-1} corresponding to characteristic bands of NiO which is also present in NiO-MWCNT-rGO (g).

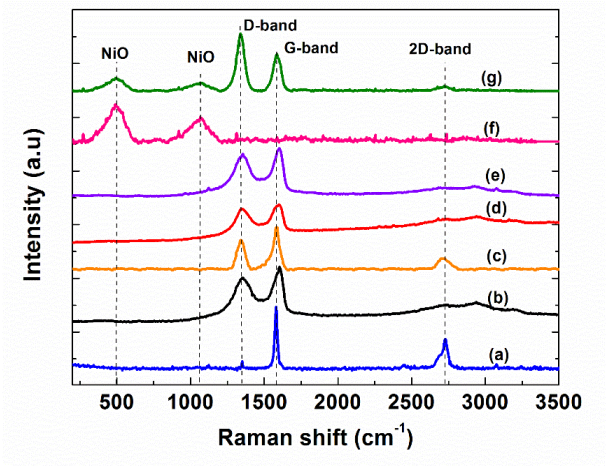

Figure 4.55 Raman spectra of graphite flake (a), GO (b), MWCNTs (c), MWCNT-GO (d), MWCNT-rGO (e), NiO (f) and 20% NiO-MWCNTs-rGO (g).

Table 4.13 Raman peak positions of D, G, 2D bands and I_D/I_G values determined for the synthesized materials.

Material	D (cm^{-1})	G (cm^{-1})	2D (cm^{-1})	I_D/I_G
Graphite	1354.9	1581.0	2727.0	0.21
GO	1348.0	1595.0	-	0.76
MWCNT	1345.2	1590.0	2720.9	0.65
MWCNT-GO	1356.5	1602.4	-	0.75
MWCNT-rGO	1351.0	1607.7	-	0.87
NiO-MWCNT-rGO	1342.0	1582.0	2726.9	1.50
NiO	-	-	-	-

4.8.2 Cyclic Voltammetry behaviour of the NiO–MWCNT-rGO/GCE

Figure 4.56 exhibits the CVs of MWCNT-rGO/GCE, NiO/GCE and 20% NiO-MWCNT-rGO/GCE in the presence and absence of 2.0 mM glucose in PBS (A) and 0.1 M NaOH solution (B) respectively. CVs recorded in PBS showed no redox peaks for the above-mentioned electrodes in both presence and absence of glucose (a-f). However, the current recorded for 20% NiO-MWCNT-rGO/GCE is much higher than the NiO/GCE and MWCNT-rGO/GCE which may be due to the synergistic effect of NiO, MWCNT and rGO. In contrast CVs recorded for these electrodes in 0.1 M NaOH solution display a distinct behaviour. In case of MWCNT-rGO/GCE (g and h) shows no redox peak in presence and absence of 2.0 mM glucose. However, well-defined redox peaks appear for NiO/GCE and NiO-MWCNT-rGO/GCE (i and k), due to the redox couple of Ni^{3+}/Ni^{2+} which cause direct oxidation of glucose to gluconic acid. Upon the addition of 2.0 mM glucose, the MWCNT-rGO/GCE (h) electrode shows insignificant change in current density. NiO-MWCNT-rGO/GCE (i) and NiO/GCE (j) records significant improvement in current density. This indicates that NiO can potentially electro-catalyse the direct glucose oxidation. Redox peaks associated with NiO-MWCNT-rGO/GCE (*l*) negatively shifted with the anodic peak at 0.55 V and cathodic peak at 0.25 V and the electrode current recorded is 2.5 times greater than the NiO/GCE. This shift in redox peak and increased current density may be due to the use of MWCNT in the NiO-rGO composite, where MWCNT acts like spacers between rGO layers and can effectively enhance the surface area of the composite which results in faster diffusion of glucose at the electrode surface improving electrochemical response.

The plausible mechanism for direct glucose oxidation on NiO based materials could be represented by the following reactions (Lu et al. 2015).

$$NiO + OH^- \rightarrow Ni(OH)_2 \quad (4.13)$$

$$Ni(OH)_2 + OH^- \rightleftharpoons NiO(OH) + H_2O + e^- \quad (4.14)$$

$$NiO(OH) + glucose \rightarrow Ni(OH)_2 + Gluconic\ acid \quad (4.15)$$

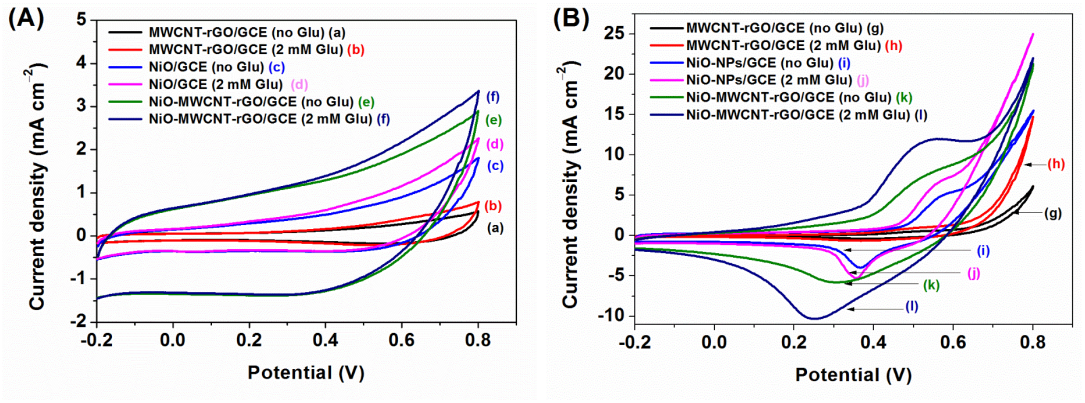

Figure 4.56 (A) CV in the presence and absence of 2.0 mM glucose at MWCNT-rGO/GCE (a and b), NiO/GCE (c and d) and NiO-MWCNT-rGO/GCE (e and f) electrodes in PBS solution and (B) CV recorded in the presence and absence of 2 mM glucose at MWCNT-rGO/GCE (g and h), NiO/GCE (i and j) and 20% NiO-MWCNT-rGO/GCE (k and l) electrodes in 0.1 M NaOH aqueous solution.

First, Ni^{2+} is electro-oxidized to Ni^{3+} in 0.1 M NaOH solution where the release of electron resulted in the formation of oxidation peak current. Then, glucose ($C_6H_{12}O_6$) is oxidized to gluconic acid ($C_6H_{12}O_7$) by reducing Ni^{3+} to Ni^{2+}. Ni^{2+} further undergo oxidation at the electrode thereby enhancing the current density. Hence, the presence of glucose lead to an increase in current.

The modified electrodes were fabricated using composites with different wt.% of Ni formate loaded namely, 10% NiO-MWCNTs-rGO/GCE, 20% NiO-MWCNTs-rGOE/GCE, 30% NiO-MWCNTs-rGO/GCE and 40% NiO-MWCNTs-rGO/GCE for 10, 20, 30, 40 wt.% NiO-MWCNTs-rGO composites, respectively (Figure 4.57, a-d). It is observed that 20% NiO-MWCNTs-rGO/GCE (a) shifted Ni^{2+} oxidation peak to lower potential with highest current density compared to 30 and 40% NiO-MWCNTs-rGO/GCE (c and d) which may due to the higher surface area offered by the MWCNTs spacers between rGO sheets. In spite of 10% NiO-MWCNTs-rGO/GCE (a) displaying the oxidation of glucose at much lower potential than the 20% NiO-MWCNTs-rGO/GCE, the electrode current recorded for 20% electrode is twice in magnitude in comparison to 10% electrode. The raise in electrode current may be due to the better surface coverage of MWCNT-rGO with NiO-NPs. Hence the 20% NiO-MWCNTs-

rGO composite was considered as the optimised ratio for the maximum electrolytic oxidation of glucose. These results correlate very well with our earlier observation.

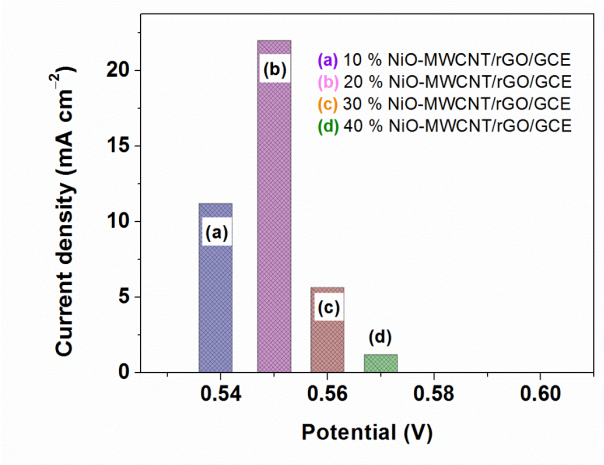

Figure 4.57 Current vs. potential plot recorded for 10% NiO-MWCNT/GCE (a), 20% NiO-MWCNT/GCE (b), 30% NiO-MWCNT/GCE (c) and 40% NiO-MWCNT/GCE (d) using 2.0 mM glucose.

The 20% NiO-MWCNTs-rGO/GCE was further investigated for the optimising NaOH concentration ranging from 0.05 M to 0.2 M NaOH solution are as shown in figure 4.58. 0.10 M NaOH (ii) shows well-defined redox peaks with significant raise in anodic peak current (E_{Pa}) and slight shift in the peak potential in comparison to 0.05 M (i), 0.15 M (iii), 0.20 M (iv) NaOH respectively. These results indicate that the hydroxyl ions (OH^-) are directly involved in electro-chemical oxidation process. The electro-adsorption of glucose with raise in OH^- concentration may retard the glucose oxidation process leading to fouling of electrodes. Therefore, 0.10 M NaOH solution was considered as the optimized concentration for further electrochemical studies.

The scan rate effect was studied on 20% NiO-MWCNTs-rGO/GCE to investigate the reaction kinetics of glucose in 0.1 M NaOH solution with 2.0 mM glucose concentration. As the scan rate was increased from 50 mV s^{-1} to 600 mV s^{-1} (Figure 4.59A), the redox peaks current increases with slight shift in anodic and cathodic peak potential toward the positive and negative sides respectively, thus leading to the substantial peak-to-peak separation. Figure 4.59B shows that the determined redox peak currents (I_P) were linearly correlated to the square root of scan rate ($\nu^{1/2}$)

with linear regression value (R^2) of 0.9717 and 0.9819 for anodic and cathodic peak potentials respectively. This result indicates that the electro-chemical process is a typical diffusion-controlled process on the surface of 20% NiO-MWCNTs-rGO/GCE which is an ideal platform for non-enzymatic glucose detection.

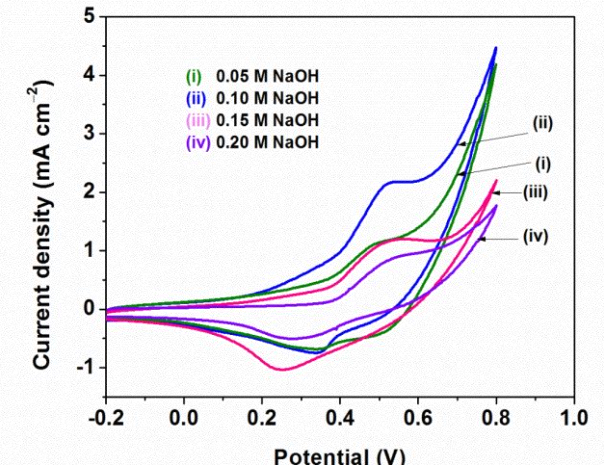

Figure 4.58 CV of 20% NiO-MWCNT/GCE at different concentration of NaOH solution.

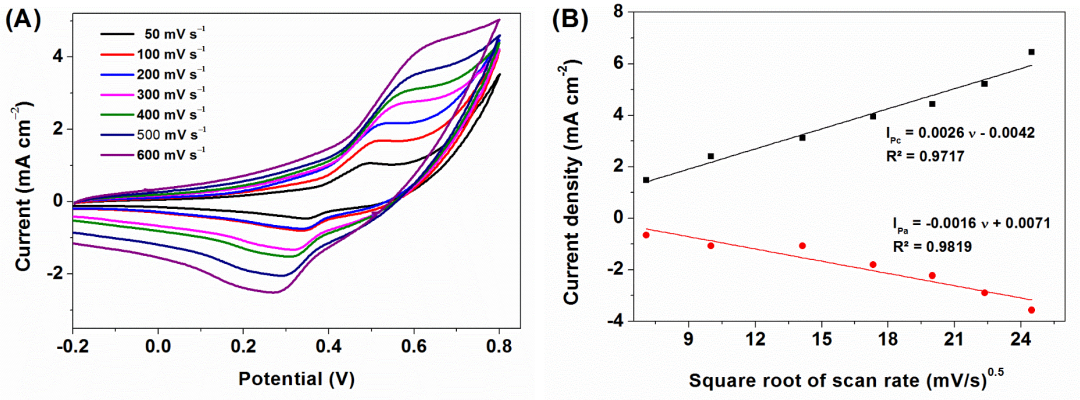

Figure 4.59 (A) Cyclic voltammograms of 20 % NiO-MWCNT/GCE at different scan rates from 50 mV s^{-1} to 600 mV s^{-1} in 0.1 M NaOH with 2.0 mM glucose and (B) A plot of peak current density vs. square root of scan rate.

4.8.3 Chronoamperometric Detection of Glucose

Figure 4.60A shows the typical current density versus time (i-t) plots obtained from the chronoamperometric response at 20% NiO–MWCNT-rGO/GCE with successive addition of 0.2 mM glucose under working potentials of 0.4 V, 0.45 V, 0.5 V, 0.55 V and 0.6 V (a-e). From the figure, it is observed that, appreciable increase in electrode current with the raise in applied potential until the potential reached +0.55 V. However, electrode current at 0.6 V start declining, which may be due the potentially interfering species which are stable only under low potential can generate many intermediate species that would probably obstruct the glucose oxidation. In addition, highest electrode current records at 0.55 V matches well with the anodic oxidation peak potential (Figure 4.56B, l) obtained from CV measurement. Thus, 0.55 V has been chosen as the optimum working potential in the following experiments. Figure 4.60B shows an chronoamperometric response recorded for 20% NiO–MWCNT-rGO/GCE in comparison with other modified electrodes like NiO /GCE, 10%, 30% and 40% NiO–MWCNT-rGO/GCE with successive addition of 0.5 mM glucose under optimal conditions of 0.55 V as working potential in 0.1 M NaOH solution. Upon each addition of glucose, a step-wise increase in current density appears while the solution was being constantly stirred. The steady-state current signal achieved for 20% NiO–MWCNT-rGO/GCE within 3 s (Figure 4.60C), suggests the faster response of the electrode. The results show that the current recorded at 20% NiO–MWCNT-rGO/GCE is 5.2, 1.5, 4.6 and 6 times greater than the NiO/GCE, 10%, 30% and 40% NiO–MWCNT-rGO/GCE, respectively. The highest current recorded for the 20% NiO–MWCNT-rGO/GCE can be attributed to the uniformly decorated NiO-NPs on the surface of MWCNT and rGO. 30% and 40% composites record lesser electrode current due to the supressed electrochemical activity and slower electron movement of dense agglomerated NiO particle in the 30 and 40% NiO–MWCNT-rGO composite modified electrodes. However, when precursor load is 10%, the electrode current recoded is lesser than 20%, which may be due to lesser active NiO available on the surface of the electrode.

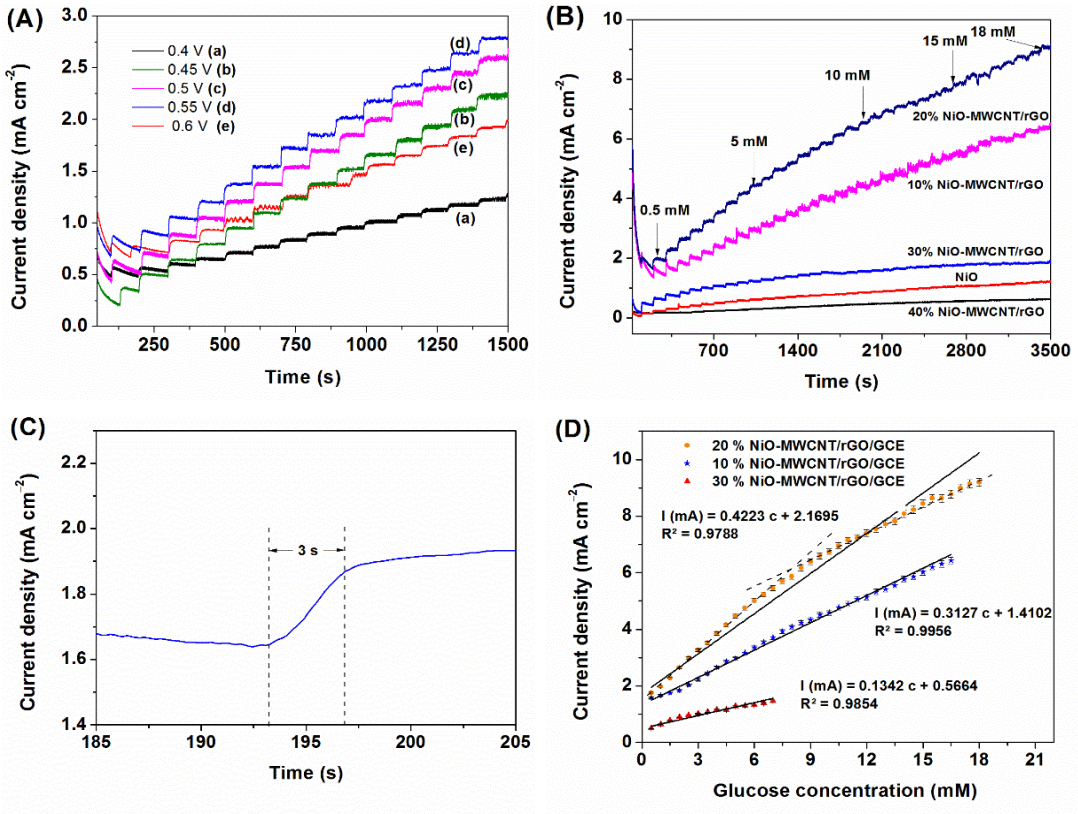

Figure 4.60 (A) Chronoamperometric responses of 20 % NiO-MWCNT/GCE at different working potentials in 0.1 M NaOH with every succsive addition of 0.2 mM glucose, (B) Current–time responses recoded for different modified electrodes fabricated at 0.55 V in 0.1 M NaOH with every succsive addition of 0.5 mM glucose (C) Response time measurement using i-t curve and (D) Electrode current density measured at 0.55 V vs. glucose concentration using different modified electrodes.

Figure 4.60D, displays the linear calibration curve over a glucose concentration ranging upto 16 mM (a), 19 mM (b) and 7.5 Mm (c) for 10, 20 and 30% NiO–MWCNT-rGO/GCE, respectively. The sensitivity for these modified electrodes were calculated to be 3126.5 μA cm^{-2} mM^{-1}, 4224.3 μA cm^{-2} mM^{-1} and 1341.5 μA cm^{-2} mM^{-1} with a limit of detection (LOD) of 2.37 μM, 0.92 μM and 1.41 μM for 10, 20 and 30% NiO–MWCNT-rGO/GCE, respectively. The corresponding regression value (R^2) for these linear curves are measured to be 0.9956, 0.9788 and 0.9854, respectively. Thus, the obtained results like sensitivity, detection limit and linear range of the proposed sensor were compared with the nickel based non-enzymatic glucose sensors reported in

literature are summarized in Table 4.14. The proposed 20 % NiO–MWCNT-rGO/GCE shows relatively fast response time with less than 3 s, low detection limits and wide linear range. These results indicated that the 20 % NiO–MWCNT-rGO/GCE exhibited remarkable electro-catalytic activity toward direct glucose oxidation which can be attributed to the synergistic effect of MWCNT, NiO- NPs and rGO. The electrical network formed through NiO-NPs on the surface of rGO sheets separated by the MWCNT spacers, will offer the intrinsic electrical conductivity and also facilitate an easy access to direct oxidation of glucose.

4.8.4 Selectivity of 20% NiO–MWCNT-rGO/GCE

The electrochemical response of the interfering species was examined for 20% NiO-MWCNT-rGO/GCE at a working potential of 0.55 V in 0.1 M NaOH solution (figure 4.61). It is observed that the significant raise in electrode current is recorded by the addition of 2.0 mM glucose. On the contrary, negligible current response was recorded with the addition of 2.0 mM of each interfering species. These factors suggest that 20% NiO-MWCNT-rGO/GCE possess excellent anti-interference properties towards many biomolecules.

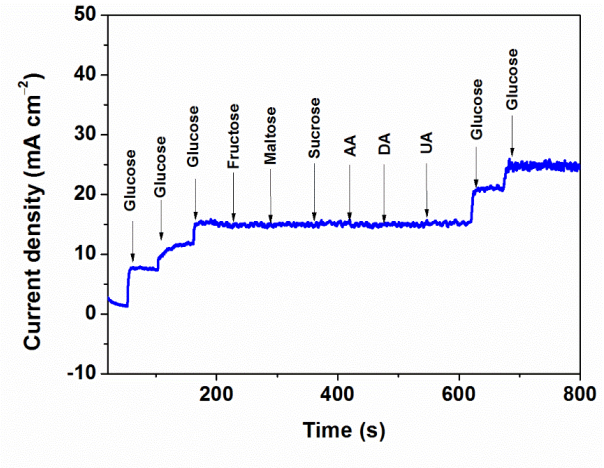

Figure 4.61 Interference test of 20% NiO-MWCNT/GCE in 0.1 M NaOH at +0.55 V with the addition of 2.0 mM glucose and other potential interferents as indicated.

Table 4.14 Performance comparision of different non-enzymatic glucose sensors reported in literature with our proposed sensor.

Electrode	**Linear range (upto mM)**	**Detection Limit (μM)**	**Sensitivity ($\mu A\ mM^{-1}\ cm^{-2}$)**
Nickel electrode (Zhao et al., 2007)	2.5	40.00	-
Ni powder modified electrode (You et al., 2003)	5.0	0.20	40.0
NiO/MWCNTs electrode (Zhang et al., 2010b)	7.0	2.00	1768.8
Ni–MWNTs (Sun et al., 2012)	17.5	0.89	67.1
Ni–Cu/TiO_2/Ti (Li et al., 2013)	4.2	5.00	1591.0
NA/NiONF-rGO/GCE (Zhang et al., 2012)	0.6	0.80	1100.0
NiO/Pt/ERGO/GCE (Li et al., 2014)	5.6	0.20	668.2
10% NiO–MWCNT-rGO/GCE (**Present work**)	16.0	2.37	3126.5
20% NiO–MWCNT-rGO/GCE (**Present work**)	**19.0**	**0.92**	**4224.3**
30% NiO–MWCNT-rGO/GCE (**Present work**)	7.5	1.41	1341.5

4.8.5 Reproducibility and Stability of NiO-MWCNT-rGO/GCE

The proposed non-enzymatic glucose sensor was investigated for the current response at a fixed concentration of 2.0 mM glucose and the current was measured at every 5 day intervals for 40-days period at 0.55 V applied potential in 0.1 M NaOH solution (Figure 4.62A). After 40 days, the sensor displayed minimal current change and it showed 85% of its initial current response suggesting the excellent stability for 20% NiO-MWCNT-rGO/GCE. Further, the reproducibility of electrode response was also investigated by measuring the current response of glucose oxidation at ten identically fabricated electrodes under same conditions (Figure 4.62B). The RSD of the current response was found to be less than 5%, suggesting greater reproducibility of the electrode. This excellent long-term storage stability and reproducibility can be attributed to the physical as well as chemical stability of NiO-NPs on the surface of rGO and MWCNTs composite.

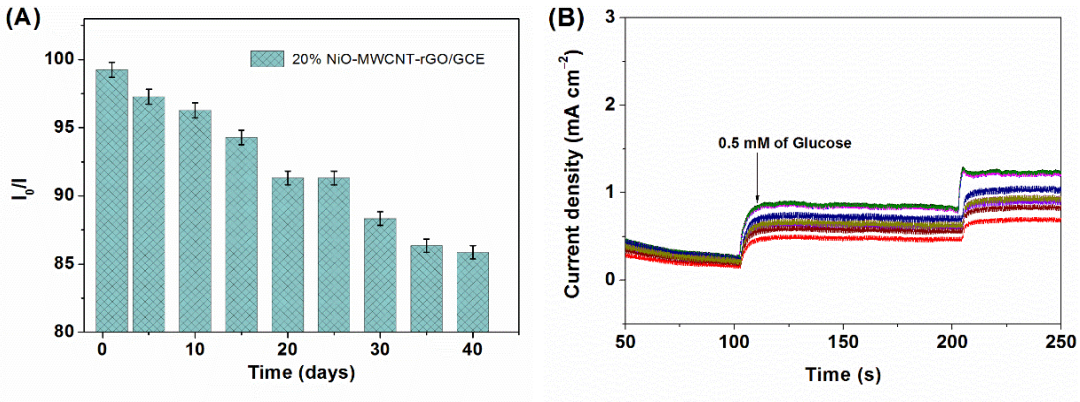

Figure 4.62 (A) Stability of 20% NiO-MWCNT-rGO/GCE stored at ambient conditions over four weeks using 0.1 M NaOH with 2.0 mM glucose at +0.55 V and (B) i-t response for stability check using ten identical 20 NiO-MWCNT/GCE.

4.8.6 Practical application of the proposed sensor in Human Blood Serum (HBS)

For practical application, 20% NiO-MWCNT-rGO/GCE was investigated to determine the glucose concentration in HBS. HBS was injected into 10 mL of 0.1 M NaOH solution at an applied potential of +0.55 V under constant stirring. The electrode current recorded was correlated with glucose concentration calibration curve (Figure

4.60D). The values obtained were compared with the results obtained using a commercial glucose meter and the measured values are tabulated in Table 4.15. The results show that accuracy of the electrodes is > 94% with the RSD less than 6 %. Hence, these results suggest that, the proposed 20% NiO-MWCNT-rGO/GCE could be used practically for routine analysis of glucose in biological samples.

Table 4.15 The detection of glucose in HBS.

Sample	**Glucose (mM) (Proposed sensor)**	**RSD* (N = 4)**	**Glucose (mM) (commercial glucose sensor)**	**Actual glucose Conc. added (mM)**	**Accuracy %**
1	4.3	5.8 %	4.5	4.5	95.5
2	6.5	4.5 %	6.6	6.6	98.5
3	5.7	2.8 %	5.7	5.7	100.0
4	4.5	4.5 %	4.8	4.6	97.8
5	5.1	4.0 %	5.2	5.0	98.0

* Average of four trials

CHAPTER 5

SUMMARY, CONCLUSIONS AND SCOPE FOR FUTURE WORK

Chapter 5 outlines the summery of the work presented in the thesis along with important conclusions drawn from the investigation. Scope for feature research has been included here.

5.1 SUMMARY

In this thesis, the electrochemical glucose sensing platforms based on metal oxide decorated carbon nanotubes are presented. The behaviour of non-enzymatic glucose sensor has been demonstrated as direct function of the electrode material on which the glucose is oxidized. The important aspect of this work is implementing eco-friendly, scalable approach to synthesise MWCNTs, metal oxide (NiO, CuO and Co_3O_4), rGO and their composites followed by fabrication of non-enzymatic electrode for glucose sensing. The carbon nanomaterials like MWCNTs and rGO act as a transducer material, whereas, the metal oxides (NiO, CuO and Co_3O_4) act as electro catalyst to catalyse the glucose under the applied potential. The nanostructured metal oxide MWCNTs modified electrode is capable of direct electrooxidation of glucose without enzyme immobilization and reduces the costs of the sensor fabrication. It is evident from the results obtained that fabricated non-enzymatic glucose electrodes offer high sensitivity, selectivity, low LOD, long term stability, low cost, simple and reproducible fabrication method. These fabricated non-enzymatic electrodes operate at low potential and hence the possible interfering signals are avoided. The catalytic oxidation mechanisms of these direct glucose oxidation process at metal oxide and carbon electrodes are clear and also debated. Nevertheless, glucose sensing based on metal-oxide nanomaterials still has many advantages in terms of miniaturization and development of semi-invasive sensing devices especially for the in vivo detection even though it requires more academic and technical studies for commercialization.

MWCNTs were grown successfully by float catalyst method using Ferrocene as catalyst precursors followed by purification. Using eco-friendly, solvent-free, thermal degradation methods, the purified MWCNTs are decorated with metal oxides (NiO, CuO, Co_3O_4) and the composites obtained as NiO-MWCNTs, CuO-MWCNTs, Co_3O_4-MWCNTs and NiO-MWCNT-rGO. Metal formate is used as precursor for synthesis of metal oxide nanoparticles used in the composite synthesis as it is eco-friendly in nature, by emission of non-toxic gasses and pure metal/metal oxide residue as by-products. The as synthesized MWCNTs and its composite samples were characterised by various techniques. The surface morphology and elemental composition were studied by FESEM, TEM, PXRD, Raman spectroscopy. These materials fabricated as non-enzymatic electrode for glucose sensing and

the electro-catalytic activity of the same are analysed by CV and chronoamperometry. Finally, the sensor parameters like sensitivity, selectivity, stability, response time and reproducibility of the fabricated electrodes were investigated. The Electrochemical findings of the work have been briefly tabulated and given below.

The MWCNT is synthesized by CVD method with less surface defects.

- Prepared NiO-MWCNTs composites show plant root nodule like morphology with NiO average particle size of 20 nm. Optimized geometric structure of NiO-MWCNT composite and charge transfer between MWCNT and NiO-NPs are visualized using DFT.
- The non-enzymatic NiO-MWCNTs/CPE glucose sensing using chronoamperometry, measurement show the sensitivity of 6527 μA $mM^{-1}cm^{-2}$, LOD of 23 μM, response time of 3 s and linear concentration range up to 14 mM. However, the NiO-MWCNTs/GCE under optimised conditions shows the 7068 μA $mM^{-1}cm^{-2}$, LOD of 0.5 μM, response time of 3s and linear concentration range up to 15 mM.

  Among CPE and GCE modified NiO-MWCNTs electrodes, the GCE shows comparatively good response. The ease of fabrication with very little composite sample required, greater conductivity, stability towards alkaline solution and reusable properties makes GCE is very promising for the non-enzymatic electrode fabrication. Hence, in our studies we employed modified GCE as a working electrode.
- In CuO decorated MWCNTs composite samples, the 10 wt% CuO-MWCNTs samples shows uniform decoration with good surface coverage and lesser agglomerated CuO-NPs with an average particle size of 12 nm. For fabricated CuO-MWCNTs/GCE under optimized electrochemical investigation, sensitivity of 3530 μA $mM^{-1}cm^{-2}$, LOD of 18 μM, response time of 5 s and linear concentration range up to 18 mM was found. These results have been attributed to the noteworthy electro-catalytic properties CuO and high conductive and high surface are of MWCNTs.
- In case of different weight ratio of Co_3O_4-MWCNTs composite samples, the 10 wt% sample is considered to be optimised ratio for uniform decoration, least surface defects, lesser agglomeration with an average particle size is about 10 nm. On electrode fabrication and non-ezymatic glucose sensing the Co_3O_4-MWCNTs/GCE shows the sensor features like high sensitivity of 5089 μA mM^{-1} cm^{-2} (R^2: 0.988) with a LOD of 10.42 μM and linear range of glucose concentration up to 12 mM.

These results have been attributed to the self-assembled Co_3O_4-NPs over the MWCNTs surface with reliable electro-catalytic properties.

- All the modified electrodes (NiO-MWCNTs/GCE, CuO-MWCNTs/GCE and Co_3O_4-MWCNTs/GCE) show desirable sensor features like greater stability, reproducibility and selectivity for glucose in compare with the potentially interference molecules like AA, UA, DA, fructose, sucrose, maltose, and UA. Besides that, the modified electrodes are also investigated for glucose response in human blood serum and obtained results correlate well with the results from WHO approved commercial glucometer.
- In NiO-MWCNT-rGO a ternary composite, the NiO is uniformly decorated on the surface of conductive carbon matrices network such as MWCNTs and reduced graphene oxide (rGO). Under the optimal conditions the 20 wt% NiO-MWCNT-rGO/GCE electrode exhibits the sensitivity of 4223.3 μA cm^{-2} mM^{-1} and LOD of 0.92 μM over a linear glucose concentration range up to 19 mM.
- The fabricated electrode was successfully examined to detect glucose in human blood serum. The fabricated electrode also exhibits an excellent selectivity, reproducibility and long-term stability.
- A Comparative Evaluation of all the fabricated biosensors in terms of their performance characteristics is given as Table 5.1.

Table 5.1: Comparative Evaluation of all the fabricated biosensors in terms of their performance characteristics

Sl. No.	Parameters	NiO-MWNCTs/ CPE	NiO-MWNCTs/GCE	CuO-MWCNT/GCE	Co_3O_4-MWCNT/GCE	NiO-MWNCTs/GCE
1.	**Electrolyte**	0.2 M NaOH	0.1 M NaOH	0.2 M NaOH	0.2 M NaOH	0.1 M NaOH
2.	**CA working potential**	0.50 V	0.50 V	+0.50	0.55	0.55
3.	**Response time**	3s	3s	4s	5s	3s
4.	**Sensitivity** ($mA\ cm^{-1}\ mM^{-1}$)	6540.0	7068.0	3530.0	5089.1	4224.3
5.	**LOD (μM)**	12.0	0.50	0.30	10.40	0.92
6.	**Selectivity**	Yes	Yes	Yes	Yes	Yes
7.	Linear Range	14.0	15.0	18.0	12.0	19.0
8.	**Stability**	30 days (> 80% response retain)	40 days (> 85% response retain)	25 days (> 85% response retain)	25 days (> 85% response retain)	40 days (> 85% response retain)

5.2 CONCLUSIONS

From the thesis, the conclusion obtained are as follows.

- Metal formate is an eco-friendly precursor to synthesize metal/metal oxide nanoparticles and their carbon nanomaterial composites at low temperature.
- The Carbon nanomaterials like CNT and rGO with the higher surface area and greater conductivity play important role in new generation sensor technology due to their effective charge transfer capability.
- Synergistic effect of carbon nanomaterials and metal oxide nanoparticles enhance the catalytic properties towards direct glucose oxidation and enhances the sensor features.
- The metal oxides nanoparticles like NiO, Co_3O_4, CuO and their carbon nanomaterial composite can be alternate electrode material to replace enzyme based glucose sensor.
- Among all the tested modified electrodes, the NiO-MWCNT/GCE showed the best glucose sensing ability when considered for selectivity, LOD and stability.

5.3 SCOPE FOR FUTURE WORK

The non-enzymatic glucose sensor developed in this study was found to respond well in alkaline condition. But this pH is fairly high when compared to the pH of physiological fluids. Further studies are planned to develop non-enzymatic sensors based on above metal oxide-MWCNT and (or) rGO composites which responds to glucose at pH of physiological fluids.

In the present study, GCE was chosen as modified working electrode. The cost effective, easy usable, screen printed electrode and disposable strip type electrode are planned to fabricate and used to explore the possible application for the sensing of glucose and other biological molecules.

The literature shows the bimetallic-carbon composite's excellent catalytic and conductive properties. Therefore, synthesis of bimetallic–CNT and (or) graphene composites in bulk scale and exploration of the plausible application in bio-molecule sensing is planned.

REFERENCES

Ahmad, R., Tripathy, N., Hahn, Y.-B., Umar, A., Ibrahim, A.A. and Kim, S.H. (2015). "A robust enzymeless glucose sensor based on CuO nanoseed modified electrodes." *Dalton Trans.*, 44 (28), 12488–12492.

Alizadeh, T. and Mirzagholipur, S. (2014). "A Nafion-free non-enzymatic amperometric glucose sensor based on copper oxide nanoparticles–graphene nanocomposite." *Sens. Actuators B Chem*., 198, 438–447.

Ang, L.M., Hor, T.S.A., Xu, G.Q., Tung, C.H., Zhao, S.P. and Wang, J.L.S. (2000). "Decoration of activated carbon nanotubes with copper and nickel." *Carbon*, 38 (3), 363–372.

Bai, H., Han, M., Du, Y., Bao, J. and Dai, Z. (2010). "Facile synthesis of porous tubular palladium nanostructures and their application in a nonenzymatic glucose sensor." *Chem. Commun*., 46 (10), 1739–1741.

Bai, Y., Du, M., Chang, J., Sun, J. and Gao, L. (2014). "Supercapacitors with high capacitance based on reduced graphene oxide/carbon nanotubes/NiO composite electrodes." *J. Mater. Chem.* A, 2 (11), 3834–3840.

Bai, Y., Yang, W., Sun, Y. and Sun, C. (2008). "Enzyme-free glucose sensor based on a three-dimensional gold film electrode." *Sens. Actuators B Chem*., 134 (2), 471–476.

Bao, J., Hou, C., Zhang, Y., Li, Q., Huo, D., Yang, M. and Luo, X. (2015). "A non-enzymatic glucose sensor based on copper oxide nanowires-single wall carbon nanotubes." *J. Electrochem. Soc.*, 162 (3), B47–B51.

Buerk, D.G. (1995). "*Biosensors: Theory and Applications* (CRC Press).

Byrappa, K., Ohara, S. and Adschiri, T. (2008). "Nanoparticles synthesis using supercritical fluid technology – towards biomedical applications." *Adv. Drug Deliv.* Rev., 60 (3), 299–327.

Cao, F., Guo, S., Ma, H., Shan, D., Yang, S. and Gong, J. (2011). "Nickel oxide microfibers immobilized onto electrode by electrospinning and calcination for

nonenzymatic glucose sensor and effect of calcination temperature on the performance." *Biosens. Bioelectron.*, 26 (5), 2756–2760.

Cass, A.E.G. (1990). "Biosensors: A Practical Approach (IRL Press at Oxford University Press).

Castro Neto, A.H., Guinea, F., Peres, N.M.R., Novoselov, K.S. and Geim, A.K. (2009). "The electronic properties of graphene." *Rev. Mod. Phys.*, 81 (1), 109–162.

Celej, M.S. and Rivas, G. (1998). "Amperometric glucose biosensor based on gold-dispersed carbon paste." *Electroanalysis*, 10 (11), 771–775.

Céspedes, F., Martínez-Fàbregas, E. and Alegret, S. (1993). "Amperometric glucose biosensor based on an electrocatalytically bulk-modified epoxy-graphite biocomposite." *Anal. Chim. Acta*, 284 (1), 21–26.

Chen, C., Xie, Q., Yang, D., Xiao, H., Fu, Y., Tan, Y. and Yao, S. (2013). "Recent advances in electrochemical glucose biosensors: a review." *RSC Adv.*, 3 (14), 4473–4491.

Chen, J., Zhang, W.-D. and Ye, J.-S. (2008). "Nonenzymatic electrochemical glucose sensor based on MnO2/MWNTs nanocomposite." *Electrochem. Commun.*, 10 (9), 1268–1271.

Chen, K.-J., Lee, C.-F., Rick, J., Wang, S.-H., Liu, C.-C. and Hwang, B.-J. (2012). "Fabrication and application of amperometric glucose biosensor based on a novel PtPd bimetallic nanoparticle decorated multi-walled carbon nanotube catalyst." *Biosens. Bioelectron.*, 33 (1), 75–81.

Chen, Q., Wang, J., Rayson, G., Tian, B. and Lin, Y. (1993). "Sensor array for carbohydrates and amino acids based on electrocatalytic modified electrodes." *Anal. Chem.*, 65 (3), 251–254.

Chen, X., Lin, Z., Chen, D.-J., Jia, T., Cai, Z., Wang, X., Chen, X., Chen, G. and Oyama, M. (2010). "Nonenzymatic amperometric sensing of glucose by using palladium nanoparticles supported on functional carbon nanotubes." *Biosens. Bioelectron.*, 25 (7), 1803–1808.

Cherevko, S. and Chung, C.-H. (2009). "Gold nanowire array electrode for non-enzymatic voltammetric and amperometric glucose detection." *Sens. Actuators B Chem.*, 142 (1), 216–223.

Clark, L.C. and Lyons, C. (1962). "Electrode systems for continuous monitoring in cardiovascular surgery." *Ann. N. Y. Acad. Sci*., 102 (1), 29–45.

Connolly, P. (1995). "Clinical diagnostics opportunities for biosensors and bioelectronics." *Biosens. Bioelectron*., 10 (1–2), 1–6.

Cooper, J.R., Bloom, F.E. and Roth, R.H. (2003). "The biochemical basis of neuropharmacology (Oxford University Press).

Coquay, P., Peigney, A., Grave, E. De, Flahaut, E., Vandenberghe, R.E. and Laurent, C. (2005). "Fe/Co alloys for the catalytic chemical vapor deposition synthesis of single- and double-walled carbon nanotubes (CNTs). 1. The CNT−Fe/Co−MgO System." *J. Phys. Chem. B*, 109 (38), 17813–17824.

Cui, H.-F., Ye, J.-S., Zhang, W.-D., Li, C.-M., Luong, J.H.T. and Sheu, F.-S. (2007). "Selective and sensitive electrochemical detection of glucose in neutral solution using platinum–lead alloy nanoparticle/carbon nanotube nanocomposites." *Anal. Chim. Acta*, 594 (2), 175–183.

Dai, Y.-Q. and Shiu, K.-K. (2004). "Highly sensitive amperometric glucose biosensor based on glassy carbon electrode with copper/palladium coating." *Electroanalysis*, 16 (21), 1806–1813.

Deng, S., Jian, G., Lei, J., Hu, Z. and Ju, H. (2009). "A glucose biosensor based on direct electrochemistry of glucose oxidase immobilized on nitrogen-doped carbon nanotubes." *Biosens. Bioelectron*., 25 (2), 373–377.

Dillon, A.C., Yudasaka, M. and Dresselhaus, M.S. (2004). "employing raman spectroscopy to qualitatively evaluate the purity of carbon single-wall nanotube materials." *J. Nanosci. Nanotechnol*., 4 (7), 691–703.

Ding, Y., Wang, Y., Su, L., Bellagamba, M., Zhang, H. and Lei, Y. (2010a). "Electrospun Co3O4 nanofibers for sensitive and selective glucose detection." *Biosens. Bioelectron*., 26 (2), 542–548.

Ding, Y., Wang, Y., Su, L., Zhang, H. and Lei, Y. (2010b). "Preparation and characterization of NiO–Ag nanofibers, NiO nanofibers, and porous Ag: towards the development of a highly sensitive and selective non-enzymatic glucose sensor." *J. Mater. Chem.*, 20 (44), 9918–9926.

Dong, X., Li, B., Wei, A., Cao, X., Chan-Park, M.B., Zhang, H., Li, L.-J., Huang, W. and Chen, P. (2011). "One-step growth of graphene–carbon nanotube hybrid materials by chemical vapor deposition." *Carbon*, 49 (9), 2944–2949.

Dong, X., Ma, Y., Zhu, G., Huang, Y., Wang, J., Chan-Park, M.B., Wang, L., Huang, W. and Chen, P. (2012b). "Synthesis of graphene–carbon nanotube hybrid foam and its use as a novel three-dimensional electrode for electrochemical sensing." *J. Mater. Chem.*, 22 (33), 17044–17048.

Dong, X.-C., Xu, H., Wang, X.-W., Huang, Y.-X., Chan-Park, M.B., Zhang, H., Wang, L.-H., Huang, W. and Chen, P. (2012a). "3D Graphene–cobalt oxide electrode for high-performance supercapacitor and enzymeless glucose detection." *ACS Nano*, 6 (4), 3206–3213.

Du, P., Zhou, B. and Cai, C. (2008). "Development of an amperometric biosensor for glucose based on electrocatalytic reduction of hydrogen peroxide at the single-walled carbon nanotube/nile blue A nanocomposite modified electrode." *J. Electroanal. Chem.*, 614 (1–2), 149–156.

Eklund, P.C., Holden, J.M. and Jishi, R.A. (1995). "Vibrational modes of carbon nanotubes; Spectroscopy and theory." *Carbon*, 33 (7), 959–972.

Erickson, D., Mandal, S., Yang, A.H.J. and Cordovez, B. (2007). "Nanobiosensors: optofluidic, electrical and mechanical approaches to biomolecular detection at the nanoscale." *Microfluid. Nanofluidics*, 4 (1-2), 33–52.

Fairclough, S.H. and Houston, K. (2004). "A metabolic measure of mental effort." *Biol. Psychol.*, 66 (2), 177–190.

Faridbod, F., Gupta, V.K. and Zamani, H.A. (2012). "Electrochemical sensors and biosensors." *Int. J. Electrochem.*, 352546.

Ferraris, R.P. (2001). "Dietary and developmental regulation of intestinal sugar transport." *Biochem. J.*, 360 (Pt 2), 265–276.

Fleischmann, M., Korinek, K. and Pletcher, D. (1971). "The oxidation of organic compounds at a nickel anode in alkaline solution." *J. Electroanal. Chem. Interfacial Electrochem.*, 31 (1), 39–49.

Frew, J.E. and Hill, H.A.O. (1987). "Electrochemical biosensors." *Anal. Chem.*, 59 (15), 933A–944A.

Gailliot, M.T. and Baumeister, R.F. (2007). "The Physiology of willpower: linking blood glucose to self-control." *Personal. Soc. Psychol. Rev.*, 11 (4), 303–327.

Gamburzev, S., Atanasov, P. and Wilkins, E. (1995). "Glucose biosensor based on oxygen electrode Part III: Long-term performance of the glucose biosensor in blood plasma at body temperature." *Anal. Lett.*, 28 (7), 1143–1157.

Gamburzev, S., Atanasov, P. and Wilkins, E. (1996). "Performance of glucose biosensor based on oxygen electrode in physiological fluids and at body temperature." *Sens. Actuators B Chem.*, 30 (3), 179–183.

Gamburzev, S., Atanasov, P. and Wilkins, E. (1997). "Oxygen electrode with pyrolyzed cotmpp catalyst: application in glucose biosensor." *Anal. Lett.*, 30 (3), 503–514.

Gan, T. and Hu, S. (2011). "Electrochemical sensors based on graphene materials." *Microchim. Acta*, 175 (1-2), 1–19.

Gangopadhyay, R. and De, A. (2000). "Conducting polymer nanocomposites: A brief overview." *Chem. Mater.*, 12 (3), 608–622.

González, V.J., Martín-Alberca, C., Montalvo, G., García-Ruiz, C., Baselga, J., Terrones, M. and Martin, O. (2014). "Carbon nanotube-Cu hybrids enhanced catalytic activity in aqueous media." *Carbon*, 78, 10–18.

Gooding, J.J. (2005). "Nanostructuring electrodes with carbon nanotubes: A review on electrochemistry and applications for sensing." *Electrochimica Acta*, 50 (15), 3049–3060.

Gorski, W. and Kennedy, R.T. (1997). "Electrocatalyst for non-enzymatic oxidation of glucose in neutral saline solutions." *J. Electroanal. Chem*., 424 (1–2), 43–48.

Guilbault, G.G. and Montalvo, J.G. (1969). "Urea-specific enzyme electrode." *J. Am. Chem. Soc*., 91 (8), 2164–2165.

Guo, C., Zhang, X., Huo, H., Xu, C. and Han, X. (2013). "Co3O4 microspheres with free-standing nanofibers for high performance non-enzymatic glucose sensor." *Analyst*, 138 (22), 6727–6731.

Guo, T., Nikolaev, P., Thess, A., Colbert, D.T. and Smalley, R.E. (1995). "Catalytic growth of single-walled manotubes by laser vaporization." *Chem. Phys. Lett.*, 243 (1–2), 49–54.

Harris, P.J.F. (2007). "Solid state growth mechanisms for carbon nanotubes." *Carbon*, 45 (2), 229–239.

He, C., Zhao, N., Shi, C., Du, X., Li, J., Li, H. and Cui, Q. (2007). "An approach to obtaining homogeneously dispersed carbon nanotubes in al powders for preparing reinforced al-matrix composites." *Adv. Mater.*, 19 (8), 1128–1132.

Heller, A. and Feldman, B. (2010). "Electrochemistry in diabetes management." *Acc. Chem. Res.*, 43 (7), 963–973.

Homola, J. (2006). "Surface plasmon resonance based sensors (springer science & business media).

Hong, T.-K., Lee, D.W., Choi, H.J., Shin, H.S. and Kim, B.-S. (2010). "Transparent, flexible conducting hybrid multilayer thin films of multiwalled carbon nanotubes with graphene nanosheets." *ACS Nano*, 4 (7), 3861–3868.

Hsieh, C.-T., Chou, Y.-W. and Chen, W.-Y. (2007). "Synthesis and electrochemical characterization of carbon nanotubes decorated with nickel nanoparticles for use as an electrochemical capacitor." *J. Solid State Electrochem*., 12 (6), 663–669.

Huang, Y. and Kim, D.-H. (2011). "Synthesis and self-assembly of highly monodispersed quasispherical gold nanoparticles." *Langmuir*, 27 (22), 13861–13867.

Huiqun, C., Meifang, Z. and Yaogang, L. (2006). "Decoration of carbon nanotubes with iron oxide." *J. Solid State Chem*., 179 (4), 1208–1213.

Iijima, S. (1991). "Helical microtubules of graphitic carbon." *Nature,* 354(6348), 56-

Jena, B.K. and Raj, C.R. (2006). "Enzyme-free amperometric sensing of glucose by using gold nanoparticles." *Chem. – Eur. J.*, 12 (10), 2702–2708.

Jiang, J. and Li, L. (2007). "Synthesis of sphere-like Co3O4 nanocrystals via a simple polyol route." *Mater. Lett.*, 61 (27), 4894–4896.

Kang, X., Mai, Z., Zou, X., Cai, P. and Mo, J. (2007). "A sensitive nonenzymatic glucose sensor in alkaline media with a copper nanocluster/multiwall carbon nanotube-modified glassy carbon electrode." *Anal. Biochem*., 363 (1), 143–150.

Karyakin, A.A., Gitelmacher, O.V. and Karyakina, E.E. (1994). "A high-sensitive glucose amperometric biosensor based on prussian blue modified electrodes." *Anal. Lett.*, 27 (15), 2861–2869.

Kenfack, F. and Langbein, H. (2005). "Synthesis and thermal decomposition of freeze-dried copper–iron formates." *Thermochim. Acta*, 426 (1–2), 61–72.

Khanderi, J., Hoffmann, R.C., Gurlo, A. and Schneider, J.J. (2009). "Synthesis and sensoric response of ZnO decorated carbon nanotubes." *J. Mater. Chem*., 19 (28), 5039–5046.

Kharat, A.N., Pendleton, P., Badalyan, A., Abedini, M. and Amini, M.M. (2002). "Decomposition of nickel formate on sol–gel alumina and characterization of product by x-ray photoelectron and tof-sims spectroscopies." *J. Catal.*, 205 (1), 7–15.

Khimchenko, Y.I., Vasilenko, V.P., Radkevich, L.S., Myalkovskii, V.V., Chubar', T.V. and Chegoryan, V.M. (1977). "Decomposition of iron, cobalt, nickel, and copper formates." *Sov. Powder Metall. Met. Ceram.,* 16 (5), 327–332.

Kim, D.-W., Rhee, K.-Y. and Park, S.-J. (2012). "Synthesis of activated carbon nanotube/copper oxide composites and their electrochemical performance." *J. Alloys Compd*., 53, 0 6–10.

Kim, S.N., Rusling, J.F. and Papadimitrakopoulos, F. (2007). "Carbon Nanotubes for electronic and electrochemical detection of biomolecules." *Adv. Mater*., 19 (20), 3214–3228.

Kim, W.J., Lee, T.J. and Han, S.H. (2014). "Multi-layer graphene/copper composites: Preparation using high-ratio differential speed rolling, microstructure and mechanical properties." *Carbon*, 69, 55–65.

Kissinger, P.T. and Heineman, W.R. (1983). "Cyclic voltammetry." *J. Chem. Educ*., 60 (9), 702.

Kresse, G. and Hafner, J. (1993). "text initio molecular dynamics for liquid metals." *Phys. Rev. B,* 47 (1), 558–561.

Kung, C.-W., Lin, C.-Y., Lai, Y.-H., Vittal, R. and Ho, K.-C. (2011). "Cobalt oxide acicular nanorods with high sensitivity for the non-enzymatic detection of glucose." *Biosens. Bioelectron.,* 27 (1), 125–131.

Kurkina, T. and Balasubramanian, K. (2011). "Towards in vitro molecular diagnostics using nanostructures." *Cell. Mol. Life Sci*., 69 (3), 373–388.

Lang, X.-Y., Fu, H.-Y., Hou, C., Han, G.-F., Yang, P., Liu, Y.-B. and Jiang, Q. (2013). "Nanoporous gold supported cobalt oxide microelectrodes as high-performance electrochemical biosensors." *Nat. Commun*., 4: 2169 ,1-8.

Laviron, E. (1979). "General expression of the linear potential sweep voltammogram in the case of diffusionless electrochemical systems." *J. Electroanal. Chem. Interfacial Electrochem*., 101 (1), 19–28.

Lee, K.K., Loh, P.Y., Sow, C.H. and Chin, W.S. (2012). "CoOOH nanosheets on cobalt substrate as a non-enzymatic glucose sensor." *Electrochem. Commun*., 20, 128–132.

Li, C., Qiao, Y., Li, Y. and Wu, Y. (2008). "Decorating multiwalled carbon nanotubes with zinc oxide nanoparticles by thermally decomposing Zn-oleate in an organic medium." *Sci. China Ser. E Technol. Sci*., 52 (5), 1254–1257.

Li, C., Su, Y., Zhang, S., Lv, X., Xia, H. and Wang, Y. (2010). "An improved sensitivity nonenzymatic glucose biosensor based on a CuxO modified electrode." *Biosens. Bioelectron.*, 26 (2), 903–907.

Li, M., Bo, X., Mu, Z., Zhang, Y. and Guo, L. (2014). "Electrodeposition of nickel oxide and platinum nanoparticles on electrochemically reduced graphene oxide film as a nonenzymatic glucose sensor." *Sens. Actuators B Chem*., 192, 261–268.

Li, S., Zhao, Z., Huang, Y., Di, J., Jia, Y. (Alec) and Zheng, H. (2015). "Hierarchically structured WO3–CNT@TiO2NS composites with enhanced photocatalytic activity." *J. Mater. Chem.* A, 3 (10), 5467–5473.

Li, W., Zhang, H., Wang, C., Zhang, Y., Xu, L., Zhu, K. and Xie, S. (1997). "Raman characterization of aligned carbon nanotubes produced by thermal decomposition of hydrocarbon vapor." *Appl. Phys. Lett.*, 70 (20), 2684–2686.

Li, X., Yao, J., Liu, F., He, H., Zhou, M., Mao, N., Xiao, P. and Zhang, Y. (2013). "Nickel/Copper nanoparticles modified TiO2 nanotubes for non-enzymatic glucose biosensors." *Sens. Actuators B Chem.*, 181, 501–508.

Li, X., Zhu, Q., Tong, S., Wang, W. and Song, W. (2009). "Self-assembled microstructure of carbon nanotubes for enzymeless glucose sensor." *Sens. Actuators B Chem.*, 136 (2), 444–450.

Li, Y., Gao, W., Ci, L., Wang, C. and Ajayan, P.M. (2010). "Catalytic performance of Pt nanoparticles on reduced graphene oxide for methanol electro-oxidation." *Carbon*, 48 (4), 1124–1130.

Li, Y., Song, Y.-Y., Yang, C. and Xia, X.-H. (2007). "Hydrogen bubble dynamic template synthesis of porous gold for nonenzymatic electrochemical detection of glucose." *Electrochem. Commun*., 9 (5), 981–988.

Liu, J., Lu, L., Li, A., Tang, J., Wang, S., Xu, S. and Wang, L. (2015). "Simultaneous detection of hydrogen peroxide and glucose in human serum with upconversion luminescence." *Biosens. Bioelectron.*, 68, 204–209.

Liu, Y., Teng, H., Hou, H. and You, T. (2009). "Nonenzymatic glucose sensor based on renewable electrospun Ni nanoparticle-loaded carbon nanofiber paste electrode." *Biosens. Bioelectron.,* 24 (11), 3329–3334.

Lu, L.-M., Zhang, L., Qu, F.-L., Lu, H.-X., Zhang, X.-B., Wu, Z.-S., Huan, S.-Y., Wang, Q.-A., Shen, G.-L. and Yu, R.-Q. (2009). "A nano-Ni based ultrasensitive nonenzymatic electrochemical sensor for glucose: Enhancing sensitivity through a nanowire array strategy*." Biosens. Bioelectron*., 25 (1), 218–223.

Lu, L.-M., Zhang, X.-B., Shen, G.-L. and Yu, R.-Q. (2012). "Seed-mediated synthesis of copper nanoparticles on carbon nanotubes and their application in nonenzymatic glucose biosensors." *Anal. Chim. Acta*, 715, 99–104.

Lu, P., Liu, Q., Xiong, Y., Wang, Q., Lei, Y., Lu, S., Lu, L. and Yao, L. (2015). "Nanosheets-assembled hierarchical microstructured Ni(OH)2 hollow spheres for highly sensitive enzyme-free glucose sensors." *Electrochimica Acta*, 168, 148–156.

Lu, X., Zhou, J., Lu, W., Liu, Q. and Li, J. (2008). "Carbon nanofiber-based composites for the construction of mediator-free biosensors." *Biosens. Bioelectron.,* 23 (8), 1236–1243.

Luo, L., Li, F., Zhu, L., Ding, Y., Zhang, Z., Deng, D. and Lu, B. (2013). "Nonenzymatic glucose sensor based on nickel(II)oxide/ordered mesoporous carbon modified glassy carbon electrode." *Colloids Surf. B Biointerfaces*, 102, 307–311.

Malhotra, B.D. and Chaubey, A. (2003). "Biosensors for clinical diagnostics industry." *Sens. Actuators B Chem.,* 91 (1–3), 117–127.

Marazuela, M. and Moreno-Bondi, M. (2002). "Fiber-optic biosensors – an overview." *Anal. Bioanal. Chem*., 372 (5-6), 664–682.

Maroto, A., Balasubramanian, K., Burghard, M. and Kern, K. (2007). "Functionalized metallic carbon nanotube devices for ph sensing." *ChemPhysChem*, 8 (2), 220–223.

McCreery, R.L. (2008). "Advanced carbon electrode materials for molecular electrochemistry." *Chem. Rev*., 108 (7), 2646–2687.

McDowell, L.R. (1989). "Vitamins in animal nutrition: comparative aspects to human nutrition (Academic Press).

Meng, L., Jin, J., Yang, G., Lu, T., Zhang, H. and Cai, C. (2009). "Nonenzymatic electrochemical detection of glucose based on palladium−single-walled carbon nanotube hybrid nanostructures." *Anal. Chem*., 81 (17), 7271–7280.

Meng, Z., Liu, B., Zheng, J., Sheng, Q. and Zhang, H. (2011). "Electrodeposition of cobalt oxide nanoparticles on carbon nanotubes, and their electrocatalytic properties for nitrite electrooxidation." *Microchim. Acta*, 175 (3-4), 251–257.

Mouche, M.-J., Mermet, J.-L., Romand, M. and Charbonnier, M. (1995). "Metal—organic chemical vapor deposition of copper using hydrated copper formate as a new precursor." *Thin Solid Films*, 262 (1–2), 1–6.

Mu, Y., Jia, D., He, Y., Miao, Y. and Wu, H.-L. (2011). "Nano nickel oxide modified non-enzymatic glucose sensors with enhanced sensitivity through an electrochemical process strategy at high potential." *Biosens. Bioelectron*., 26 (6), 2948–2952.

Mun, J., Ha, H.-W. and Choi, W. (2014). "Nano LiFePO4 in reduced graphene oxide framework for efficient high-rate lithium storage." *J. Power Sources*, 251, 386–392.

Nagy, L., Nagy, G. and Hajós, P. (2001). "Copper electrode based amperometric detector cell for sugar and organic acid measurements." *Sens. Actuators B Chem*., 76 (1–3), 494–499.

Nakada, K., Fujita, M., Dresselhaus, G. and Dresselhaus, M.S. (1996). "Edge state in graphene ribbons: Nanometer size effect and edge shape dependence." *Phys. Rev. B*, 54 (24), 17954–17961.

Newman, J.D., Turner, A.P.F. and Marrazza, G. (1992). "Ink-jet printing for the fabrication of amperometric glucose biosensors." *Anal. Chim. Acta*, 262 (1), 13–17.

Niu, X., Lan, M., Zhao, H. and Chen, C. (2013). "Highly sensitive and selective nonenzymatic detection of glucose using three-dimensional porous nickel nanostructures." *Anal. Chem*., 85 (7), 3561–3569.

Park, J.Y., Kim, Y.H., Seong, A. and Yoo, Y.J. (2008). "Amperometric determination of glucose, based on the direct electron transfer between glucose oxidase and tin oxide." *Biotechnol. Bioprocess Eng*., 13 (4), 431–435.

Park, S., Boo, H. and Chung, T.D. (2006). "Electrochemical non-enzymatic glucose sensors." *Anal. Chim. Acta,* 556 (1), 46–57.

Park, S., Chung, T.D. and Kim, H.C. (2003). "Nonenzymatic glucose detection using mesoporous platinum." *Anal. Chem*., 75 (13), 3046–3049.

Park, Y.S., Kim, K.S., Jeong, H.J., Kim, W.S., Moon, J.M., An, K.H., Bae, D.J., Lee, Y.S., Park, G.-S. and Lee, Y.H. (2002). "Low pressure synthesis of single-walled carbon nanotubes by arc discharge." *Synth. Met*., 126 (2–3), 245–251.

Ping, C., Li, F., Jian, Z. and Wei, J. (2006). "Preparation of Cu/CNT Composite Particles and Catalytic Performance on Thermal Decomposition of Ammonium Perchlorate." *Propellants Explos. Pyrotech*., 31 (6), 452–455.

Pohanka, M. (2013). "Cholinesterases in Biorecognition and Biosensors Construction: A Review." *Anal. Lett*., 46 (12), 1849–1868.

Pomeranz, Y. (2013). "Food analysis: Theory and practice (Springer Science & Business Media).

Popov, V.N. (2004). "Carbon nanotubes: properties and application." *Mater. Sci. Eng. R Rep*., 43 (3), 61–102.

Pujadó, M.P. (2012). "Carbon nanotubes as platforms for biosensors with electrochemical and electronic transduction (Springer Science & Business Media).

Qiao, N. and Zheng, J. (2012). "Nonenzymatic glucose sensor based on glassy carbon electrode modified with a nanocomposite composed of nickel hydroxide and graphene." *Microchim. Acta*, 177 (1-2), 103–109.

Rajarao, R. and Bhat, B.R. (2013). "Large-scale synthesis of high purity carbon nanotubes by novel catalytic route." *Synth. React. Inorg. Met.-Org. Nano-Met. Chem*., 43 (10), 1418–1422.

Reich, S. and Thomsen, C. (2004). "Raman spectroscopy of graphite." *Philos. Trans. R. Soc*. Lond. *Math. Phys. Eng. Sci.,* 362 (1824), 2271–2288.

Reimhult, E. and Höök, F. (2015). "Design of surface modifications for nanoscale sensor applications." *Sensors*, 15 (1), 1635–1675.

Reitz, E., Jia, W., Gentile, M., Wang, Y. and Lei, Y. (2008). "CuO nanospheres based nonenzymatic glucose sensor." *Electroanalysis*, 20 (22), 2482–2486.

Ren, H., Liu, Y., Jiao, Q., Fu, X. and Yang, T. (2010). "Preparation of nanocomposite PbO·CuO/CNTs via microemulsion process and its catalysis on thermal decomposition of RDX." *J. Phys. Chem. Solids*, 71 (2), 149–152.

Saito, R., Hofmann, M., Dresselhaus, G., Jorio, A. and Dresselhaus, M.S. (2011). "Raman spectroscopy of graphene and carbon nanotubes." *Adv. Phys*., 60 (3), 413–550.

Salimi, A. and Roushani, M. (2005). "Non-enzymatic glucose detection free of ascorbic acid interference using nickel powder and nafion sol–gel dispersed renewable carbon ceramic electrode*." Electrochem. Commun*., 7 (9), 879–887.

Shahriary, L., Nair, R., Sabharwal, S. and Athawale, A.A. (2015). "One-step synthesis of Ag–reduced graphene oxide–multiwalled carbon nanotubes for enhanced antibacterial activities*." New J. Chem*., 39 (6), 4583–4590.

Shan, C., Yang, H., Song, J., Han, D., Ivaska, A. and Niu, L. (2009). "Direct electrochemistry of glucose oxidase and biosensing for glucose based on graphene." *Anal. Chem*., 81 (6), 2378–2382.

Shang, N.G., Papakonstantinou, P., McMullan, M., Chu, M., Stamboulis, A., Potenza, A., Dhesi, S.S. and Marchetto, H. (2008). "Catalyst-free efficient growth, orientation and biosensing properties of multilayer graphene nanoflake films with sharp edge planes." *Adv. Funct. Mater*., 18 (21), 3506–3514.

Sharifi, E., Salimi, A., Shams, E., Noorbakhsh, A. and Amini, M.K. (2014). "Shape-dependent electron transfer kinetics and catalytic activity of NiO nanoparticles immobilized onto DNA modified electrode: Fabrication of highly sensitive enzymeless glucose sensor." *Biosens. Bioelectron*., 56, 313–319.

Shen, J., Dudik, L. and Liu, C.-C. (2007). "An iridium nanoparticles dispersed carbon based thick film electrochemical biosensor and its application for a single use, disposable glucose biosensor." *Sens. Actuators B Chem.*, 125 (1), 106–113.

Shin, Y.J., Wang, M. and Kameoka, J. (2009). "Electrospun nanofiber biosensor for measuring glucose concentration." *J. Photopolym. Sci. Technol*., 22 (2), 235–237.

Si, P., Huang, Y., Wang, T. and Ma, J. (2013). "Nanomaterials for electrochemical non-enzymatic glucose biosensors." *RSC Adv.*, 3 (11), 3487–3502.

Simpson, G.L.W. and Ortwerth, B.J. (2000). "The non-oxidative degradation of ascorbic acid at physiological conditions." *Biochim. Biophys. Acta BBA - Mol. Basis Dis*., 1501 (1), 12–24.

Singh, A.P., Mishra, M., Hashim, D.P., Narayanan, T.N., Hahm, M.G., Kumar, P., Dwivedi, J., Kedawat, G., Gupta, A., Singh, B.P., Chandra, A., Vajtai, R., Dhawan, S.K., Ajayan, P.M. and Gupta, B.K. (2015). "Probing the engineered sandwich network of vertically aligned carbon nanotube–reduced graphene oxide composites for high performance electromagnetic interference shielding applications." *Carbon*, 85, 79–88.

Soomro, R.A., Nafady, A., Ibupoto, Z.H., Sirajuddin, Sherazi, S.T.H., Willander, M. and Abro, M.I. (2015). "Development of sensitive non-enzymatic glucose sensor using complex nanostructures of cobalt oxide." *Mater. Sci. Semicond. Process*., 34 373–381.

Strasinger, S.K. and Lorenzo, M.S.D. (2001). "Urinalysis and body fluids (F.A. Davis Company).

Strømme, M., Niklasson, G.A. and Granqvist, C.G. (1995). "Voltammetry on fractals." *Solid State Commun.*, 96 (3), 151–154.

Sun, A., Zheng, J. and Sheng, Q. (2012). "A highly sensitive non-enzymatic glucose sensor based on nickel and multi-walled carbon nanotubes nanohybrid films fabricated by one-step co-electrodeposition in ionic liquids." *Electrochimica Acta*, 65 64–69.

Sun, S., Sun, Y., Chen, A., Zhang, X. and Yang, Z. (2015). "Nanoporous copper oxide ribbon assembly of free-standing nanoneedles as biosensors for glucose." *Analyst*, 140 (15), 5205–5215.

Sun, Y., Buck, H. and Mallouk, T.E. (2001). "Combinatorial discovery of alloy electrocatalysts for amperometric glucose sensors." *Anal. Chem*., 73 (7), 1599–1604.

Tian, K., Prestgard, M. and Tiwari, A. (2014). "A review of recent advances in nonenzymatic glucose sensors." *Mater. Sci. Eng*. C, 41, 100–118.

Tominaga, M., Shimazoe, T., Nagashima, M., Kusuda, H., Kubo, A., Kuwahara, Y. and Taniguchi, I. (2006). "Electrocatalytic oxidation of glucose at gold–silver alloy, silver and gold nanoparticles in an alkaline solution*." J. Electroanal. Chem*., 590 (1), 37–46.

Updike, S.J. and Hicks, G.P. (1967). "Reagentless substrate analysis with immobilized enzymes." *Science*, 158 (3798), 270–272.

Vassilev, P., Kanazirska, M. and Tien, H.T. (1985). "Intermembrane linkage mediated by tubulin." *Biochem. Biophys. Res. Commun*., 126 (1), 559–565.

Vassilyev, Y.B., Khazova, O.A. and Nikolaeva, N.N. (1985). "Kinetics and mechanism of glucose electro oxidation on different electrode-catalysts: Part II. Effect of the nature of the electrode and the electrooxidation mechanism." *J. Electroanal. Chem. Interfacial Electrochem*., 196 (1), 127–144.

Wang, B., Li, S., Liu, J. and Yu, M. (2014). "Preparation of nickel nanoparticle/graphene composites for non-enzymatic electrochemical glucose biosensor applications." *Mater. Res. Bull*., 49, 521–524.

Wang, G., He, X., Wang, L., Gu, A., Huang, Y., Fang, B., Geng, B. and Zhang, X. (2012a). "Non-enzymatic electrochemical sensing of glucose." *Microchim. Acta*, 180 (3-4), 161–186.

Wang, G., Lu, X., Zhai, T., Ling, Y., Wang, H., Tong, Y. and Li, Y. (2012b). "Free-standing nickel oxide nanoflake arrays: synthesis and application for highly sensitive non-enzymatic glucose sensors." *Nanoscale*, 4 (10), 3123–3127.

Wang, H., Wang, X., Zhang, X., Qin, X., Zhao, Z., Miao, Z., Huang, N. and Chen, Q. (2009a). "A novel glucose biosensor based on the immobilization of glucose oxidase onto gold nanoparticles-modified Pb nanowires." *Biosens. Bioelectron*., 25 (1), 142–146.

Wang, J. (2005a). "Carbon-nanotube based electrochemical biosensors: A Review." *Electroanalysis*, 17 (1), 7–14.

Wang, J. (2005b). "Nanomaterial-based electrochemical biosensors." *Analyst*, 130 (4), 421–426.

Wang, J. (2008). "Electrochemical glucose biosensors*." Chem. Rev*., 108 (2), 814–825.

Wang, J., Bao, W. and Zhang, L. (2012c). "A nonenzymatic glucose sensing platform based on Ni nanowire modified electrode." *Anal. Methods*, 4 (12), 4009–4013.

Wang, J., Sun, X., Cai, X., Lei, Y., Song, L. and Xie, S. (2007). "Nonenzymatic glucose sensor using freestanding single-wall carbon nanotube films." *Electrochem. Solid-State Lett.*, 10 (5), J58–J60.

Wang, J.X., Sun, X.W., Wei, A., Lei, Y., Cai, X.P., Li, C.M. and Dong, Z.L. (2006). "Zinc oxide nanocomb biosensor for glucose detection." *Appl. Phys. Lett.*, 88 (23), 233106.

Wang, L., Lu, X., Ye, Y., Sun, L. and Song, Y. (2013). "Nickel-cobalt nanostructures coated reduced graphene oxide nanocomposite electrode for nonenzymatic glucose biosensing." *Electrochimica Acta*, 114, 484–493.

Wang, P.P. and Liu, D.Q. (2011). Biosensors and measurement. in biomedical sensors and measurement, (Springer Berlin Heidelberg), pp 199–275.

Wang, W., Zhang, L., Tong, S., Li, X. and Song, W. (2009b). "Three-dimensional network films of electrospun copper oxide nanofibers for glucose determination." *Biosens. Bioelectron*., 25 (4), 708–714.

Wang, X., Hu, C., Liu, H., Du, G., He, X. and Xi, Y. (2010). "Synthesis of CuO nanostructures and their application for nonenzymatic glucose sensing." *Sens. Actuators B Chem.*, 144 (1), 220–225.

Wei, F., Zhang, Q., Qian, W.-Z., Yu, H., Wang, Y., Luo, G.-H., Xu, G.-H. and Wang, D.-Z. (2008). "The mass production of carbon nanotubes using a nano-agglomerate fluidized bed reactor: A multiscale space–time analysis." *Powder Technol.*, 183 (1), 10–20.

Wilson, R. and Turner, A.P.F. (1992). "Glucose oxidase: an ideal enzyme." *Biosens. Bioelectron.*, 7 (3), 165–185.

Wring, S.A., Hart, J.P. and Birch, B.J. (1990). "Voltammetric behaviour of ascorbic acid at a graphite—epoxy composite electrode chemically modified with cobalt phthalocyanine and its amperometric determination in multivitamin preparations." *Anal. Chim. Acta*, 229, 63–70.

Wu, H.-Q., Wei, X.-W., Shao, M.-W., Gu, J.-S. and Qu, M.-Z. (2002). "Synthesis of copper oxide nanoparticles using carbon nanotubes as templates." *Chem. Phys. Lett.*, 364 (1–2), 152–156.

Wu, H.-X., Cao, W.-M., Li, Y., Liu, G., Wen, Y., Yang, H.-F. and Yang, S.-P. (2010). "In situ growth of copper nanoparticles on multiwalled carbon nanotubes and their application as non-enzymatic glucose sensor materials." *Electrochimica Acta*, 55 (11), 3734–3740.

Xiao, X., Michael, J.R., Beechem, T., McDonald, A., Rodriguez, M., Brumbach, M.T., Lambert, T.N., Washburn, C.M., Wang, J., Brozik, S.M., Wheeler, D.R., Burckel, D.B. and Polsky, R. (2012). "Three dimensional nickel–graphene core–shell electrodes." *J. Mater. Chem.*, 22 (45), 23749–23754.

Xu, Q., Zhao, Y., Xu, J.Z. and Zhu, J.-J. (2006). "Preparation of functionalized copper nanoparticles and fabrication of a glucose sensor." *Sens. Actuators B Chem.*, 114 (1), 379–386.

Yang, J., Jiang, L.-C., Zhang, W.-D. and Gunasekaran, S. (2010a). "A highly sensitive non-enzymatic glucose sensor based on a simple two-step electrodeposition of cupric

oxide (CuO) nanoparticles onto multi-walled carbon nanotube arrays." *Talanta*, 82 (1), 25–33.

Yang, J., Zhang, W.-D. and Gunasekaran, S. (2010b). "An amperometric non-enzymatic glucose sensor by electrodepositing copper nanocubes onto vertically well-aligned multi-walled carbon nanotube arrays." *Biosens. Bioelectron*., 26 (1), 279–284.

Yang, W., Ratinac, K.R., Ringer, S.P., Thordarson, P., Gooding, J.J. and Braet, F. (2010c). "Carbon nanomaterials in biosensors: Should you use nanotubes or graphene?" *Angew. Chem. Int. Ed*., 49 (12), 2114–2138.

Ye, J.-S., Wen, Y., Zhang, W. De, Ming Gan, L., Xu, G.Q. and Sheu, F.-S. (2004). "Nonenzymatic glucose detection using multi-walled carbon nanotube electrodes." *Electrochem. Commun*., 6 (1), 66–70.

Yeo, I.-H. and Johnson, D.C. (2001). "Electrochemical response of small organic molecules at nickel–copper alloy electrodes." *J. Electroanal. Chem*., 495 (2), 110–119.

Yoo, E.-H. and Lee, S.-Y. (2010). "Glucose biosensors: An overview of use in clinical practice." *Sensors*, 10 (5), 4558–4576.

You, T., Niwa, O., Chen, Z., Hayashi, K., Tomita, M. and Hirono, S. (2003). "An Amperometric detector formed of highly dispersed ni nanoparticles embedded in a graphite-like carbon film electrode for sugar determination." *Anal. Chem*., 75 (19), 5191–5196.

Yuan, J.H., Wang, K. and Xia, X.H. (2005). "Highly ordered platinum-nanotubule arrays for amperometric glucose sensing." *Adv. Funct. Mater*., 15 (5), 803–809.

Yun, Y.-H., Eteshola, E., Bhattacharya, A., Dong, Z., Shim, J.-S., Conforti, L., Kim, D., Schulz, M.J., Ahn, C.H. and Watts, N. (2009). "Tiny medicine: Nanomaterial-based biosensors." *Sensors*, 9 (11), 9275–9299.

Zhang, C. and Wang, K. (2002). "An Amperometric glucose biosensor incorporating a permeable pre-oxidation layer." *Anal. Lett*., 35 (5), 869–880.

Zhang, W., Peigen, S., Haifeng, X. and Qian, D. (2010b). Design and implement of management clustering primitives based on satellite networks. In 2010 2nd International Conference on Advanced Computer Control (ICACC), pp 259–263.

Zhang, W.-D., Chen, J., Jiang, L.-C., Yu, Y.-X. and Zhang, J.-Q. (2010a). "A highly sensitive nonenzymatic glucose sensor based on NiO-modified multi-walled carbon nanotubes." *Microchim. Acta*, 168 (3-4), 259–265.

Zhang, X., Wang, G., Zhang, W., Wei, Y. and Fang, B. (2009). "Fixure-reduce method for the synthesis of Cu2O/MWCNTs nanocomposites and its application as enzyme-free glucose sensor." *Biosens. Bioelectron*., 24 (11), 3395–3398.

Zhang, Y., Wang, Y., Jia, J. and Wang, J. (2012). "Nonenzymatic glucose sensor based on graphene oxide and electrospun NiO nanofibers." *Sens. Actuators B Chem*., 172, 580–587.

Zhao, C., Shao, C., Li, M. and Jiao, K. (2007). "Flow-injection analysis of glucose without enzyme based on electrocatalytic oxidation of glucose at a nickel electrode." *Talanta*, 71 (4), 1769–1773.

Zhao, X., Mai, Z., Kang, X. and Zou, X. (2008). "Direct electrochemistry and electrocatalysis of horseradish peroxidase based on clay–chitosan-gold nanoparticle nanocomposite." *Biosens. Bioelectron*., 23 (7), 1032–1038.

Zhu, H., Lu, X., Li, M., Shao, Y. and Zhu, Z. (2009). "Nonenzymatic glucose voltammetric sensor based on gold nanoparticles/carbon nanotubes/ionic liquid nanocomposite." *Talanta*, 79 (5), 1446–1453.

Zhu, J., Jiang, J., Liu, J., Ding, R., Li, Y., Ding, H., Feng, Y., Wei, G. and Huang, X. (2011). "CNT-network modified Ni nanostructured arrays for high performance non-enzymatic glucose sensors." *RSC Adv.*, 1 (6), 1020–1025.

Zhuang, Z., Su, X., Yuan, H., Sun, Q., Xiao, D. and Choi, M.M.F. (2007). "An improved sensitivity non-enzymatic glucose sensor based on a CuO nanowire modified Cu electrode." *Analyst*, 133 (1), 126–132.

PUBLICATIONS AND CONFERENCES

Papers published in international journals

1. **Prasad**. R, Ganesh. V and B. R. Bhat (2016), Nickel-oxide multiwall carbon-nanotube/reduced graphene oxide a ternary composite for enzyme-free glucose sensing. *RSC Advances***,** 6, 62491-62500.
2. **Prasad, R.** and Bhat, B.R. (2015a). "Multi-wall carbon nanotube–NiO nanoparticle composite as enzyme-free electrochemical glucose sensor." *Sens. Actuators B Chem.*, *220* 81–90.
3. **Prasad, R**. and Bhat, B.R. (2015b). "Self-assembly synthesis of Co_3O_4/multiwalled carbon nanotube composites: an efficient enzyme-free glucose sensor." *New J. Chem.*, *39* (12), 9735–9742.
4. **Prasad, R**., Gorjizadeh, N., Rajarao, R., Sahajwalla, V. and Bhat, B.R. (2015). "Plant root nodule like nickel-oxide–multi-walled carbon nanotube composites for non-enzymatic glucose sensors." *RSC Adv.*, *5* (56), 44792–44799.
5. **Prasad, R**. and Bhat, B.R. (2016) Nickel oxide - multi walled carbon nanotube composite as non-enzymatic electrochemical glucose sensor, *Advanced Science Letters*, 22 (1), 219-222.
6. **Prasad. R** and B. R. Bhat (2016), Eco-friendly synthesis of copper-oxide decorated multi-wall carbon nanotube composites for enzyme-free glucose sensing, **Analytical chemical acta, (**Submitted**).**

Papers presented in conferences

1. **Prasad. R.** and Bhat, B.R. (2015), Eco-friendly synthesis of Co_3O_4-carbon nanotube/reduced graphene oxide ternary composite for non-enzymatic glucose sensor application, **Nanos-15**, Gitum University, Vizag, AP, India, December 2015

2. **Prasad. R.** and Bhat, B.R. (2015) Nickel oxide - multi walled carbon nanotube composite as non-enzymatic electrochemical glucose sensor **EMCA-2014**, CSIR-CRCRI and NIT Durgapur, Kolaktta, West Bengal, India-700032, December-2014

3. **Prasad. R,** Ravindra Rajarao, VeenaSahajwalla, Badekai Ramachandra Bhat. (2014). Green Approach to Decorate Multi-Walled Carbon Nanotubes by Metal/Metal Oxide Nanoparticles, International Conference on Advances in Manufacturing and Materials Engineering, (**ICAMME-2014**), National Institute of Technology Karnataka, Surathkal, Mangalore, 27-29 March, 2014.

4. **Prasad. R** and B.R Bhat (2015). Eco-friendly synthesis of Co_3O_4-carbon nanotube/reduced graphene oxide ternary composite for non-enzymatic glucose sensor. International Conference on "Nanoscience, Nanotechnology & Advanced Materials" (NANOS 2015), 14-17 December 2015, GITUM University, Vishakapattanam, AP, India.

RAGHAVENDRA PRASAD J, (Ph.D)
Catalysis and Materials Laboratory, Department of Chemistry,
National Institute of Technology Karnataka, Surathkal, Srinivasnagar-575025, India
E-mail: raghavendra.raki@gmail.com, rpj.cy12f08@nitk.edu.in
Phone: +91-**9886525882**

CAREER INTEREST

Fundamental science of nano- micro-, meso-, and macro-scale aspects of materials and technologies for sustainable material development with special attention to contributions that reduce the knowledge gap between materials and system designs.

EDUCATION

PhD in Chemistry (Submitted)

Area: Nanomaterials, Electrochemistry, Biosensor, Catalysis, Energy storage.
Thesis title: Carbon nanocomposites material for enzyme-free glucose sensing.
Institute: National Institute of Technology Karnataka, India
Year: Jan 2013 – 2016

Masters in Chemistry (2007-2009)

Area: Organic/analytical chemistry
Thesis title: Potassium Hydride in Paraffin: A Useful Base for Organic Synthesis
Institute: Bangalore University, India
Year: 2007-2009

PROFESSIONAL EXPERIENCE

Senior scientist (**R&D)**

Anthem Bio-Science Pvt, Ltd, Bangalore, (Nov 2009 to Dec 2012).

Team Lead

Designing new processes or improving the existing ones for effective synthesis.

Technology transfer from **R&D to** production.

Synthesizing target compounds utilizing a blend of both classical and modern technology.

Structural elucidation of organic compounds by latest spectroscopic techniques such as NMR Spectroscopy, chiral HPLC, GC, FT-IR, UV-Vis Spectrometer, Fluorescence Spectrometer, TEM, LC-MS etc.

Chromatographic methods.

Communicating effectively in verbal and written form on research results, issues and plans.

RESEARCH AWARDS AND ACHIEVEMENTS

- Received International Travel Grant from TEQIP-II for **research interaction on sustainable material: design, synthesis, characterisation and recovery of the materials, at University of New South Wales (UNSW), Sydney, Australia**, during May to June, 2016.
- The best research award in 6th Annual Karnataka Science and Technology Academy Conference, India

RESEARCH EXPERIENCE

- Extensive knowledge on principle and interpretation of data from Gas Chromatography, Mass spectroscopy, Hyphenated TGA-FTIR, Hyphenated TGA-FTIR-GCMS, TGA, Raman spectroscopy, ICP-MS, XRF, XPS, XRD, UV-Visible spectroscopy, Scanning Electron Microscope, Transmission Electron Microscope, FTIR, LECO carbon analyser, BET surface area analyser, CHNS analyser, Chemical vapour deposition techniques.
- Experience in studying the gas evolution and pyrolytic catalysis reactions by using hyphenated TGA-FTIR-GC/MS technique.
- Experience in synthesis of zero/one dimensional nanoparticles by techniques such as chemical vapour deposition, combustion, carbothermal techniques and their characterisation by analytical techniques.
- Experience in developing novel and innovative materials and processes by utilizing waste materials.
- Experience in synthesis of organic molecules and inorganic metal complexes and their characterisation.
- Experience in homogeneous and heterogeneous catalytic studies.
- Experience incharacterisation of various waste materials.
- Experience in writing research articles, reports and research proposals.
- Experience in co-supervising Bachelors and Masters Students on their projects.
- Presented many talks in industrial meeting and research papers in conferences.
- Ability to conduct experiments in lab and proficient in IT with excellent computer skills.

EXPERIENCE IN HANDLING ANALYTICAL INSTRUMENTS

Trained and experienced in **state of art** instruments :

- Hyphenated **TGA- FTIR-GCMS** (Make: PerkinElmer)
- Hyphenated **TGA- FTIR** (Make: PerkinElmer)
- Gas Chromatography (**GC,** Make: Shimadzu)
- Mass Spectroscopy (**MS,** Make: PerkinElmer)
- Laser Raman spectrometer (**LRS,** Make: Reinshaw)
- Scanning Electron Microscope (**SEM,** Make: Hitachi)
- Powder X-ray diffraction (**XRD**, Make: PANalytical)
- Infrared Spectroscopy (**FTIR**, Make: Thermo Fischer)
- BET surface area analyser (Make: Quanta Chrome)
- Electrochemical techniques (Make: Autolab)

RESEARCH PUBLICATIONS

1. **R. Prasad**. Ganesh. V and B. R. Bhat (2016), Nickel-oxide multiwall carbon-nanotube/reduced graphene oxide a ternary composite for enzyme-free glucose sensing. *RSC Advances***,** 6, 62491-62500

2. **R. Prasad**. and Bhat, B.R. (2016). "Electrochemical determination of dopamine using zinc-oxide rod modified carbon paste electrode." *Adv. Sci. Lett*. 22, 921-924.

3. **R. Prasad** and Badekai Ramachandra Bhat (2016), rGO supported Co-Ni bimetallic magnetically separable nanocatalysts for the reduction of 4-Nitrophenol, *Synthetic metals*, 219, 26-32.

4. **R. Prasad** and Bhat, B.R. (2016) Nickel oxide - multi walled carbon nanotube composite as non-enzymatic electrochemical glucose sensor, *Advanced Science Letters*, 22 (1), 219-222.

5. **R. Prasad** and Badekai Ramachandra Bhat (2015), Self-assembly synthesis of Co_3O_4/multiwalled carbon nanotube composites: an efficient enzyme-free glucose sensor, New J. Chem., 39, 9735 – 9742.

6. **R. Prasad** and Badekai Ramachandra Bhat (2015), Multi-wall carbon nanotube–NiO nanoparticle composite as enzyme-free electrochemical glucose sensor, Sensors and Actuators B: Chemical 220, 81-90.

7. **Raghavendra Prasad**, NarjesGorjizadeh, RavindraRajarao, VeenaSahajwalla and Badekai Ramachandra Bhat (2015), Plant root nodule like nickel-oxide–multi-walled carbon nanotube composites for non-enzymatic glucose sensors, RSC Adv., 5, 44792-44799.

8. RavindraRajarao, **Raghavendra Prasad J**, VeenaSahajwalla, Badekai Ramachandra Bhat, Green Approach to Decorate Multi-Walled Carbon Nanotubes by Metal/Metal Oxide Nanoparticles, Elsevier Publication, Procedia Material Science. 2014, 5, 69-75.

9. **R. Prasad** and B. R. Bhat (2016), Eco-friendly synthesis of copper-oxide decorated multi-wall carbon nanotube composites for enzyme-free glucose sensing, **Analytical chemicaacta, (**Submitted**).**

10. **R. Prasad** and B. R. Bhat (2016), Pyrolysis and mechanical properties of β-SiC powder obtained from waste tires. Journal of American ceramic society, **(**Submitted**).**

RESEARCH WORKS PRESENTED IN CONFERENCES

1. National Conference on Recent Trends in Chemical Sciences (NCRTCS 2016), Manipal University, India (2013)
2. International conference on Nanoscience, Nanotechnology and advanced materials, (NANOS-15) Gitum University, Vizag, India (2015).
3. Emerging Materials: Characterization &Application (EMCA-2014), India (2014).

4. International Conference on Advances in Manufacturing and Materials Engineering, (ICAMME-2014), Mangalore, India (2014).
5. International conference on nanotechnology (NANOCON-14), Pune, India (2014).
6. 6th Annual conference on "science & technology (KSTA), Bangalore, India (2013).
7. Indian council of chemist conference (ICC) – Dharwad India, (2013).